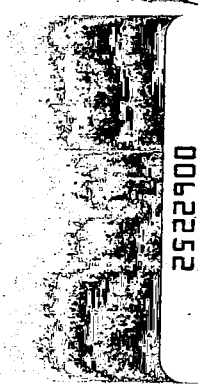

NASA Contractor Report 3494

Turbofan Forced Mixer-Nozzle Internal Flowfield

III - A Computer Code for 3-D Mixing in Axisymmetric Nozzles

J. P. Kreskovsky, W. R. Briley,
and H. McDonald

CONTRACT NAS3-20951
APRIL 1982

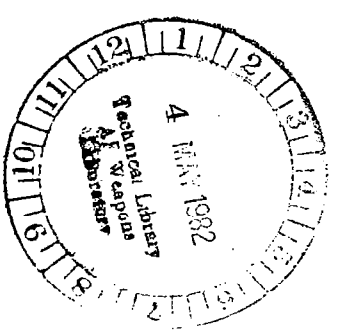

NASA

NASA Contractor Report 3494

Turbofan Forced Mixer-Nozzle Internal Flowfield

III - A Computer Code for 3-D Mixing in Axisymmetric Nozzles

J. P. Kreskovsky, W. R. Briley,
and H. McDonald
Scientific Research Associated, Inc.
Glastonbury, Connecticut

Prepared for
Lewis Research Center
under Contract NAS3-20951

NASA
National Aeronautics
and Space Administration

Scientific and Technical
Information Branch

1982

TABLE OF CONTENTS

Page

INTRODUCTION

The lobe mixer is a device currently being used for thrust augmentation on a variety of turbofan engines. The forced mixer is designed to mix primary (core) and secondary (fan) flow streams before they enter the exhaust nozzle, thus providing the nozzle with air having a more uniform energy which results in a more uniform velocity at the nozzle exit. It has long been known that by mixing the fan and turbine exhaust streams of a turbofan engine in this manner prior to expansion through the exhaust nozzle, a small but significant performance gain may be realized. The level of these gains depends on trade-offs between the degree of mixing of the two streams and the viscous losses incurred in the mixing process.

To date, the performance of lobe mixers has been determined almost entirely through experiments. These experiments are sufficient to determine the relative merits of one mixer configuration as compared to another, but in the absence of detailed understanding, it is both expensive and time consuming to develop unproved lobe mixers in this manner. The overall mixer flow field consists of two major flow regions: (1) the flow upstream of the lobe exit plane (within the lobes) and (2) the flow downstream of the lobe exit plane where the mixing actually takes place. The present study concentrates upon the actual mixing process downstream of the lobe exit plane, through development of a computational procedure applicable in this region and capable of predicting the three-dimensional mixing process in detail. The present analysis and computational procedure represent a capability which can provide further understanding of the mechanism by which mixers produce a gain in performance. Ultimately, the present analysis may enable designers to predict practical mixer flows in detail and to screen or otherwise evaluate alternative mixer configurations.

Although the geometry of the mixing duct itself is axisymmetric and thus effectively contains only radial and axial variations, the flow entering the mixing duct is normally three-dimensional and consists of two streams, the cold fan stream and the hot core stream. The inlet flow contains free shear layers and thermal mixing layers downstream of the mixer lobes. Since the

mixer lobe geometry forces an azimuthal variation in the flow, the mixing layers of primary importance in the present analysis are inherently three-dimensional, and thus various methods of analysis based on two-dimensional theories were excluded from consideration. The flow field downstream of the lobe exit plane and within the mixing duct can be treated, however, within the general framework recently developed by Briley & McDonald (Ref. 1) for the prediction of three-dimensional viscous subsonic flows with large secondary velocities. The analysis of Briley & McDonald was developed for three-dimensional subsonic viscous flows at high Reynolds number which have a predominant primary flow direction with secondary flow in transverse planes. A key restriction of the analysis is that once a primary flow direction is established, reversed flow in the primary flow direction (flow separation) does not occur. The analysis synthesizes concepts from potential flow theory, secondary flow theory, and from an extension of three-dimensional boundary layer theory in a manner which allows efficient solution by forward-marching numerical integration techniques, given only knowledge of the potential flow. Repeated and costly (iterative) sweeping of the entire three-dimensional flow field is not necessary to obtain a valid approximation to the flow. As a consequence, numerical solution of the derived governing equations generally requires considerably less computer time than would a solution of the full three-dimensional Navier-Stokes equations. An *a priori* potential flow solution nevertheless accounts at least approximately for the important elliptic influence of downstream boundary conditions and determines the primary flow direction. In Ref. 1, the analysis was employed to compute laminar flow in curved rectangular ducts and a turbine blade passage at high Reynolds number but relatively low Mach number. In that application, the strong secondary flows and corner vortices associated with the endwall regions and caused by large turning angles of the passage, were of primary interest. The present application to lobe mixer flows includes a two-equation turbulence model, and solves an energy equation to account for thermal effects arising from large temperature differences between the hot turbine exhaust and cool fan streams. The analysis is designed for internal flows which have a maximum average Mach number less than 1.0 at each axial station, although Mach numbers exceeding unity may occur locally within the flow field.

ANALYSIS

General Approach

The present analysis includes a development in a general vector form which follows Ref. 1, and other material which pertains to the application to turbulent flow in lobe mixers. The analysis is based on approximations made relative to a curvilinear but not necessarily orthogonal coordinate system fitted to and aligned with the flow geometry under consideration (cf. Fig. 1). The coordinate system is chosen such that the streamwise or marching coordinate either coincides with or is at least approximately aligned with a known inviscid primary flow direction, as determined for example by a potential flow for the given geometry. Transverse coordinate surfaces must be either perpendicular or nearly perpendicular to solid walls or bounding surfaces, since diffusion is permitted only in these transverse coordinate surfaces. One obvious coordinate system would take the local direction of the velocity from an inviscid potential flow as the marching coordinate, and curvilinear surfaces of constant potential as transverse coordinate surfaces, although such a "potential flow coordinate system" is not essential (and may not even be convenient).

Equations governing streamwise vorticity and a scalar viscous correction u_v to a known inviscid primary flow velocity $\bar{U}_I$ are derived utilizing assumptions which permit forward-marching solution, provided reversal of the composite streamwise velocity does not occur. Terms representing diffusion normal to transverse coordinate surfaces are neglected. Approximate pressure gradients are derived from the inviscid primary flow and imposed in the streamwise momentum equation. These pressure gradients are the sole means of accounting for the elliptic influence of downstream boundary conditions in curved flow geometries, although they may be corrected as part of the forward-marching process if a suitable correction is available. Secondary flow velocities are determined by scalar and vector potentials in the transverse coordinate surfaces, to suppress streamwise elliptic behavior requiring downstream boundary conditions.

The use of streamwise vorticity in obtaining secondary flow velocities avoids the use of transverse momentum equations and hence the major influence of transverse pressure gradients in predicting secondary flow velocity.

As a consequence, the method does not require or yield a direct prediction for the overall viscous pressure field. The viscous pressure field can nevertheless be determined *a posteriori* using the computed composite velocity as input for a scalar three-dimensional solution of the Poisson equation for pressure, obtained as the divergence of the vector momentum equation. Although the presence of reversed flow in the primary flow coordinate direction (flow separation) normally precludes the use of forward-marching solution procedures as described here, special treatments which exclude the separated region from the computational domain are both possible and useful in some applications.

This general approach has been applied to flow in smoothly curved internal flow passages with large turning by Briley & McDonald [1 & 2], to the airfoil tip vortex generation process by Shamroth & Briley [3], and is also applicable to the forced lobe mixer problem considered here.

Primary-Secondary Velocity Decomposition

The analysis is based on decomposition of the overall velocity vector field $\bar{U}$ into a primary flow velocity $\bar{U}_p$ and a secondary flow velocity $\bar{U}_s$. The overall or composite velocity is determined from the super-position

$$\bar{U} = \bar{U}_p + \bar{U}_s \tag{2.1}$$

The primary flow velocity is represented as

$$\bar{U}_p = \bar{U}_I u_v \tag{2.2}$$

where $\bar{U}_I$ is a known inviscid primary flow velocity satisfying slip conditions and determined for example from an *a priori* potential flow solution in the geometry under consideration. The (non-dimensional) scalar quantity u_v is a viscous velocity profile factor which introduces viscous shear layers and may also correct for internal flow blockage effects. In the present case of the lobe mixer u_v accounts for both boundary layers and the free shear layer which exists between the fan and turbine streams. The viscous velocity correction u_v is determined from solution of a primary flow momentum equation. As will become apparent, for the lobe mixer it is convenient to solve for the component of $\bar{U}_p$ in the primary flow direction rather than u_v.

To suppress streamwise elliptic behavior, the secondary flow velocity $\bar{U}_s$ is defined by and thus presumed derivable from scalar and vector surface potentials denoted ϕ and ψ, respectively. If $\hat{i}_1$ denotes the unit vector normal to transverse coordinate surfaces (also presumed here to be in the direction of the marching coordinate), if ρ is density, and if ρ_o is an arbitrary constant reference density, then $\bar{U}_s$ is defined by

$$\bar{U}_s \equiv \nabla_s\phi + (\rho_o/\rho)\nabla\times\hat{i}_1\psi \tag{2.3}$$

where ∇_s is the surface gradient operator defined by

$$\nabla_s \equiv \nabla - \hat{i}_1(\hat{i}_1\cdot\nabla) \tag{2.4}$$

It follows that $\hat{i}_1 \cdot \bar{U}_s = 0$ and thus $\bar{U}_s$ lies entirely within transverse coordinate surfaces. Equation (2.3) is a general form permitting both rotational and irrotational secondary flows and will lead to governing equations which are elliptic in transverse coordinate surfaces and which are therefore solvable within a forward-marching context. The overall velocity decomposition (2.1) can be written

$$\begin{aligned}\bar{U} &= \bar{U}_I u_v + \nabla_s\phi + (\rho_o/\rho)\nabla\times\hat{i}_1\psi \\ &= \bar{u}_p + \nabla_s\phi + (\rho_o/\rho)\nabla\times\hat{i}_1\psi\end{aligned} \tag{2.5}$$

Surface Potential Equations

Equations relating ϕ and ψ with u_v, ρ, and the streamwise vorticity component Ω_1 can be derived from Eq. (2.5) as follows:

$$\nabla\cdot\rho\bar{U} = 0 = \nabla\cdot\rho\bar{U}_I u_v + \nabla\cdot\rho\nabla_s\phi + \rho_o\nabla\cdot\nabla\times\hat{i}_1\psi \tag{2.6}$$

$$\hat{i}_1\cdot\nabla\times\bar{U} \equiv \Omega_1 = \hat{i}_1\cdot\nabla\times\bar{U}_I u_v + \hat{i}\cdot\nabla\times(\rho_o/\rho)\nabla\times\hat{i}_1\psi + \hat{i}_1\cdot\nabla\times\nabla_s\phi \tag{2.7}$$

Since the last term in each of Eqs. (2.6, 2.7) is zero by vector identity, Eqs. (2.6, 2.7) can be written as

$$\nabla\cdot\rho\nabla_s\phi = -\nabla\cdot\rho\bar{U}_I u_v \tag{2.8}$$

$$\hat{i}_l\cdot\nabla\times(\rho_o/\rho)\nabla\times\hat{i}_l\psi = \Omega_l - \hat{i}_l\cdot\nabla\times\bar{U}_I u_v \tag{2.9}$$

which are elliptic for ϕ and ψ in transverse coordinate surfaces. The last term in Eq. (2.9) is identically zero in a potential flow coordinate system for which $\hat{i}_1$ and $\bar{U}_I$ have the same direction, and is small if $\hat{i}_1$ and $\bar{U}_I$ are approximately aligned. Given a knowledge of u_v, Ω, and ρ, the surface potentials ϕ and ψ can be determined by a two-dimensional elliptic calculation in transverse coordinate surfaces at each streamwise location. In turn, $\bar{U}_s$ can be computed from Eq. (2.3), and the composite velocity $\bar{U}$ will satisfy continuity. Equations for u_v and Ω_1 are obtained from the equations governing momentum and vorticity, respectively.

Primary Momentum and Pressure Approximation

The streamwise momentum equation is given by

$$\hat{i}_l\cdot\left[(\bar{U}\cdot\nabla)\bar{U} + (\nabla p)/\rho\right] = \hat{i}_l\cdot\bar{F} \tag{2.10}$$

where p is pressure and $\rho\bar{F}$ is force due to viscous stress. Terms in F representing streamwise diffusion are neglected; however, since the viscous terms are complex for compressible flow, the modified viscous force is temporarily denoted $\bar{F}'$, and further consideration of viscous terms is deferred to a later section.

The remaining assumption for Eq. (2.10) concerns the pressure gradient term and is designed to permit numerical solution as an initial value problem. An obvious pressure approximation for curved flow geometries is to impose pressure gradients from an inviscid potential flow (Briley [4]), and for internal flows, to correct these with a mean pressure gradient term depending only on the x_1 coordinate (Patankar & Spalding [5]). This approximation is appropriate both for flows consisting of an irrotational core region with thin shear layers on bounding surfaces, and also for some fully viscous flows. Depending on the particular application, approximate downstream boundary

conditions such as the commonly used "Kutta condition" may be required, and periodicity conditions may be imposed to simulate cascades of airfoils. This approximation invokes the boundary layer concept that, to first order, shear layers do not alter inviscid pressure gradients.

A somewhat more general approximation (in that $\bar{U}_I$ need not be a potential flow) can be derived, and the consequences of such an assumption are clarified on examination of the inviscid momentum equation written as

$$\nabla p + \rho\nabla(q^2/2) = \rho\bar{U} \times \bar{\Omega} \tag{2.11}$$

where $q^2 = \bar{U} \cdot \bar{U}$, and vorticity $\bar{\Omega} = \nabla \times \bar{U}$. In an orthogonal coordinate system, the $\hat{i}_1$ component of Eq. (2.11) is

$$\hat{i}_1 \cdot \left[\nabla p + \rho\nabla(q^2/2) \right] = \rho(u_2\Omega_3 - u_3\Omega_2) \tag{2.12}$$

For small transverse vorticity Ω_2, Ω_3 and small transverse velocities u_2, u_3 (relative to the coordinate system being used), the right-hand side of Eq. (2.12) is of second order and may be neglected. This small shear assumption is familiar as part of the "secondary flow approximation" (cf. Hawthorne [6]), although it should be emphasized that the present analysis accounts for "distortion of Bernoulli surfaces" by means of u_v.

If the right side of Eq. (2.12) is neglected, if pressure gradients are derived from the inviscid velocity $\bar{U}_I$ by setting $q^2 = \bar{U}_I \cdot \bar{U}_I$, and if a mean viscous pressure correction $p_v(x_1)$ is introduced, the pressure approximation can be written as

$$\begin{aligned} \hat{i}_1 \cdot \nabla p &\doteq \hat{i}_1 \cdot \left[\nabla p_v(x_1) - \rho\nabla(\bar{U}_I \cdot \bar{U}_I)/2 \right] \\ &\equiv \hat{i}_1 \cdot \nabla(p_I + p_v) \end{aligned} \tag{2.13}$$

where p_I is the imposed pressure. Typically, for internal flows, p_v is determined to ensure that an integral mass flux condition is satisfied, such as

$$\int_A \hat{i}_1 \cdot \rho\bar{U}\, dA = \text{constant} \tag{2.14}$$

For external flows, $p_v = 0$. If an internal flow has an average Mach number of 1.0 and thus becomes choked, it is not possible to determine a value for p_v such that Eq. (2.14) is satisfied. In this instance, the solution downstream is indeterminant for the given set of initial conditions, and cannot be continued. However, the inlet mass flux or Mach number can be adjusted and iterated if necessary to obtain a flow which is choked at any given axial location. In addition, if it is necessary to pass through the throat of a choked nozzle, this could be accomplished by local perturbation of the throat geometry in a manner similar to that used by Kreskovsky and Shamroth [7] in two dimensions. Finally, if the flow is purely supersonic, there is no need for any pressure approximation such as Eq. (2.13), and such flows have been treated by McDonald and Briley [8].

Arguments favoring subsonic pressure approximation as in Eq. (2.13) lose some validity in strongly curved corner regions, where strong cross flows in the inviscid outer region of shear layers are deflected. Nevertheless, the approximation may not be seriously in error when considering its overall and somewhat limited role in the present context. Finally, this type of pressure approximation is questionable for strongly deflected <u>inviscid</u> flows having large transverse vorticity.

Combining Eqs. (2.10) and (2.13) and setting $\bar{F} \doteq \bar{F}'$ provides an equation nominally governing u_v:

$$\hat{i}_1 \cdot \left[(\bar{U} \cdot \nabla)\bar{U} + (\nabla p_v)/\rho - \nabla(\bar{U}_I \cdot \bar{U}_I)/2 \right] = \hat{i}_1 \cdot \bar{F}' \tag{2.15}$$

where $\bar{U}$ is to be written as

$$\bar{U} = \hat{i}_1 u_I u_v + \hat{i}_2 (v_I u_v + v_s) + \hat{i}_3 (w_I u_v + w_s) \tag{2.16}$$

where u_I, v_I, w_I are components of $\bar{U}_I$, and v_s, w_s are components of $\bar{U}_s$.

<u>Secondary Vorticity</u>

An equation governing Ω_1 in compressible flow can be obtained from an approximate application of secondary flow theory. The equation governing the growth of vorticity Ω_s along a streamline for compressible flow with constant viscosity is given by Lakshminarayana & Horlock [9] and may be written for variable viscosity as

$$\frac{\partial}{\partial s}\left(\frac{\Omega_s}{\rho q}\right) = \frac{2\Omega_n}{\rho q R} - \frac{1}{\rho q^2}\,\hat{s}\cdot\nabla\times\frac{1}{\rho}\nabla p + \frac{1}{\rho q^2}\,\hat{s}\cdot\bar{G} \qquad (2.17)$$

where q is velocity magnitude, $\hat{s}$ is the unit vector along a streamline, s is distance along a streamline, Ω_n is vorticity in the direction of the unit principal normal vector $\hat{n}$ of the streamline, for which R is the principal radius of curvature. These quantities are related by the Frenet formula $\hat{n}/R = \partial\hat{s}/\partial s = \hat{s}\cdot\nabla\hat{s}$. In Eq. (2.17), $\bar{G} \equiv \nabla \times \bar{F}$, and the term containing p vanishes if ρ is constant. Since an intrinsic coordinate system formulation as in Eq. (2.17) provides an "inverse" coordinate system if used to compute $\bar{U}$, and since intrinsic coordinates are degenerate on no-slip surfaces and nonorthogonal for general rotational flows, intrinsic coordinates are not attractive for numerical computation. However, if the coordinate system used for computation is approximately aligned with the flow direction, then an approximate equation governing Ω, can be derived from Eq. (2.17) by replacing $\hat{s}$ by $\hat{i}$, as in the following development:

$$\frac{\Omega_s}{q} = \frac{\hat{s}\cdot\bar{\Omega}}{\hat{s}\cdot\bar{U}} \doteq \frac{\hat{i}_1\cdot\bar{\Omega}}{\hat{i}_1\cdot\bar{U}} = \frac{\Omega_1}{u_1} \qquad (2.18a)$$

$$\frac{\Omega_n}{qR} = \frac{(\hat{s}\cdot\nabla\hat{s})\cdot\bar{\Omega}}{\hat{s}\cdot\bar{U}} \doteq \frac{(\hat{i}_1\cdot\nabla\hat{i}_1)\cdot\bar{\Omega}}{\hat{i}_1\cdot\bar{U}} = \frac{\Omega_{n1}}{u_1 R_1} \qquad (2.18b)$$

where $u_1 = u_I u_v$; R_1 is the principal radius of curvature of the x_1 coordinate, and Ω_{n1} is vorticity in the direction of $\hat{n}_1$, the principal normal of the x_1 coordinate line. The quantities $\hat{n}_1$ and R_1 are defined by the Frenet formula $\hat{n}_1/R_1 = \hat{i}_1\cdot\nabla\hat{i}_1$. To illustrate, in an orthogonal coordinate system,

$$\frac{\hat{n}_1}{R_1} = -\left[\frac{\hat{i}_2}{h_1 h_2}\frac{\partial h_1}{\partial x_2} + \frac{\hat{i}_3}{h_1 h_3}\frac{\partial h_1}{\partial x_3}\right] \qquad (2.19)$$

where h_1, h_2, h_3 denote metric coefficients. If ρ varies, p is replaced by the imposed pressure p_I as defined in Eq. (2.13). Finally, taking $q^2 \doteq u_1^2$ and $\hat{s} \doteq \hat{i}_1$ in the last two terms in Eq. (2.17), and neglecting streamwise

diffusion, Eq. (2.17) becomes

$$\bar{U}\cdot\nabla\left(\frac{\Omega_1}{\rho u_1}\right) = \frac{2\Omega_{n1}}{\rho u_1 R_1} - \frac{1}{\rho u_1^2}\hat{i}_1\cdot\nabla\times\left(\frac{\nabla p_I}{\rho}\right) + \frac{1}{\rho u_1^2}\hat{i}_1\cdot\bar{G}' \qquad (2.20)$$

where $\bar{G}'$ does not contain streamwise diffusion.

The transverse vorticity Ω_{n1} in Eq. (2.20) contains components which, in orthogonal coordinates and assuming an irrotational $\bar{U}_I$, are given by

$$\Omega_2 = \hat{i}_2\cdot\nabla\times\bar{U} = \frac{u_I}{h_3}\frac{\partial u_v}{\partial x_3} - \frac{w_I}{h_1}\frac{\partial u_v}{\partial x_1} - \frac{1}{h_1 h_3}\frac{\partial}{\partial x_1}(h_3 w_s) \qquad (2.21a)$$

$$\Omega_3 = \hat{i}_3\cdot\nabla\times\bar{U} = -\frac{u_I}{h_2}\frac{\partial u_v}{\partial x_2} + \frac{v_I}{h_1}\frac{\partial u_v}{\partial x_1} + \frac{1}{h_1 h_2}\frac{\partial}{\partial x_1}(h_3 v_s) \qquad (2.21b)$$

In the applications contemplated here, the first term on the right-hand side of each of Eqs. (2.21a - b) is expected to dominate, and the remaining terms may be neglected as a convenience, if desired.

Energy Equation

Since the flow being considered is nonadiabatic, solution of an equation governing energy is required. The energy equation can be written in a variety of forms, one of which is

$$\rho\bar{U}\cdot\nabla E = \nabla\cdot k\nabla T + \bar{U}\cdot\bar{F} + \Phi \qquad (2.22)$$

where E is total enthalpy, T is temperature, k is thermal conductivity, and ϕ is the dissipation function. Solution of Eq. (2.22) by forward marching integration requires only that terms representing streamwise conduction of heat and also streamwise viscous diffusion in $\bar{F}$ be neglected.

Compressibility Relations

In the imposition of streamwise pressure gradients compressibility effects are represented by introducing the perfect gas equation of state $p = \rho RT$. No other assumptions are necessary for consideration of compressible flow. For moderate subsonic Mach numbers, inviscid pressure gradients would

ideally be obtained from a compressible potential flow calculation or otherwise from an incompressible potential flow corrected for compressibility using either the Prandtl-Glauert formula or Laitone's variant [10]. Replacing p in Eq. (2.13) by the state equation and eliminating temperature using the temperature-enthalpy relation

$$E = c_p T + \frac{\bar{U}\cdot\bar{U}}{2} \tag{2.23}$$

where c_p denotes specific heat, the following auxiliary equation relating the imposed pressure gradients with density, velocity, and total enthalpy is obtained:

$$\hat{i}_1 \cdot \nabla\left[p_I + p_v(x_1)\right] = \hat{i}_1 \cdot \nabla\left[\frac{\gamma-1}{\gamma}\rho\left(E - \frac{\bar{U}\cdot\bar{U}}{2}\right)\right] \tag{2.24}$$

where γ is specific heat ratio. A slight simplification results if $\bar{U} \cdot \bar{U}$ is replaced by $(\hat{i}_1 \cdot \bar{U})^2$ in Eq. (2.24).

Typically, the treatment of nonconstant total enthalpy is of interest for predicting heat transfer levels in shear layers. However, it should be noted that the geometrical pattern of streamlines for steady inviscid flow of a perfect gas depends only on the total pressure gradient and not on the distribution of total enthalpy (cf. Hawthorne [6]). Thus, within an assumption of small transverse total pressure gradient in the free stream or core region, it is possible to consider core flows with two separate streams having large differences in total enthalpy and velocity and hence separated by thermal and viscous shear layers, provided the two streams have about the same static and total pressure. In addition, the analysis can be applied to flows with two streams at different total pressure provided the static pressure is continuous across the interface. Although inviscid pressure gradients can no longer be represented by a two-dimensional potential flow, the error thus introduced by the present analysis may not be serious. Since the mean pressure level is determined accurately by p_v, the primary source of error in this instance would be that due to the assumed transverse variation in imposed streamwise pressure gradients, which in turn is associated with streamline curvature. For geometries without appreciable turning, this error

may be acceptable. The foregoing observations regarding two stream flows were used to advantage in the present application to flow in turbofan lobe mixers.

Viscous and Heat Conduction Terms

A variety of techniques for suppressing streamwise diffusion is possible, and the particular choice in any given application may depend on the complexity one is willing to tolerate in the viscous terms. For example, the complete set of viscous terms can be written out and all derivatives in the streamwise direction neglected. Alternatively, only second derivatives in the streamwise direction may be neglected. Here, attention is restricted to incompressible flow but with variable viscosity. In the momentum equation (2.10), $\bar{F} \equiv -\nabla \times \nu\nabla \times \bar{U}$, where ν is kinematic viscosity. A particularly simple expression which neglects contributions from $\bar{U}_s$ is given by

$$\hat{i}_1 \cdot \bar{F} \doteq -\hat{i}_1 \cdot \nabla \times \nu \nabla \times \hat{i}_1 u_I u_V = \bar{F}' \tag{2.25}$$

Alternatively, contributions from $\bar{U}_s$ may be retained as in the approximation

$$\hat{i}_1 \cdot \bar{F} \doteq -\hat{i}_1 \cdot \nabla \times \nu \nabla_s \times \bar{U} = \bar{F}' \tag{2.26}$$

Similarly, in the vorticity equation (2.17), $\bar{G}$ is defined by $\bar{G} = -\nabla \times \nabla \times \nu\bar{\Omega}$ and approximated by

$$\hat{i}_1 \cdot \bar{G} \doteq -\hat{i}_1 \cdot \nabla \times \nabla \times \hat{i}_1 \nu \Omega_1 = \bar{G}' \tag{2.27}$$

Streamwise heat conduction in Eq. (2.22) is suppressed by the approximation

$$\nabla \cdot k\nabla T \doteq \nabla \cdot k\nabla_s T \tag{2.28}$$

Governing System of Equations

A complete system of six coupled equations governing u_v, Ω_1, Φ, ψ, E, and ρ is given by Eqs. (2.8), (2.9), (2.15), (2.22), (2.24), and (2.20). Ancillary relations are given by Eq. (2.5) for composite velocity, Eq. (2.14) for mass flux, and Eqs. (2.21a-b) for transverse vorticity.

The Turbulence Model

The present analysis is to be used to predict a turbulent flow field, thus the stress terms F' and G' in Eqs. (2.15), (2.20), and (2.22) contain turbulent shear terms in the form of fluctuating velocity and velocity-temperature correlations. These terms may be modeled using any of a number of turbulence models. In the present application to lobe mixer flows, these turbulent shear terms are modeled through the introduction of a turbulent eddy viscosity determined from solution of two partial differential equations governing the transport of the turbulence kinetic energy and the turbulent dissipation. The particular model used in the present application is described by Launder and Spalding [11]. Using Cartesian tensor notation, and overbars to indicate time averaging the turbulence kinetic energy is defined as

$$k = \frac{1}{2}\overline{u_i' u_i'} \tag{2.29}$$

and the dissipation as

$$\epsilon = \nu \overline{\frac{\partial u_i'}{\partial x_j}\frac{\partial u_i'}{\partial x_j}} \tag{2.30}$$

By hypothesis, Prandtl and Kolmogorov have suggested that the effective viscosity is proportional to the local density and the product of a characteristic turbulent velocity and length scale. The characteristic velocity is assumed equal to the square root of the local value of turbulence kinetic energy, thus $\mu_T = c\rho\ell k^{1/2}$ where c is a constant of proportionality. Through dimensional arguments, the length scale may be related to the turbulence kinetic energy and dissipation as

$$\ell = C^3 k^{3/2}/\epsilon \tag{2.31}$$

and from the Prandtl-Kolmogorov hypothesis it follows that the turbulent viscosity may be expressed in terms of k and ϵ as

$$\mu_T = C^4 \rho k^2/\epsilon \tag{2.32}$$

Based on an examination of a large amount of experimental data Launder [11] has recommended that $c^4 = 0.09 \equiv c_\mu$, and under these conditions the length scale may be thought of as the conventional mixing length.

The transport equations governing k and ε at high Reynolds number are given in vector form [11] as

$$\rho \frac{\partial k}{\partial t} + \rho U \cdot \nabla k = \nabla \cdot (\mu + \mu_T/\sigma_k) \nabla k + P - \rho \epsilon \tag{2.33}$$

$$\rho \frac{\partial \epsilon}{\partial t} + \rho U \cdot \nabla \epsilon = \nabla \cdot (\mu + \mu_T/\sigma_\epsilon) \nabla k + C_1 \frac{\epsilon}{k} P - C_2 \frac{\rho \epsilon^2}{k} \tag{2.34}$$

In Eqs. (2.33, 2.34), P is the turbulence production and is given in the APPENDIX. The quantities $\sigma_k, \sigma_\epsilon$, C_1, C_2 are empirical constants which, as recommended by Launder & Spalding [11] , are taken as 1.0, 1.3, 1.44, and 1.92, respectively.

Although the k-ε turbulence model provides a general means by which turbulence effects may be modeled, experience with the model has indicated that it may not be completely reliable. Negative values of dissipation may develop under certain conditions at isolated points in the flow field leading to a breakdown of the calculation. To provide a means to circumvent this problem an optional turbulence model was included in the analysis.

This turbulence model is referred to as a wake turbulence model and is derived from the definition of turbulent viscosity μ_t and Prandtl's suggestion that the diffusional flux of some property $\phi = \bar{\phi} + \phi'$ may be expressed

$$-\overline{v'\phi'} = \frac{1}{\sigma_\phi} k^{1/2} \ell \frac{\partial \bar{\phi}}{\partial y} = \frac{\mu_t}{\rho} \frac{\partial \bar{\phi}}{\partial y} \tag{2.35}$$

hence one obtains the Prandtl-Kolmogorov relationship

$$\mu_t = \frac{1}{\sigma_\phi} k^{1/2} \ell \rho \tag{2.36}$$

The wake turbulence model is obtained by assuming that the turbulent length scale and velocity scales are constant throughout the flow field. From equations 2.31 and 2.32 it follows that the constant $1/\sigma_\phi$ is simply $C^{1/4}$. The velocity scale is taken as the square root of the initially specified turbulence kinetic energy k. The length scale is specified using the geometric constraints of the mixer as a guide, for instance assuming that the initial length scale would not be smaller than the inlet boundary layer or larger than the duct height. As a consequence of this formulation, the turbulent viscosity is dependent only upon the initial choices of k and ℓ, and the local density which is determined as the solution progresses.

APPLICATION TO FLOW IN A LOBE MIXER

In this section, specific details arising in the application of the foregoing analysis to lobe mixer problems are given. A cross section of a typical lobe mixer geometry is shown in Fig. 2. The area immediately downstream of the nozzle plug is faired in with an assumed streamline to model the reversed flow region expected in this region. Since the flow area thus excluded from consideration is very small, this treatment is not believed to introduce significant error. A more detailed analysis of this separated flow region could be performed following a zone embedding approach using the Navier-Stokes equations (cf. [12]). Although the mixer geometry is axisymmetric, the flow is three-dimensional due to the azimuthal variation of the hot and cold streams. However, due to observed symmetry, only a pie-shaped region of the transverse coordinate surface need be considered. The shape of this region and the extent of typical hot and cold streams at the mixer exit surface are shown in Fig. 3.

Coordinate System

Curvilinear orthogonal coordinates x, y, z are constructed to fit the flow passage boundaries as shown in Fig. 2. Metric coefficients h_1, h_2, h_3 are defined such that incremental distance s is determined by $(\delta x)^2 = (h_1 \delta x)^2 + (h_2 \delta y)^2 + (h_3 \delta z)^2$. In planes of constant z, azimuth, orthogonal streamlines, and velocity potential lines from a two-dimensional planar incompressible potential flow analysis are utilized as the coordinate lines for constant y and x, respectively. This x-y coordinate system is then rotated about an axis representing the centerline of the lobe mixer, to form an axisymmetric coordinate system. Thus the z direction can be regarded as cylindrical (i.e., θ) and $h_3 = r$. The x coordinate is taken as the primary flow or axial coordinate, and is associated with surfaces for which the two-dimensional potential is constant. The y and z coordinates define transverse secondary flow planes at any given x location. In this coordinate system, the normals $\bar{i}_n$ to the transverse planes coincide with $\bar{i}_1$ the unit vector in the x direction. A two-dimensional incompressible potential flow analysis and computer program developed by Anderson [13] was employed in the present investigation, without modification, to compute the necessary coordinate data.

The Axisymmetric Pressure Field

Since the coordinate system is based on a two-dimensional planar potential calculation, the coordinate lines are not precisely aligned with the axisymmetric potential flow appropriate for the mixer geometry. For the purpose of setting the primary and secondary flow directions, however, the two-dimensional solution provides a good approximation and thus the direction of $\bar{i}_1$, the unit vector in the x coordinate direction, is taken as the primary flow direction. This assumption is justified since surfaces of constant potential from the two-dimensional solution remain surfaces of nearly constant potential even though the value of the potential at each surface may be altered significantly in the axisymmetric case. The two-dimensional potential flow is not suitable for approximating the axisymmetric potential flow pressure gradients, however, and consequently an axisymmetric potential flow is computed in the given coordinate system, prior to the forward marching calculation.

Since a compressible potential flow solver was not readily available, an incompressible axisymmetric potential flow was computed and then corrected for compressibility during the forward-marching solution procedure, using Laitone's rule (Ref. 10). Although the Laitone compressibility correction is expected to become inaccurate at high subsonic Mach numbers, this error is mitigated both by the computed correction p_v for mean pressure drop, and by certain mixer flow characteristics. Since the mean pressure level is determined accurately by p_v at each axial location, influence of the imposed inviscid pressure p_I is limited to approximating the transverse variation of axial pressure gradient and hence is associated only with curvature of potential flow streamlines. The axial development of mean pressure drop and average Mach number is thus influenced only indirectly by the imposed pressure and should be predicted with reasonably accuracy. Furthermore, in most mixer geometries, curvature effects are more pronounced in the upstream region and near the end of the center plug, where the Mach number is relatively low. In the region of strong acceleration and high subsonic Mach number near the exit, streamlines tend to have small curvature, and hence the flow has small transverse variation in axial pressure gradients.

The incompressible potential flow is determined by solution of the axisymmetric potential equation

$$\frac{h_2 h_3}{h_1}\frac{\partial^2\phi}{\partial x^2} + \frac{\partial}{\partial x}\left[\frac{h_2 h_3}{h_1}\right]\frac{\partial\phi}{\partial x} + \frac{h_1 h_3}{h_2}\frac{\partial^2\phi}{\partial y^2} + \frac{\partial}{\partial y}\left[\frac{h_1 h_3}{h_2}\right]\frac{\partial\phi}{\partial y} = 0 \quad (3.1)$$

using an efficient iterative ADI procedure and the solution, which represents the correct axisymmetric potential, is used to obtain the axisymmetric pressure field, $P_I(x,y)$. In setting boundary conditions for the axisymmetric potential, the inlet and exit planes are assumed to be surfaces of constant (but differing) potential, and normal derivatives are set to zero elsewhere.

Since Eq. (3.1) may be considered a dimensionless equation with the dimensionless potential ϕ given by

$$\phi = \frac{\phi^*}{U_r L_r} \quad (3.2)$$

where ϕ^* has units of ft^2/sec, the resulting potential field may be arbitrarily scaled to give a mean dimensionless velocity of unity at the mixer exit plane. This normalized potential field is then used in the computation of $P_I(x,y)$.

Governing Equations in Orthogonal Coordinates

A general model for three-dimensional flows which may have large secondary velocities was given in vector form in the preceding section. The governing equations are given here for the orthogonal coordinate system used to represent the mixer passage geometry. Throughout the remaining discussion, all variables in the governing equations are nondimensional, having been normalized by the following reference quantities: distance, L_r; velocity, U_r; density, ρ_r; temperature, T_r; total enthalpy, U_r^2; pressure, $\rho_r U_r^2$; viscosity, μ_r. Here the subscript r denotes a reference quantity. This normalization leads to the following nondimensional parameters: Mach number, M; Reynolds number, Re; Prandtl number, Pr; and specific heat ratio, γ. These parameters are defined by

$$M = U_r/c \ , \ Re = \rho_r U_r L_r/\mu_r \ , \ Pr = c_p \mu_r / k \ , \ \gamma = c_p / c_v \quad (3.3)$$

where μ_r is the molecular viscosity, k is thermal conductivity, and c_p and c_v are the specific heats at constant pressure and volume. The reference speed of sound, c, is defined by $c^2 = \gamma R_g T_r$, where R_g is the gas constant. Since the flow is assumed to be turbulent, the dependent variables are taken to be

the time-averaged quantities in the usual sense; however, third order correlation as well as second order correlations including the fluctuating density have been neglected. The decomposition of the velocity vector thus can be written

$$\bar{U} = \bar{i}_1 u + \bar{i}_2 v + \bar{i}_3 w \tag{3.4}$$

Where $\bar{i}_1$, $\bar{i}_2$, and $\bar{i}_3$ are the unit vectors in the x, y, and z coordinate directions, respectively. Since $\bar{i}_1$ is closely aligned with the primary flow direction, v_I is small and is neglected as a minor convenience. This approximation is of little consequence since the neglected quantity v_I effectively reappears as part of v_s and is thus determined from solution of the continuity equation during the forward-marching solution process, instead of being imposed a priori from the potential flow. Since w_I is zero by definition, the velocity decomposition can be written as

$$\bar{u} = \bar{i}_1 u_p + \bar{i}_2 v_s + \bar{i}_3 w_s \tag{3.5}$$

Since u_p is the only streamwise component of $\bar{U}$ the subscript "p" is dropped. Under the stated assumptions the streamwise momentum equation can be written as

$$\begin{aligned} &\rho u h_2 h_3 \frac{\partial u}{\partial x} + \rho(v_s) h_1 h_3 \frac{\partial u}{\partial y} + \rho(w_s) h_1 h_2 \frac{\partial u}{\partial z} \\ &\quad + \rho(v_s) u h_3 \frac{\partial h_1}{\partial y} - \rho(v_s)^2 h_3 \frac{\partial h_2}{\partial x} \\ &\quad - \rho(w_s)^2 h_2 \frac{\partial h_3}{\partial x} + h_2 h_3 \frac{\partial p_I}{\partial x} + h_2 h_3 \frac{dp_v(x)}{dx} \\ &= \frac{1}{Re} \frac{\partial}{\partial y}\left[\frac{(\mu+\mu_T) h_1 h_3}{h_2} \frac{\partial u}{\partial y}\right] + \frac{h_1 h_2}{Re h_3} \frac{\partial}{\partial z}\left[\frac{(\mu+\mu_T)\partial u}{\partial z}\right] \end{aligned} \tag{3.6}$$

The energy equation is approximated by

$$\rho u h_2 h_3 \frac{\partial E}{\partial x} + \rho(v_s) h_1 h_3 \frac{\partial E}{\partial y} + \rho(w_s) h_1 h_2 \frac{\partial E}{\partial z}$$
$$= \frac{1}{Re} \frac{\partial}{\partial y}\left[\left(\frac{\mu}{Pr} + \frac{\mu_T}{Pr_T}\right)\frac{h_1 h_3}{h_2}\frac{\partial E}{\partial y}\right.$$
$$\left. + \frac{h_1 h_3}{2h_2}\left(\mu + \mu_T - \frac{\mu}{Pr} - \frac{\mu_T}{Pr_T}\right)\frac{\partial}{\partial y}(\bar{u}^2 + \bar{w}_s^2)\right] \qquad (3.7)$$
$$+ \frac{1}{Re}\frac{h_1 h_2}{h_3}\frac{\partial}{\partial z}\left[\left(\frac{\mu}{Pr} + \frac{\mu_T}{Pr_T}\right)\frac{\partial \bar{E}}{\partial z}\right.$$
$$\left. + 1/2\left(\mu + \mu_T - \frac{\mu}{Pr} - \frac{\mu_T}{Pr_T}\right)\frac{\partial}{\partial z}(\bar{u}^2 + \bar{v}^2)\right]$$

with the Prandtl number Pr and turbulent Prandtl number Pr_T assumed to be 1.0. From the axisymmetric potential flow,

$$u_I = \frac{1}{h_1}\frac{\partial \phi}{\partial x}, \quad v_I = \frac{1}{h_2}\frac{\partial \phi}{\partial y} \qquad (3.8)$$

Substituting these velocity components into the inviscid, incompressible momentum equation

$$\nabla\left(\frac{\bar{U}_I \cdot \bar{U}_I}{2}\right) - \bar{U}_I \times (\nabla \times \bar{U}_I) = -\frac{1}{\rho}\nabla P_{M=0} \qquad (3.9)$$

and integrating Eq. (3.9) with the observation that $\nabla \times \bar{U}_I = 0$ the inviscid incompressible pressure field $P_{M=0}(x,y)$ is obtained from the relationship

$$P_{M=0}(x,y) + \frac{\rho(u_I^2 + v_I^2)}{2} = \text{constant} = P_{TOT} \qquad (3.10)$$

The imposed compressible pressure gradients are then determined from $P_{M=0}$ as

$$\frac{\partial P_I}{\partial x} = \frac{1}{\sqrt{1 - M_L^2}}\frac{\partial P_{M=0}}{\partial x} \qquad (3.11)$$

where M_L is the local Mach number. The imposed pressure gradient is related to the dependent variables using the following form of the auxiliary gas law

$$\frac{\partial}{\partial x}\left[\left(\frac{\gamma-1}{\gamma}\right)\rho\left(E-\frac{u^2}{2}\right)\right] = \frac{\partial P_I}{\partial x} + \frac{dP_v(x)}{dx} \tag{3.12}$$

The integral mass flux relation is

$$\iint_A h_2 h_3 \rho u dy dz = C \tag{3.13}$$

To obtain the rotational secondary flow components of the velocity, the streamwise vorticity equation is written as

$$\begin{aligned}
&\frac{u}{Q}\left(\rho u\frac{\partial \xi}{\partial x} - \xi\frac{\partial \rho u}{\partial x}\right) + \frac{v_s}{Q}\frac{h_1}{h_2}\left(\rho u\frac{\partial \xi}{\partial y} - \xi\frac{\partial \rho u}{\partial y}\right) \\
&+ \frac{w_s}{Q}\frac{h_1}{h_3}\left(\rho u\frac{\partial \xi}{\partial z} - \xi\frac{\partial \rho u}{\partial z}\right) = -\frac{2}{h_2}\frac{\partial h_1}{\partial y}\rho u\frac{1}{h_3}\frac{\partial u}{\partial z} \\
&- \frac{h_1}{h_2 h_3}\frac{1}{\rho}\left[\frac{\partial P}{\partial y}\frac{\partial \rho}{\partial z} - \frac{\partial \rho}{\partial y}\frac{\partial P}{\partial z}\right] \\
&+ \frac{\rho}{Re}\left\{\frac{h_1}{h_2 h_3}\frac{\partial}{\partial y}\left[\frac{h_3}{h_1 h_2 \rho}\frac{\partial h_1(\mu+\mu_T)\xi}{\partial y}\right] + \frac{h_1}{h_3^2}\frac{\partial}{\partial z}\left[\frac{1}{\rho}\frac{\partial(\mu+\mu_T)\xi}{\partial z}\right]\right\}
\end{aligned} \tag{3.14}$$

where $Q^2 = u^2 + v_x^2 + w_s^2$ and the vorticity is related to velocity by

$$\xi_n = \xi = \frac{1}{h_2 h_3}\left(\frac{\partial h_3 w_s}{\partial y} - \frac{\partial h_2 v_s}{\partial z}\right) \tag{3.15}$$

The vector potential $\bar{\psi}_s$ is determined from

$$\frac{1}{h_2 h_3}\frac{\partial}{\partial y}\left[\left(\frac{h_3}{\rho h_1 h_2}\right)\frac{\partial(h_1\psi_s)}{\partial y}\right] + \frac{1}{h_1 h_3^2}\frac{\partial}{\partial z}\left[\left(\frac{1}{\rho}\right)\frac{\partial(h_1\psi_s)}{\partial z}\right] = -\xi \tag{3.16}$$

and the rotational secondary flow velocities are determined as

$$v_\psi = \frac{1}{\rho h_1 h_3}\frac{\partial(h_1\psi_s)}{\partial z} \tag{3.17a}$$

$$w_\psi = -\frac{1}{\rho h_1 h_2}\frac{\partial(h_1\psi_s)}{\partial y} \tag{3.17b}$$

The scalar potential is governed by

$$\frac{\partial}{\partial y}\left[\frac{\rho h_1 h_3}{h_2}\frac{\partial\phi_s}{\partial y}\right] + \frac{\partial}{\partial z}\left[\frac{\rho h_1 h_2}{h_3}\frac{\partial\phi_s}{\partial z}\right] = -\frac{\partial(h_2 h_3 \rho u)}{\partial x} \tag{3.18}$$

The velocity components v_ϕ and w_ϕ are found to be

$$v_\phi = \frac{1}{h_2}\frac{\partial\phi_s}{\partial y} \tag{3.19a}$$

$$w_\phi = \frac{1}{h_3}\frac{\partial\phi_s}{\partial z} \tag{3.19b}$$

The secondary flow velocities are thus

$$v_s = v_\psi + v_\phi \tag{3.20a}$$

$$w_s = w_\psi + w_\phi \tag{3.20b}$$

The turbulence model equations (Eqs. 2.33 & 2.34) must also be expressed in orthogonal coordinates. It is assumed that the turbulence equations are tensor invariant [14] and thus may be expressed directly in orthogonal coordinates by performing vector operations in such a coordinate system. With streamwise diffusion neglected to allow forward-marching solution, the result for the turbulence kinetic energy equation in steady flow is

$$\begin{aligned}\rho u h_2 h_3\frac{\partial k}{\partial x} + \rho v_s h_1 h_3\frac{\partial k}{\partial y} + \rho w_s h_1 h_2\frac{\partial k}{\partial z} \\ = \frac{1}{Re}\left\{\frac{\partial}{\partial y}\left[\frac{h_1 h_3}{h_2}\left(\mu + \frac{\mu_T}{\sigma_k}\right)\frac{\partial k}{\partial y}\right]\right. \\ \left. + \frac{h_1 h_2}{h_3}\frac{\partial}{\partial z}\left[\left(\mu + \frac{\mu_T}{\sigma_k}\right)\frac{\partial k}{\partial z}\right]\right\} - h_1 h_2 h_3 \rho\epsilon + P\end{aligned} \tag{3.21}$$

and similarly the turbulence dissipation equation is given by

$$\rho u h_2 h_3 \frac{\partial \epsilon}{\partial x} + \rho v_s h_1 h_3 \frac{\partial \epsilon}{\partial y} + \rho w_s h_1 h_2 \frac{\partial \epsilon}{\partial z}$$
$$= \frac{1}{Re}\left\{ \frac{\partial}{\partial y}\left[\frac{h_1 h_3}{h_2}\left(\mu + \frac{\mu_T}{\sigma_\epsilon}\right)\frac{\partial \epsilon}{\partial y}\right] \right. \tag{3.22}$$
$$\left. + \frac{h_1 h_2}{h_3}\frac{\partial}{\partial z}\left[\left(\mu + \frac{\mu_T}{\sigma_\epsilon}\right)\frac{\partial \epsilon}{\partial z}\right]\right\}$$
$$- h_1 h_2 h_3 C_2 \rho \frac{\epsilon^2}{k} + C_1 \frac{\epsilon}{k} P$$

The turbulent viscosity is then

$$\mu_T = \frac{C_\mu \rho k^2}{\epsilon} Re \tag{3.23}$$

and the length scale may be determined as

$$\ell = \frac{C_\mu^{3/4} k^{3/2}}{\epsilon} \tag{3.24}$$

Numerical Method

The governing equations are approximated by finite differences. Three point central differences are used for all transverse derivatives. An analytical coordinate transformation devised by Roberts [15] can be employed as a means of introducing a nonuniform grid in each transverse coordinate direction to concentrate grid points near walls while maintaining second-order accuracy. In the computation presented here a uniform mesh spacing in each transverse direction was used. The streamwise vorticity equation is decoupled from other equations in the system and linearized with respect to ξ by an ad hoc process consisting of lagging quantities not yet available at the implicit level. The resulting implicit difference equation for ξ is solved using a scalar ADI scheme based on the technique of Douglas & Gunn [16] for generating ADI schemes as perturbations of fundamental implicit schemes. Equations (3.16 & 3.18) for the vector and scalar potential functions ψ_s and ϕ_s are elliptic in the transverse planes and are solved, given values for

the right-hand sides, using scalar iterative ADI. Specifically, the Douglas-Gunn perturbation of the Crank-Nicolson scheme is used for Eqs. (3.13 & 3.16) while perturbation of the backward difference scheme is used for Eq. (3.18). With regard to the streamwise momentum and energy equations (3.6 & 3.7), since the transverse velocity components are determined separately from elliptic equations the coefficients of the transverse convective terms are lagged. Formal linearization of the streamwise convective terms following Briley and McDonald [17] as extended to nonconservation law form by Kreskovsky and Shamroth [7] also indicates that to first order the coefficients of these derivatives may also be lagged. The energy and momentum equations thus become decoupled while maintaining first-order accuracy in the spatial marching direction. The resulting difference equations may then be grouped by coordinate direction and solved using an efficient ADI scheme. The turbulence model equations form a similar system, but these equations remain coupled through the source terms. In this case, the resulting difference equations can be written in block-tridiagonal matrix form and solved efficiently using linearized block implicit (LBI) techniques.

A summary of the overall algorithm used to advance the solution a single axial step follows. It is assumed that the solution is known at the n level x^n and is desired at x^{n+1}.

1) The imposed pressure gradients are determined from Eqs. (3.10) and (3.11).

2) A value for the mean viscous pressure drop $dp_v(x)/dx$ is assumed. Initially, the value from the previous step is used.

3) Equations (3.6), (3.7) and (3.12) are solved to obtain values of u^{n+1}, E^{n+1} and ρ^{n+1}. In general, the integral mass flux relation (3.13) will not be satisfied.

4) Return to step (2) and repeat this process iteratively using the standard secant method [18] to find the value of the mean viscous pressure drop which leads to u^{n+1} and ρ^{n+1} which satisfies the integral mass flux relation (3.13). The secant method was found in practice to converge the integral mass flux to five figures on the third iteration, unless the flow is near transonic.

5) The turbulence model equations (3.21 & 3.22) are solved using a split LBI scheme.

6) The streamwise vorticity equation (3.14) is solved using scalar ADI to obtain ξ^{n+1}.

7) The vector potential equation (3.16) is solved using scalar iterative ADI to obtain ψ_s^{n+1}.

8) Values for solenoidal secondary flow velocities v_ψ and w_ψ are computed using Eq. (3.17).

9) Using values now available for $\partial\rho u/\partial x$, the scalar potential (3.18) is solved using scalar ADI to obtain ϕ_s^{n+1} to assure that the solution at level n+1 satisfies continuity on a differential basis, and the irrotational secondary flow velocity components v_ϕ and w_ϕ are determined from Eq. (3.19).

To ensure that the initial conditions satisfy continuity on a differential basis, steps 2 through 4 and step 9 are performed to obtain ϕ^n at the initial station either using estimated values of the transverse velocities (obtained from experimental data) or assuming the transverse velocity components are zero.

Specification of Initial Conditions

The initial conditions for a lobe mixer calculation may be specified by using either an automated starting routine or by reading in experimental data. The fully automated procedure is considered first.

To obtain initial conditions for a lobe mixer calculation, it is necessary to specify the velocity and total temperature of the respective hot and cold streams in addition to a mean value of static pressure. The lobe shape is specified, and based on the specified lobe shape, a decision is made as to whether a grid point lies in the hot or cold stream. The appropriate values for velocity, temperature and density are then assigned to the grid point. The total energy is assumed to be constant but may differ in both streams. The velocity in the two respective streams is assigned its nondimensional reference value which is then corrected to account for normal pressure gradients present at the initial plane as determined from the axisymmetric potential flow. To account for boundary layers on the lobe, hub and shroud surfaces, the free stream velocity profiles are further scaled in accordance with an assumed turbulent boundary layer velocity profile, and the distance from the lobe surface.

Referring to Fig. 3, the position of the line representing the lobe shape, S_L, is determined by specifying its r and θ coordinates at a sufficient number of points to describe the lobe shape, thus

$$S_L = S_L(r,\theta) \tag{3.25}$$

where S_L may have an arbitrary shape subject only to the following restrictions (see Fig. 3).

1) S_L must enter the computation region along r_{min} or along θ_{max}.

2) S_L must exit the computation region along θ_{min} or along r_{max}.

3) In the specification of the r, θ coordinates of S_L, r must increase monotonically, i.e., any line of constant radius may intersect S_L only once when moving along S_L in the direction indicated in Fig. 3. No restriction is made on θ. An example of the lobe shapes which may be specified is shown in Fig. 4. The initial velocity profile with boundary layers are given by

$$u = u(u_{STRM}, \delta_{BL}, y/\delta_{BL}, \delta^*, H) \tag{3.26}$$

where U_{STRM} is the velocity of the appropriate stream, δ_{BL} is the boundary layer thickness, y/δ represents the shortest distance from a surface (hub, shroud or lobe) to the grid point in question, δ^* is the local displacement thickness and H is the shape factor. For grid points near the lobe the distance, y/δ, is determined as shown in Fig. 5a by constructing a triangle given two data points on the lobe and the grid point in question. The normal to the base of the triangle (the line segment between the two lobe data points) is constructed and its length determined. If a normal cannot be constructed such that it intersects the line of which the base is a segment between the lobe data points, the distance to the lobe is taken as the distance to the nearest data point as shown in Fig. 5b. For grid points near the hub or shroud the calculation of y/δ is straightforward. Thus having determined y/δ, the velocity at the grid point in question can be scaled to account for the boundary layer. The assumed boundary layer profile used in the present code is a Coles-type profile modified as suggested by Waltz [19].

$$u = u_\tau\left[(-.3y^+ - 5)e^{-3y^+} + \frac{1}{\kappa}\ln(1+y^+) + C + \frac{\Pi}{\kappa}w\left(\frac{y}{\delta}\right)\right] \tag{3.27}$$

Since the turbulence model used is valid only at high Reynolds numbers, the low Reynolds number sublayer flow in the immediate region of walls must be treated in an approximate manner. This is accomplished by using wall functions

which assume that locally between the wall and the first grid point away from the wall the velocity profile is logarithmic such that

$$u = u_\tau\left(\frac{1}{\kappa}\ln\frac{u_\tau y}{\nu} + C\right) \tag{3.28}$$

where u_τ is the friction velocity, $\kappa = 0.43$ is the von Karman constant, and c is taken as 5.0. It follows that

$$\frac{\partial u}{\partial y} = \frac{u_\tau}{\kappa y} \tag{3.29}$$

Equation (3.29) is used to determine a wall slip velocity such that the finite differenced form of the velocity gradient one point off the wall is consistent with the assumed law of the wall profiles. The density is then computed to be consistent with the temperature and the local static pressure as determined from the mean static pressure corrected for the normal pressure gradients.

Initial conditions for the turbulence model are determined through specification of a reference length scale, ℓ_{ref} and free stream turbulence levels. Near the hub and shroud the length scale is determined from the McDonald-Camarata [20] relationship

$$\ell = \ell_{ref}\tanh\left(\frac{\kappa y}{\ell_{ref}}\right) \tag{3.30}$$

where y is the distance from the surface in question. In the region about the lobe surface the distribution of Eq. (3.30) may be used with y representing the distance to the lobe from the grid point in question. However, since the lobe may pass arbitrarily close to a grid point the length scale determined from Eq. (3.30) will approach 0.0 as y approaches 0.0. This results in a low Reynolds number region in the initial flow field which can create problems with the turbulence model. This problem is circumvented through use of an option which renders the length scale constant in the region near the lobe, and the distribution of Eq. (3.30) is used only near the hub or casing if boundary layers are specified there. With the length scale distribution known, the initial turbulent viscosity is obtained from the generalized mixing length relationship

$$\mu_T = \rho\ell^2\left[\left(\frac{1}{h_2}\frac{\partial\bar{u}}{\partial y}\right)^2 + \left(\frac{1}{h_2}\frac{\partial\bar{w}}{\partial y}\right)^2 + \left(\frac{1}{h_3}\frac{\partial\bar{u}}{\partial z}\right)^2 + \left(\frac{1}{h_3}\frac{\partial\bar{v}}{\partial z}\right)^2\right]^{1/2} \tag{3.31}$$

The initial turbulence kinetic energy and dissipation are then determined from simultaneous solution of Eqs. (3.23) and (3.24). The kinetic energy is modified slightly following McDonald and Kreskovsky [21] to account for the free stream turbulence, and the turbulent viscosity is then recomputed from k and ε to be consistent.

Under certain conditions, neither the wall length scale option Eq. (3.30) nor the wake length scale option (constant length scale) will provide satisfactory initial values of k, ε and μ_T. This may occur when the mesh is coarse and the velocity gradients in Eq. (3.31) vary greatly between adjacent grid points. Under these circumstances, it can be useful to initiate the turbulence quantities using an option which specifies the turbulent kinetic energy, dissipation and viscosity as essentially constant throughout the flow field. Such an approach has also been used previously by Launder, Morse, Rodi and Spalding [22] in the computation of free shear flows.

If experimental profiles are read in, the specification of initial conditions is similar. The velocity and static temperature are input at each grid point. The lobe shape is specified as in the automated starting procedure, and a reference length scale and free stream turbulence intensities must be provided. Additionally, estimates of the boundary layer thickness on the hub, shroud and lobe must be specified for use in setting up the initial turbulence quantities. Initialization of the turbulence quantities is similar to that used in the automated procedure.

Boundary Conditions

To march the solution downstream, it is necessary to apply boundary conditions in each transverse plane. Boundary conditions are needed for the energy equation, the primary flow momentum equation, the streamwise vorticity equation, the vector and scalar potential equations, and the turbulence model equations. Referring to Fig. 3, the boundaries at θ_{min} and θ_{max} represent symmetry planes. Boundary conditions on these surfaces are therefore straightforward and are as follows:

1) azimuthal gradients of u_p, E, k and ε are set to zero,
2) the vorticity is set to zero, and
3) the normal velocity component is zero, and thus the vector potential is zero and the azimuthal gradient of the scalar potential is zero.

Boundary conditions on the hub and shroud surface are specified as follows: 1) the normal velocity is zero along these surfaces, and the vector potential and the normal gradient of the scalar potential are thus set to zero, and 2) these surfaces are taken as adiabatic, and thus the normal gradient of energy is set to zero. (Although not included in the present version of the code, thermal wall functions can be developed which would allow specification of the wall temperature. These boundary conditions could be easily implemented.)

Boundary conditions for the primary flow velocity, u_p, and the turbulence quantities k and ε are treated in a manner consistent with the high Reynolds number limitation of the turbulence model. These boundary conditions are based on the same logarithmic profile assumption used in the initial conditions (Eq. (3.28)). The gradient condition of Eq. (3.29) is used to determine a slip value of the primary velocity, u_p. Furthermore, consistency with the log law implies that the turbulence is in local equilibrium and that the shear stress is constant near the wall. From this it may be deduced that

$$k = \frac{u_\tau^2}{C_\mu^{1/2}} \tag{3.32}$$

in the near wall region, and

$$\frac{\partial k}{\partial y} = 0 \tag{3.33}$$

Equation (3.32) is used to specify the value of k one point off a wall with Eq. (3.33) giving the wall value. Additionally, the log law implies that the length scale, ℓ, varies linearly with distance from a wall ($\ell = \kappa y$). Thus initially the turbulent dissipation one point off a wall was specified using Eq. (3.24). However, problems were encountered with this boundary condition which led to negative values of ε. This problem was traced to the linearization of $k^{3/2}$ in Eq. (3.24) and was resolved by combining Eqs. (3.24) and (3.32) to give the linear relationship

$$\epsilon = \frac{u_\tau^3}{\kappa y} \tag{3.34}$$

which performed satisfactorily.

With regard to the boundary conditions for the secondary vorticity, it is observed that the generation of vorticity is most likely to occur in the free

shear layer downstream of the lobe rather than within the hub and shroud boundary layer. Thus the secondary vorticity is assumed zero in the near wall region. It should also be noted that as the flow proceeds past the hub region, provisions are made to change from wall boundary conditions on the hub to symmetry conditions at the centerline.

COMPUTED RESULTS

Several flow calculations were performed to assess the computational procedure and turbulence model. These flows include a simple coaxial turbulent jet, used to validate the turbulence model, and both laminar and turbulent mixer calculations in two different geometries typical of modern designs.

Coaxial Jet Flow

The first flow considered is that of a coaxial jet experimentally investigated by Forstall and Shapiro [23] and used as a test case in the NASA Langley Free Turbulent Shear Flow Conference [24]. This test case was chosen in part since other predictors at this conference were able to obtain good agreement with this data, using the same two-equation turbulence model as is used in the present lobe mixer program. These experimental measurements were obtained with a .25 in. diameter nozzle exhausting into a 4 in. diameter pipe. The velocity ratio of the nozzle stream to the outer stream was 4 to 1. Tabulated values for the initial streamwise velocity profile are given in [24] as are values for the jet spread rate and the centerline velocity decay. Profile data at various downstream locations may be found in [23].

Since the shear layer is very thin in the upstream region near the jet, a very fine mesh would be required to resolve the flow both near the jet and at large distances downstream, where the shear layer thickness increases many fold. For convenience, the flow was computed in two parts with different outer boundaries and grids, upstream and downstream of X/D = 1.0. The first calculation had an outer pipe radius of 16 nozzle radii, utilized 20 radial grid points concentrated near $r/R_N = 1$, and was started at X/D = 1. The initial velocity profile was chosen to agree with the measured profile of Sami, Carmody and Rouse [25] at X/D = 1.0. Turbulence quantities were initialized using a constant length scale across the shear layer in conjunction with Eqs. (3.23), (3.24) and (3.31). The calculation was marched to X/D = 37.

Comparisons of the predicted and measured centerline velocity decay and jet spread rate are presented in Figs. 6 and 7, respectively. The predicted centerline velocity decay is in very good agreement with the measurements, and the predicted spread rate is only slightly above the trend of the data. It should be noted that these calculations did not utilize the modifications to C_2 and c_μ suggested by Launder and Spalding [9] to improve predictions of

the spread rate. Recently, Janicka and Kollmann [26] also observed good agreement between predicted and measured spread rate and velocity decay using the unmodified turbulence model. Figure 8 shows the predicted streamwise velocity profiles (normalized by jet half radius) at various X/D locations and the range of data measured by Forstall. Again the agreement is good despite a slight under resolution of the outer region at X/D = 37, which is evident from the grid point locations in the figure.

The second part of this flow calculation was performed in the upstream region $0 \leq X/D \leq 1.0$, with a computational domain limited to $0.5 \leq r/R_w \leq 1.5$. As shown in Fig. 9, the initial profile was chosen to match the experimental data of Forstall and Shapiro [23 & 24], and includes a small slip velocity at the nozzle edge. The distribution of grid points is shown in Fig. 9 and provides adequate resolution in the region near the nozzle. Turbulence variables were again initialized using a constant length scale. In Fig. 10, the computed velocity profile at X/D = 1.0 is compared with that used as the initial profile in the previous calculation with expanded computational domain. The good agreement between the velocity profiles in Fig. 10 justifies the initial conditions used for the previous solution obtained in the region downstream of X/D = 1.0. The calculations of coaxial jet flow given in this section confirm that the turbulence model being used performs satisfactorily for this relatively simple flow for which adequate experimental documentation is available. Further, the predictions of the lobe mixer deck for this case are in essential agreement with predictions made by other investigators using the same turbulence model [24].

Lobe Mixer Flows

Several calculations of lobe mixer flows were performed to demonstrate the overall method in its present state of development and to explore the potential of the method for making detailed predictions of the flow and mixing process. A summary of the calculations performed is presented in Table I. The test cases include both hot and cold flow calculations in two different geometries, and with different inlet velocity ratios and average Mach number. All calculations were made using 20 equally spaced grid points in the radial coordinate direction and 10 equally spaced points in the azimuthal direction. Twenty to twenty-two axial stations were computed.

Before discussing results from these calculations, it is useful to define average values of total pressure loss coefficient, ideal thrust coefficient, and Mach number at each axial location, to aid in the evaluation of flow properties. A mass-averaged total pressure loss coefficient C_{PT} is defined as

$$C_{PT} = \frac{\int_A \frac{2(P_{T_{ref}} - P_T)}{(\rho u^2)_{ref}} \rho \bar{U} \cdot d\bar{A}}{\int_A \rho \bar{U} \cdot d\bar{A}} \tag{4.1}$$

where $P_{T_{ref}}$ is a reference total pressure associated with the turbine stream reference conditions, and ρ_{ref} and u_{ref} are the reference density and velocity associated with the turbine stream. The value of C_{PT} at the starting plane is usually not zero due to the presence of shear layers in the initial conditions, and for clarity this starting value is subtracted from C_{PT} in the presentation of results. The distributions of C_{PT} presented thus represent losses incurred downstream of the starting plane. An ideal thrust coefficient is defined and based on the thrust which would be obtained by isentropic expansion from local conditions to a predetermined exit pressure. The ratio of the local value of this thrust T to the value T_i based on the initial flow field is defined as the ideal thrust coefficient, T/T_i. The thrust is obtained from the relationship

$$T = \int_{A_e} \gamma P_e M_e^2 dA_e \tag{4.2}$$

where P_e is the assumed exit pressure, $\bar{M}_e$ is the Mach number based on isentropic expansion from the local pressure to P_e, and $\bar{A}_e$ is the effective exit area, again based on isentropic expansion to P_e. Finally, an area-averaged Mach number is defined as

$$\bar{M} = \frac{\int_A M dA}{\int_A dA} \tag{4.3}$$

Results for Geometry A

The first two solutions were obtained for geometry A, which is shown in Fig. 11. The lobe shape specified for this geometry represents a high bypass ratio configuration and is shown in Fig. 12. As indicated in Table I, Case 1

is a laminar flow calculation at a Reynolds number of 1280, based on fan stream properties and the initial mixer diameter. Boundary layers on the hub and shroud were neglected in this calculation, and instead slip conditions were imposed on these boundaries. Case 2 is identical to Case 1 except that the flow is turbulent flow with Reynolds number of 2.9×10^6, and plug, casing and lobe boundary layers are included. In each case, the ratio of fan to turbine temperature is 0.5, and the ratio of fan to turbine velocity is 0.707. These conditions result in matched Mach numbers for the fan and turbine streams. The average inlet Mach number is 0.34 in each instance.

The streamwise distribution of total pressure loss coefficient is shown in Fig. 13 for Cases 1 and 2. The laminar flow has higher loss levels despite its neglect of wall boundary layers, a consequence of the lower Reynolds number. The predicted axial variation of the ideal thrust coefficient is shown in Fig. 14. Here it is observed that the turbulent flow calculation exhibits a significantly higher gain in gross thrust than the laminar calculation. These higher thrust levels presumably reflect both increased mixing and lower losses in the turbulent flow case. It is also noted that the exit Mach number for these two cases was about 0.5 to 0.6, whereas actual full scale mixers would normally be choked at design conditions.

Results for Geometry B

The remaining mixer flow calculations were performed for geometry B, which is shown in Fig. 15. Two lobe shapes were considered, and these are shown in Fig. 16. Each of these lobe shapes provides a mixer with high lobe penetration and a bypass ratio significantly lower than that of geometry A.

The first set of flow calculations considered here consists of Cases 3 and 4, which correspond to lobe shape B-1 in Fig. 16. These two cases represent both hot and cold flow conditions for which the inlet Mach numbers (and total pressures) of the fan and turbine streams are matched. In each case, the average initial Mach number is 0.194 and was estimated to give nearly choked flow at the nozzle exit. The fan stream Reynolds number is 2.6×10^6 in each case, and boundary layers on the plug, casing and lobe were included in all of the turbulent flow calculations. Test Case 3 is typical of flight cruise conditions and has a fan to turbine temperature ratio of 0.4 and velocity ratio of 0.7. In Case 4, the fan stream conditions were identical

to those of Case 3, but the turbine stream temperature was reduced to match that of the fan stream, and in addition the velocity of the turbine stream was adjusted to produce the same Mach number and total pressure ratio as Case 3. Taken as a set, Cases 3 and 4 simulate a common experimental procedure for testing lobe mixer designs whereby both hot and cold flow measurements are taken with the same conditions for stagnation pressure. Since the cold flow measurements provide an indication of losses associated with plug, casing, and lobe boundary layers, the differences between hot and cold flow measurements provide an indication of thrust gains and total pressure losses due to the mixing process itself. The set of test Cases 3 and 4 thus demonstrate one potential use of the present calculation procedure for aiding in the design and evaluation of lobe mixers.

Comparisons of the computed axial development of total pressure losses, Mach number, and thrust are given in Figs. 17-19, respectively, for Cases 3 and 4. The total pressure losses for the hot flow case are somewhat higher than those of the cold flow case, although the distributions are similar. The predicted loss levels within the mixing duct are of the order of one dynamic head at fan stream inlet conditions. The higher loss levels present in the hot flow case are presumably a result of higher losses in the mixing layer between the hot and cold streams, since the difference in velocity between the two streams is much higher in the hot flow case. The axial variation in Mach number is shown in Fig. 18. Although the initial development of Mach number is very nearly the same for the two cases, as a result of higher losses the hot flow case undergoes stronger acceleration near the exit and attains an exit Mach number of 0.91, as compared with 0.8 for the cold flow case. The rapid acceleration downstream of $X/L_r = 1.6$ occurs primarily because of the change in area of the geometry but is due in part to frictional losses. On the other hand, since loss levels increase with Mach number, the total pressure losses in Fig. 17 are seen to increase rapidly downstream of $X/L_r = 1.6$.

The final flow parameter of interest here is the thrust coefficient, which is shown in Fig. 19. As is to be expected, the thrust coefficient for the cold flow case undergoes a monotonic decrease, as viscous losses accumulate. In the hot flow case, the effects of thermal mixing provide a significant increase in thrust over most of the mixing duct. Beginning at about $X/L_r = 2.0$,

the high loss levels associated with the nozzle-induced acceleration outweigh any further thrust augmentation due to mixing, and the thrust coefficient decreases from this point onward. At the nozzle exit, the thrust coefficient is about 1.0, which indicates that the mixing gain has offset the decrease in thrust attributable to viscous losses. In turn, the thrust coefficient at the nozzle exit is 0.98 for the cold flow case, and thus the net gain in thrust due to mixing is about 2 percent.

The final set of flow calculations considered here consists of Cases 5 and 6, which correspond to lobe shape B-2 in Fig. 16. These cases represent cold flow conditions with equal fan and turbine static temperatures, but with different average inlet Mach numbers and Reynolds numbers. The ratio of fan to turbine inlet Mach number and velocity is 0.5 in each case. These flow conditions attain a large velocity difference between the fan and turbine streams as a result of mismatched total pressures and Mach numbers. Similar flow conditions are present in a related experimental study of flows in this same mixer geometry, being performed as part of this overall contract effort. These cases also serve to test the present calculation procedure under conditions of significant mismatch in fan and turbine total pressures and Mach numbers. The axial variation of Mach number and total pressure loss coefficient for Cases 5 and 6 are shown in Figs. 20 and 21. The total pressure losses in Fig. 21 are seen to be higher for the flow with higher initial Mach number, as is to be expected. These cases serve to demonstrate the capability of the present calculation procedure for treating flows with mismatched Mach number and total pressure.

SUMMARY AND CONCLUSIONS

A finite-difference method has been developed for detailed computation of three-dimensional subsonic turbulent flows in turbofan lobe mixers. The method is based on a decomposition of the velocity field into primary and secondary flow components which are determined by solution of equations governing primary momentum, secondary vorticity, thermal energy, and continuity. A two-equation turbulence model for turbulent kinetic energy and dissipation rate is used to construct the required Reynolds shear stress correlation coefficients. The governing equations are solved by a forward-marching solution procedure which corrects an a priori inviscid potential flow solution for viscous and thermal effects, secondary flows, total pressure distortion and losses, internal flow blockage and pressure drop.

Test calculations for a turbulent coaxial jet flow were performed to verify that the turbulence model would perform satisfactorily for this relatively simple flow for which adequate experimental measurements are available. Several calculations for lobe mixer flows were performed for two geometries typical of current mixer design. These calculations included both hot and cold flow conditions, and both matched and mismatched Mach number and total pressure in the fan and turbine streams. The axial development of cross-sectional averages of Mach number, total pressure losses, and thrust were presented for these mixer flows, and these predictions are consistent with the behavior expected for this type of mixer flow. The results of this study serve to demonstrate the potential value of the present calculation procedure to aid in the design and evaluation of turbofan lobe mixers. Further evaluation of the procedure will require careful comparison with sufficiently detailed and accurate experimental measurements.

References

1. Briley, W. R. and H. McDonald: Analysis and Computation of Viscous Subsonic Primary and Secondary Flows. AIAA Paper No. 79-1453, July, 1979.

2. Briley, W. R. and H. McDonald: An Approximate Analysis for Three-Dimensional Viscous Subsonic Flows with Large Secondary Velocities. SRA Report R78-300001-4, March, 1978.

3. Shamroth, S. J. and W. R. Briley: A Viscous Flow Analysis of the Tip Vortex Generation Process. AIAA Paper No. 79-1546, 1979.

4. Briley, W. R.: Numerical Method for Predicting Three-dimensional Steady Viscous Flow in Ducts. J. Comp. Phys., Vol. 14, 1974, p. 8.

5. Patankar, S. V. and D. B. Spalding: A Calculation Procedure for Heat, Mass, and Momentum Transfer in Three-dimensional Parabolic Flows. Int. J. Heat and Mass Transfer, Vol. 15, 1972, p. 1787.

6. Hawthorne, W. R.: The Applicability of Secondary Flow Analyses to the Solution of Internal Flow Problems. Fluid Mechanics of Internal Flow, ed. G. Sovran, (Elsevier), 1967, p. 263.

7. Kreskovsky, J. P. and S. J. Shamroth: An Implicit Marching Method for the Two-Dimensional Reduced Navier-Stokes Equations at Arbitrary Mach Number. Computer Methods in Applied Mechanics and Engineering, Vol. 13, 1978, pp. 307-334.

8. McDonald, H. and W. R. Briley: Three-Dimensional Supersonic Flow of a Viscous or Inviscid Gas. J. Comp. Phys., Vol. 19, 1975, pp. 150-178.

9. Lakshminarayana, B. and J. H. Horlock: Generalized Expressions for Secondary Vorticity Using Intrinsic Coordinates. J. Fluid Mech., Vol. 59, 1973, p. 97.

10. Shapiro, A. H.: The Dynamics and Thermodynamics of Compressible Fluid Flow, Vol. I. Ronald Press, New York, 1955.

11. Launder, B. E. and D. B. Spalding: The Numerical Computation of Turbulent Flows. Computer Methods in Applied Mechanics and Engineering, Vol. 3, 1974, p. 269.

12. McDonald, H. and W. R. Briley: Computational Aspects of Internal Flows. AIAA Paper No. 79-1445, 1979.

13. Anderson, O. L.: User's Manual for a Finite-Difference Calculation of Turbulent Swirling Compressible Flow in Axisymmetric Ducts with Struts and Slot Cooled Walls. USAAMRDL-TR-74-50, Vol. I, 1974.

14. Patankar, S. V., V. S. Pratap and D. B. Spalding: Prediction of Turbulent Flow in Curved Pipes. J. Fluid Mech., Vol. 67, 1975, pp. 583-595.

15. Roberts, G. O.: Computational Meshes for Boundary Layer Problems. Proceedings of the Second International Conference on Numerical Methods in Fluid Dynamics. Springer-Verlag, New York, 1971, p. 171.

16. Douglas, J. and J. E. Gunn: A General Formulation of Alternating Direction Methods, Part I. Parabolic and Hyperbolic Problems. Numerische Mathematik, Vol. 6, 1964, p. 428.

17. Briley, W. R. and H. McDonald: Solution of the Multidimensional Compressible Navier-Stokes Equations by a Generalized Implicit Method. J. Comp. Phys., Vol. 24, 1977, p. 372.

18. Ralston, A.: A First Course in Numerical Analysis. (McGraw-Hill), 1965, p. 323.

19. Waltz, A.: Boundary Layers of Flow and Temperature. MIT Press, 1969, p. 115.

20. McDonald, H. and F. J. Camarata: An Extended Mixing Length Approach for Computing the Turbulent Boundary-Layer Development. In Proceedings, Stanford Conference on Computation of Turbulent Boundary Layers, Vol. I, published by Stanford University, 1969, pp. 83-98.

21. McDonald, H. and J. P. Kreskovsky: Effect of Free-Stream Turbulence on the Turbulent Boundary Layer. International Journal of Heat and Mass Transfer, Vol. 17, No. 7, 1974, p. 705.

22. Launder, B. E., A. Morse, W. Rodi and D. B. Spalding: Prediction of Free Shear Flows - A Comparison of the Performance of Six Turbulence Models. NASA SP-321, Vol. I, 1972, pp. 361-426.

23. Forstall, W. Jr., and A. H. Shapiro: Momentum and Mass Transfer in Coaxial Gas Jets. ASME J. Applied Mechanics, Vol. 17, 1950, pp. 399-408.

24. Free Turbulent Shear Flows, Volume II - Summary of Data, NASA SP-321, Vol. II, 1972, p. 36.

25. Sami, S., T. Carmody and H. Rouse: Jet Diffusion in the Region of Flow Establishment. J. Fluid Mech., Vol. 27, 1967, pp. 231-252.

26. Janicka, J. and W. Kollmann: Prediction Model for the PDF of Turbulent Temperature Fluctuations in a Heated Round Jet. Second Symposium on Turbulent Shear Flows, Imperial College, London, 1979, pp. 1.7-1.11.

TABLE I

SUMMARY OF LOBE MIXER CALCULATIONS

CASE #	GEOMETRY	T_F/T_T	u_F/U_T	M_F/M_T	AVERAGE INLET M	FAN STREAM Re	LAMINAR OR TURBULENT
1	A	0.5	0.707	1.0	0.34	1280	L
2	A	0.5	0.707	1.0	0.34	2.9×10^6	T
3	B	0.4	0.7	1.107	0.194	2.6×10^6	T
4	B	1	1.107	1.107	0.194	2.6×10^6	T
5	B	1	0.5	0.5	0.0529	4.75×10^5	T
6	B	1	0.5	0.5	0.171	1.54×10^6	T

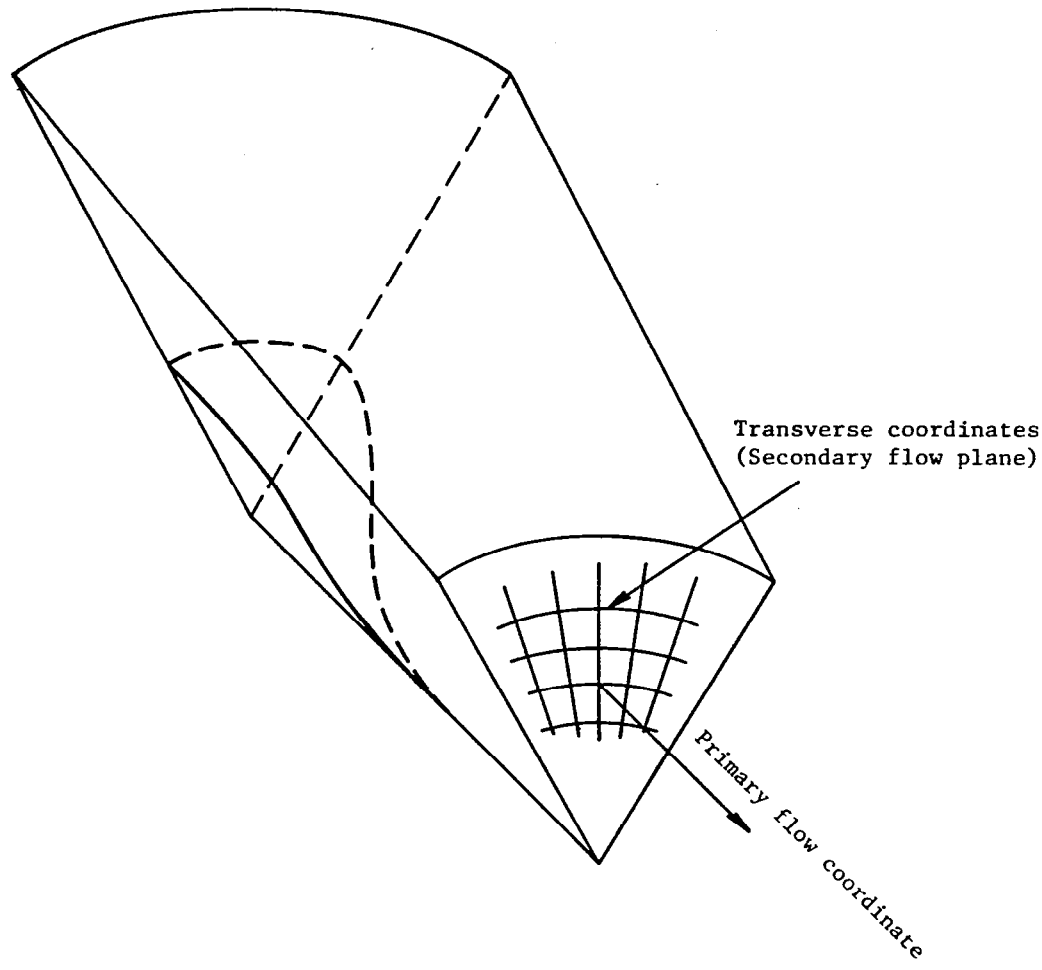

Figure 1. - Schematic of coordinate system for three-dimensional flow problem.

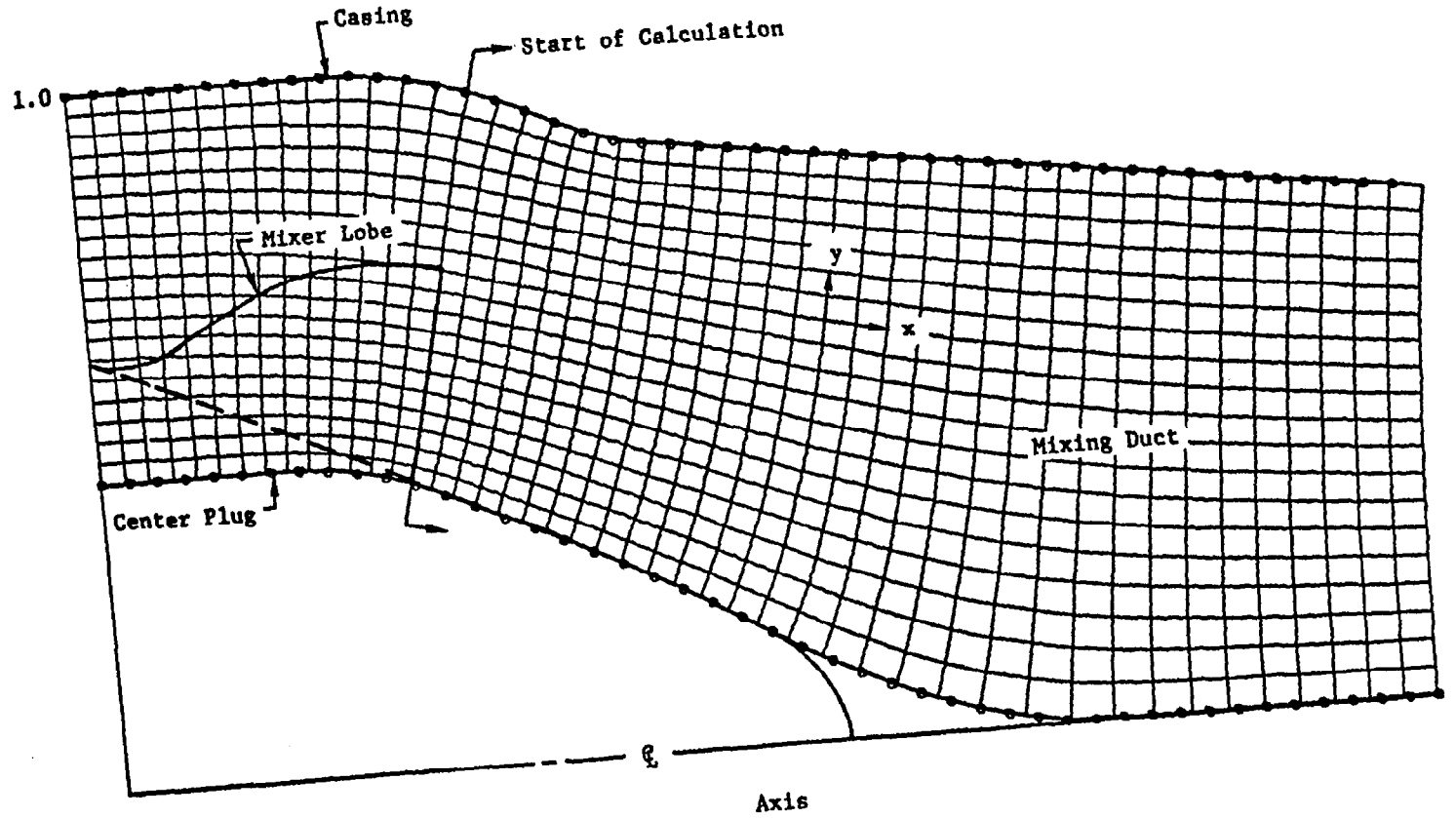

Figure 2. - Typical lobe mixer geometry and potential flow coordinate system.

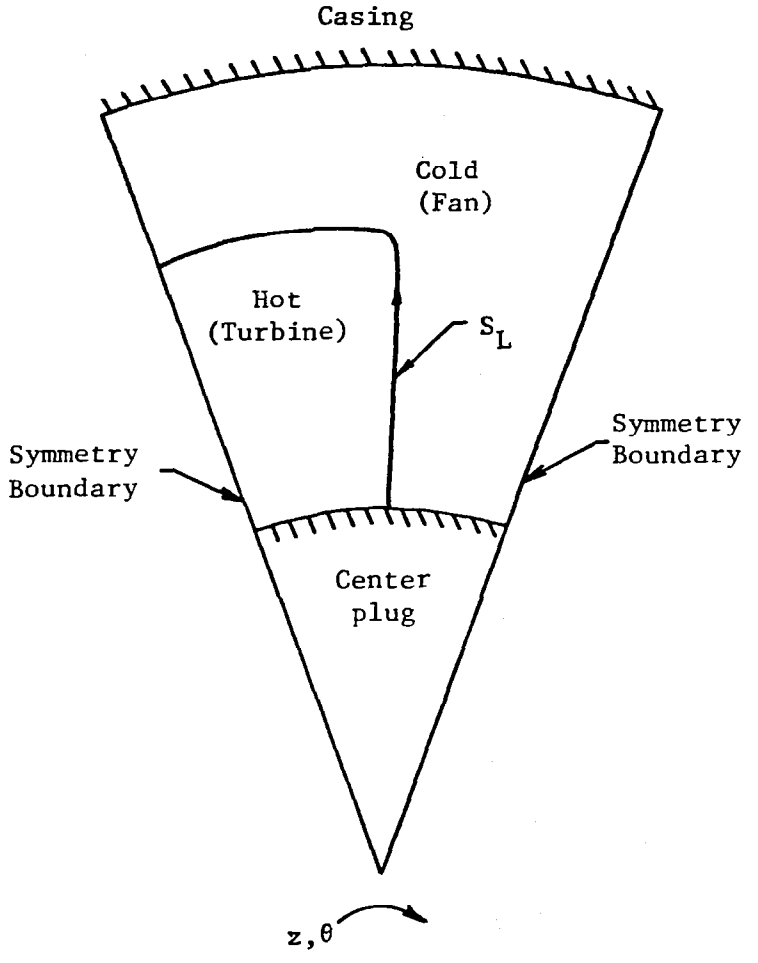

Figure 3. - Typical cross section at mixer exit surface.

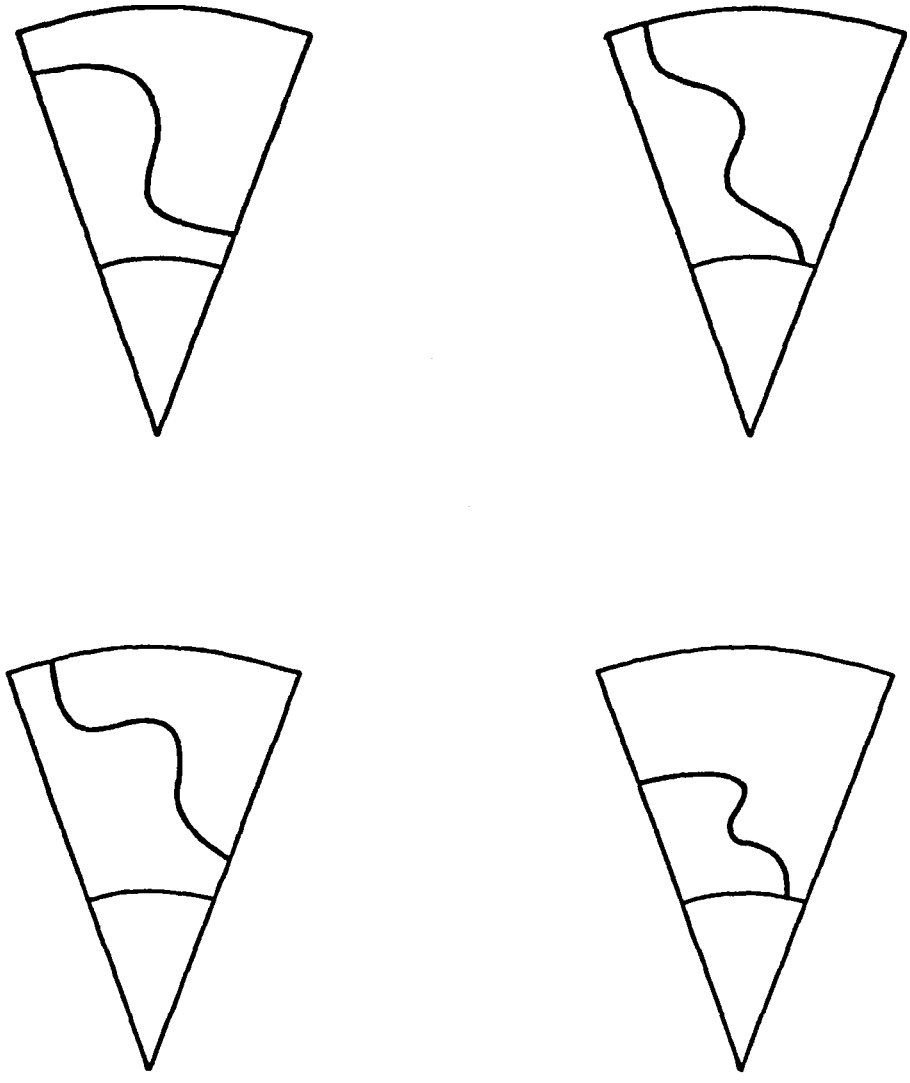

Figure 4. - Family of lobe contours which may be specified.

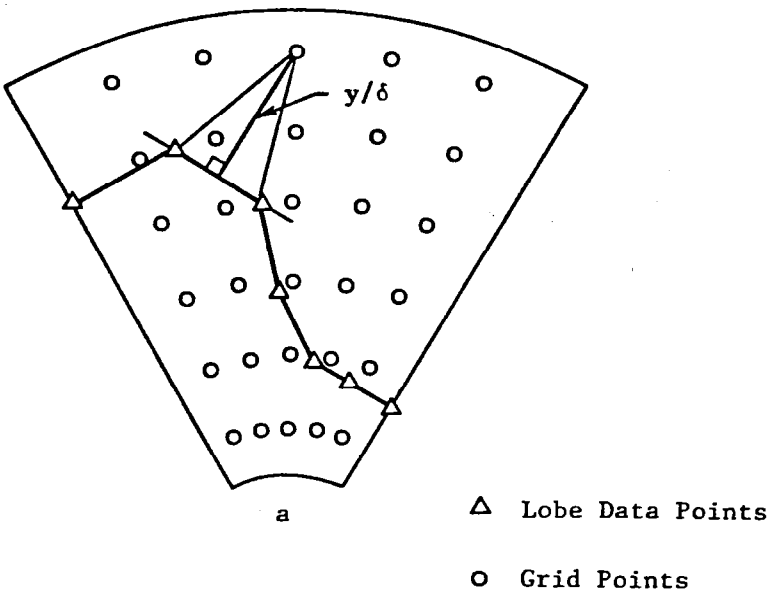

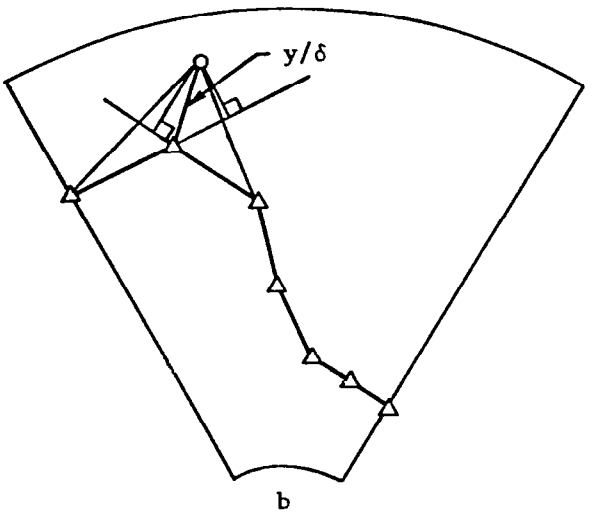

Figure 5. - Determination of distance to lobe boundary.

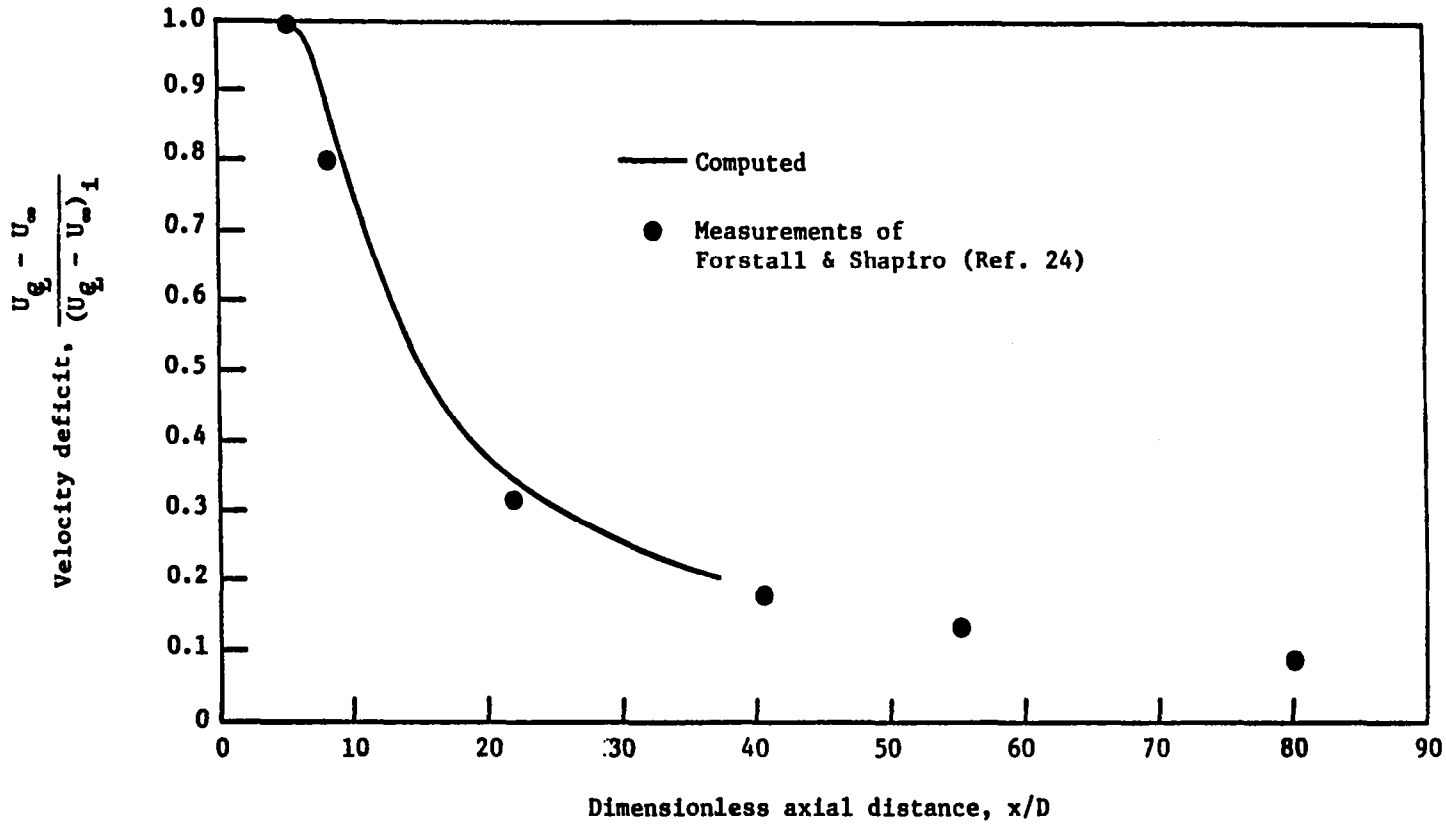

Figure 6. - Comparison of predicted and measured centerline velocity decay.

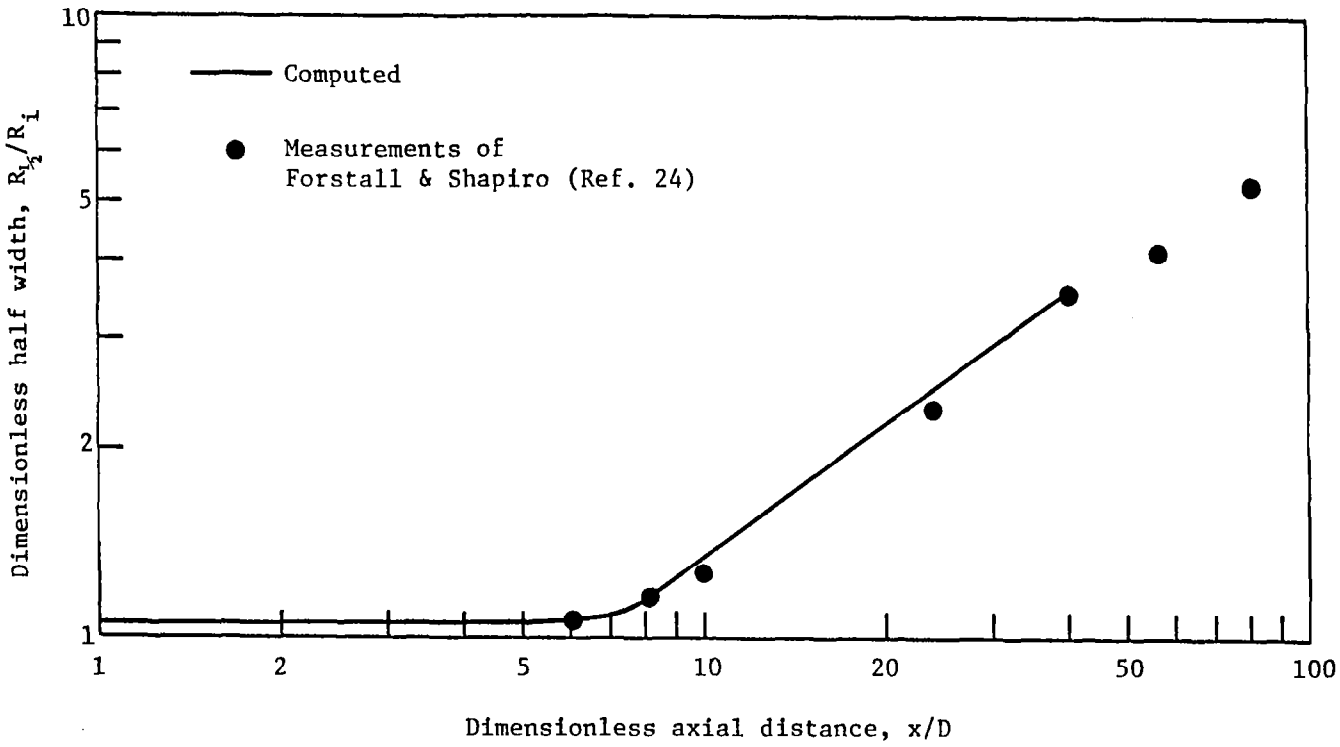

Figure 7. - Comparison of predicted and measured spread rate.

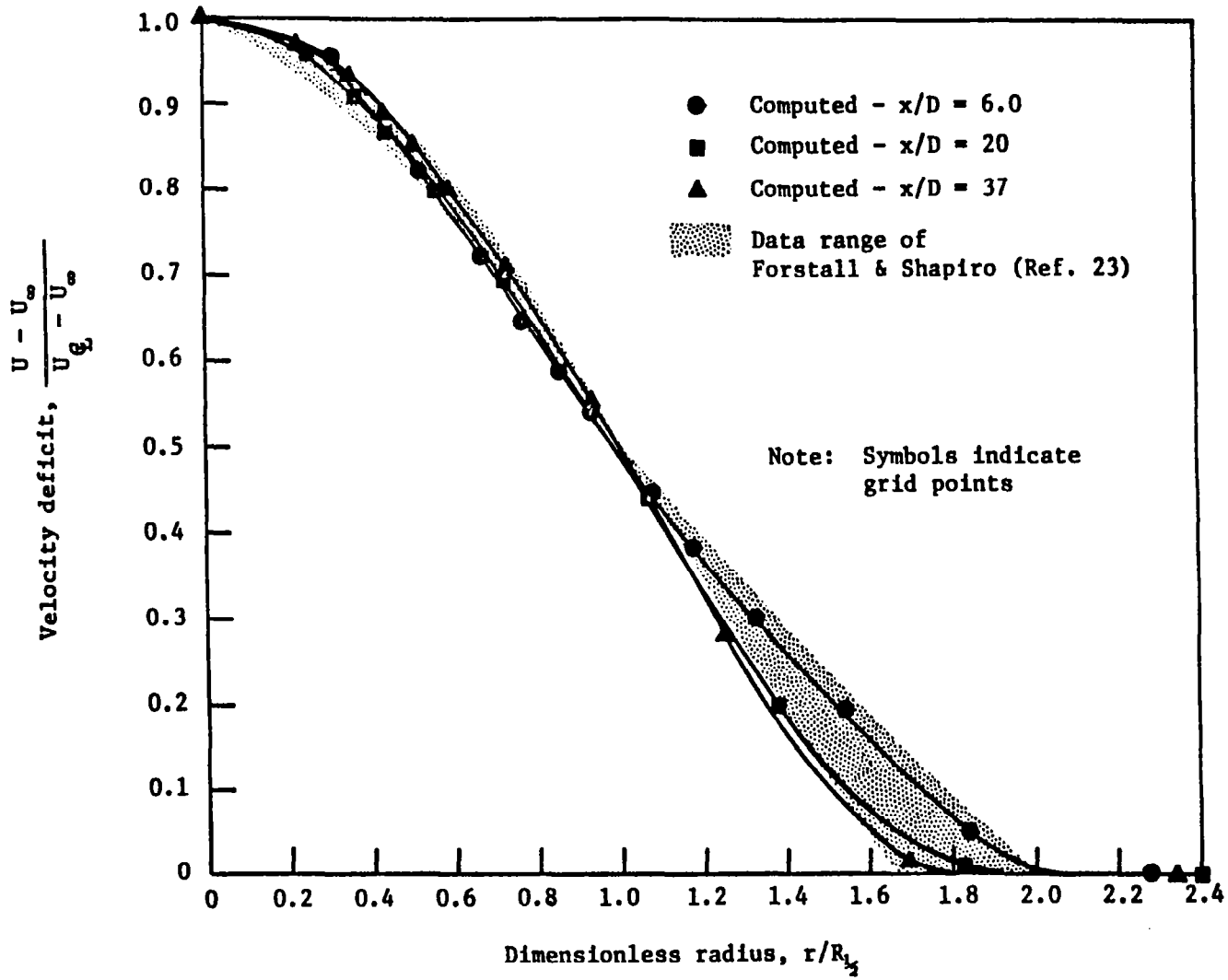

Figure 8. - Comparison of predicted and experimental velocity profiles.

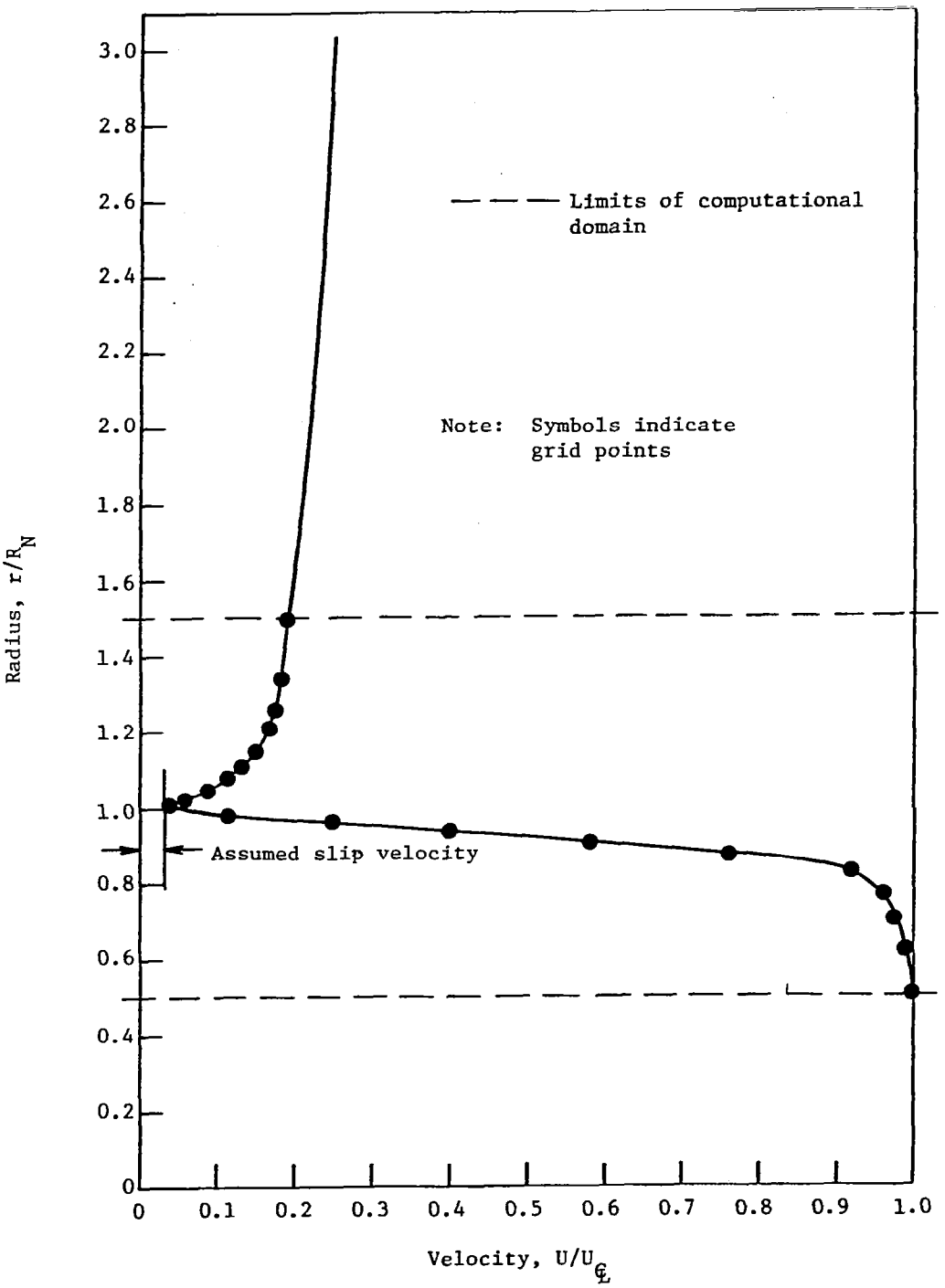

Figure 9. - Initial velocity profile used for starting refined mesh calculation.

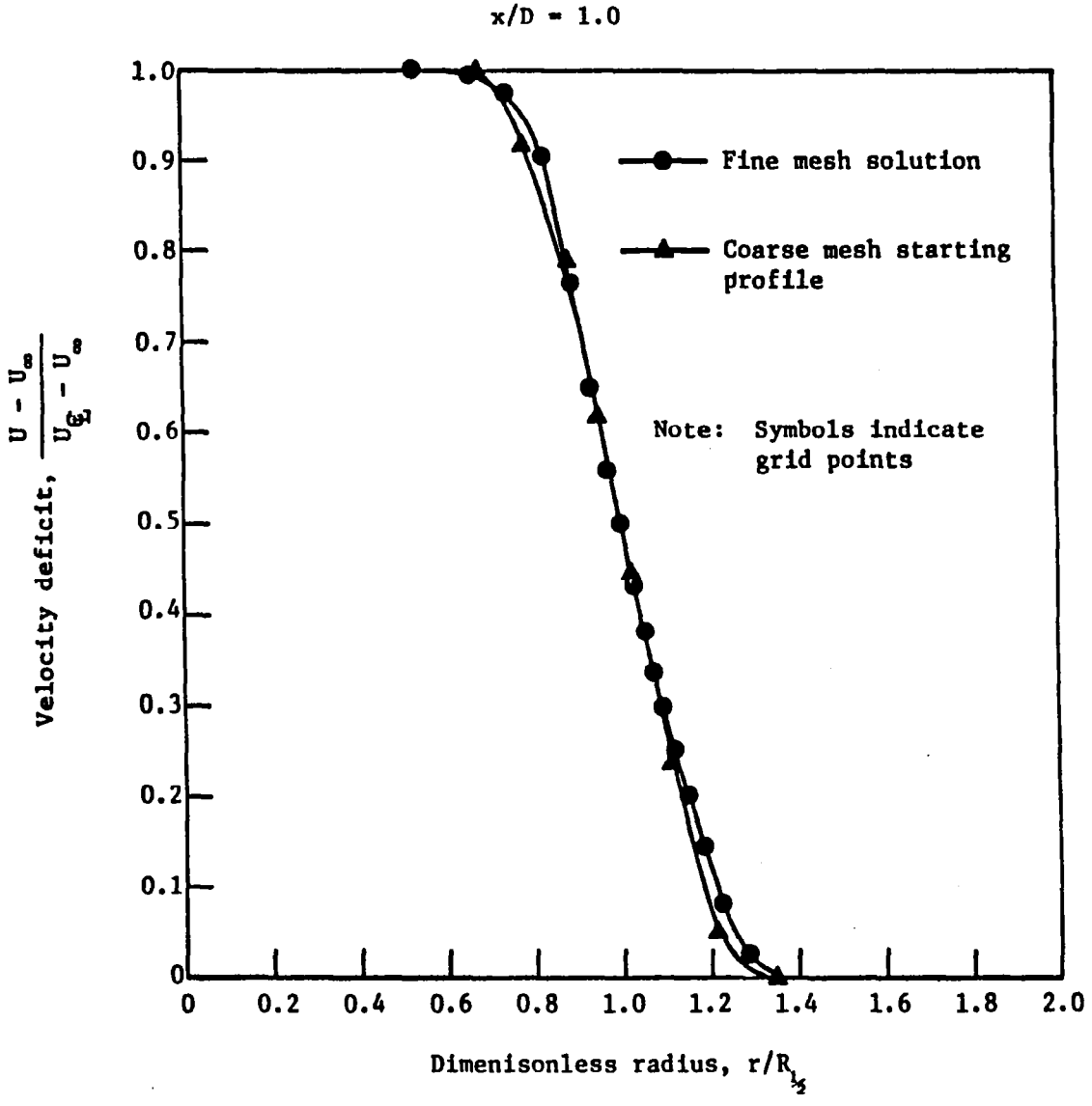

Figure 10. - Comparison of computed fine mesh velocity profile with assumed coarse mesh starting profile.

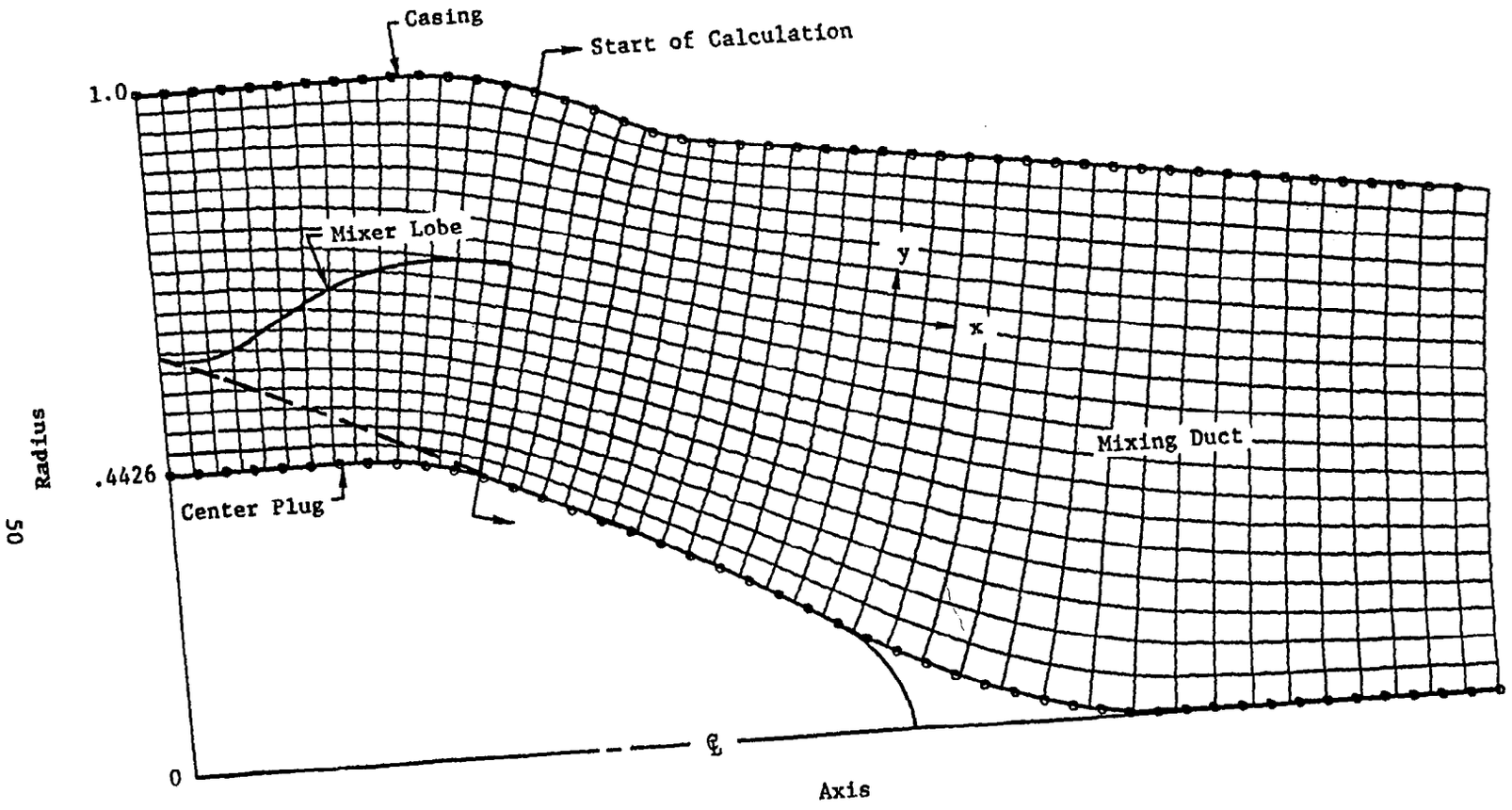

Figure 11. - Computed coordinate system for mixer Geometry A.

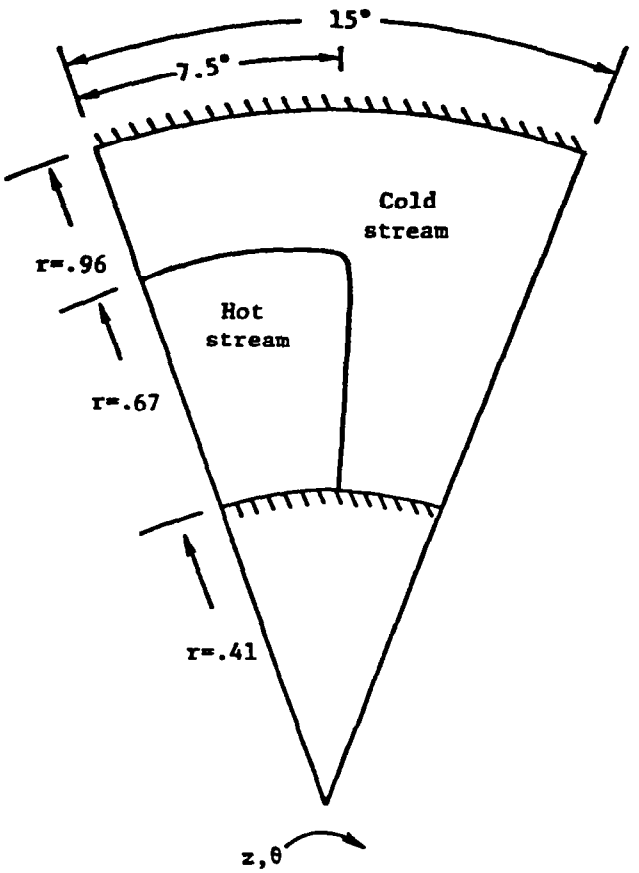

(not to scale)

Figure 12. - Lobe shape at mixer exit surface for Geometry A.

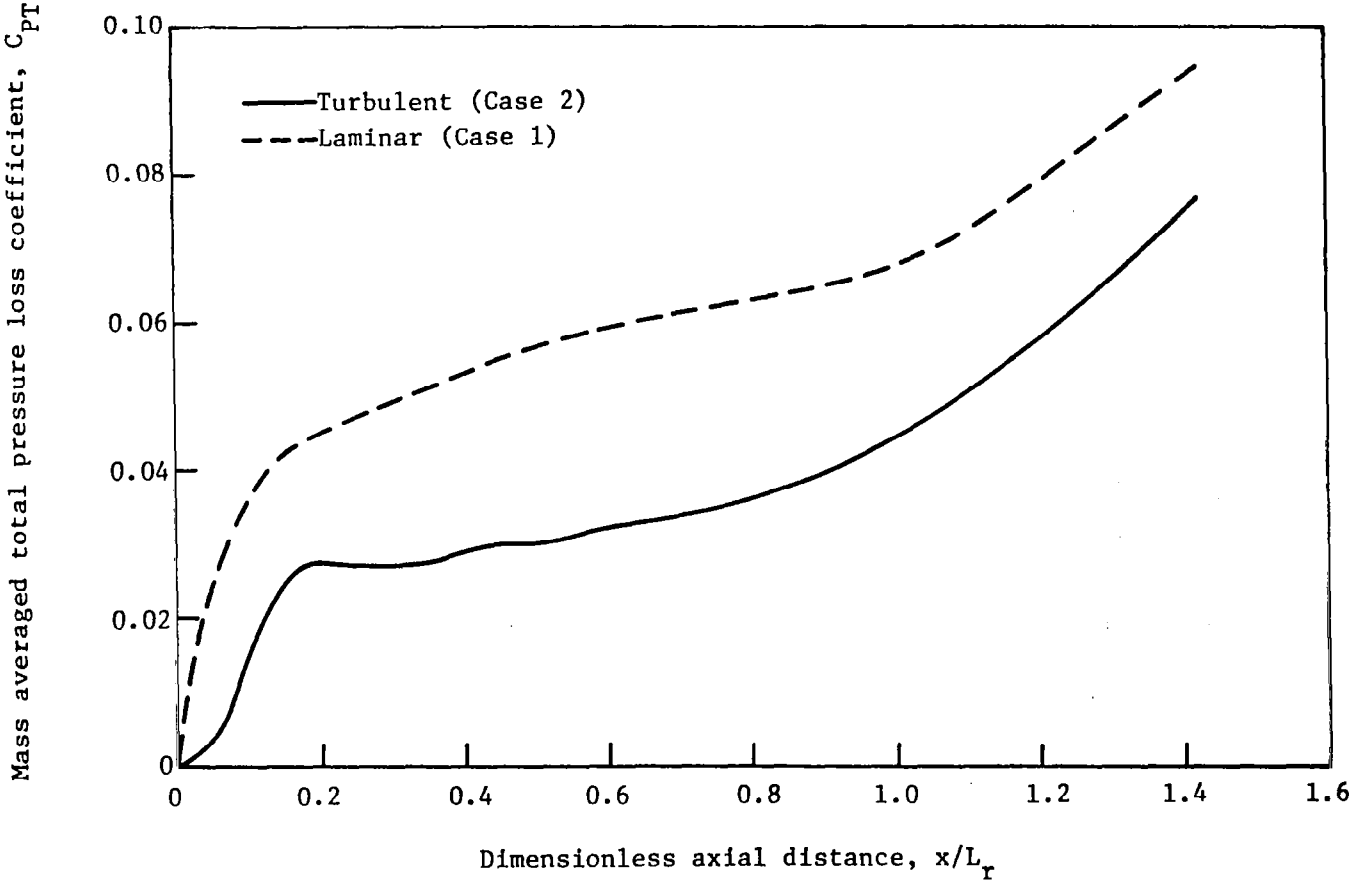

Figure 13. - Comparison of laminar and turbulent losses in mixer Geometry A.

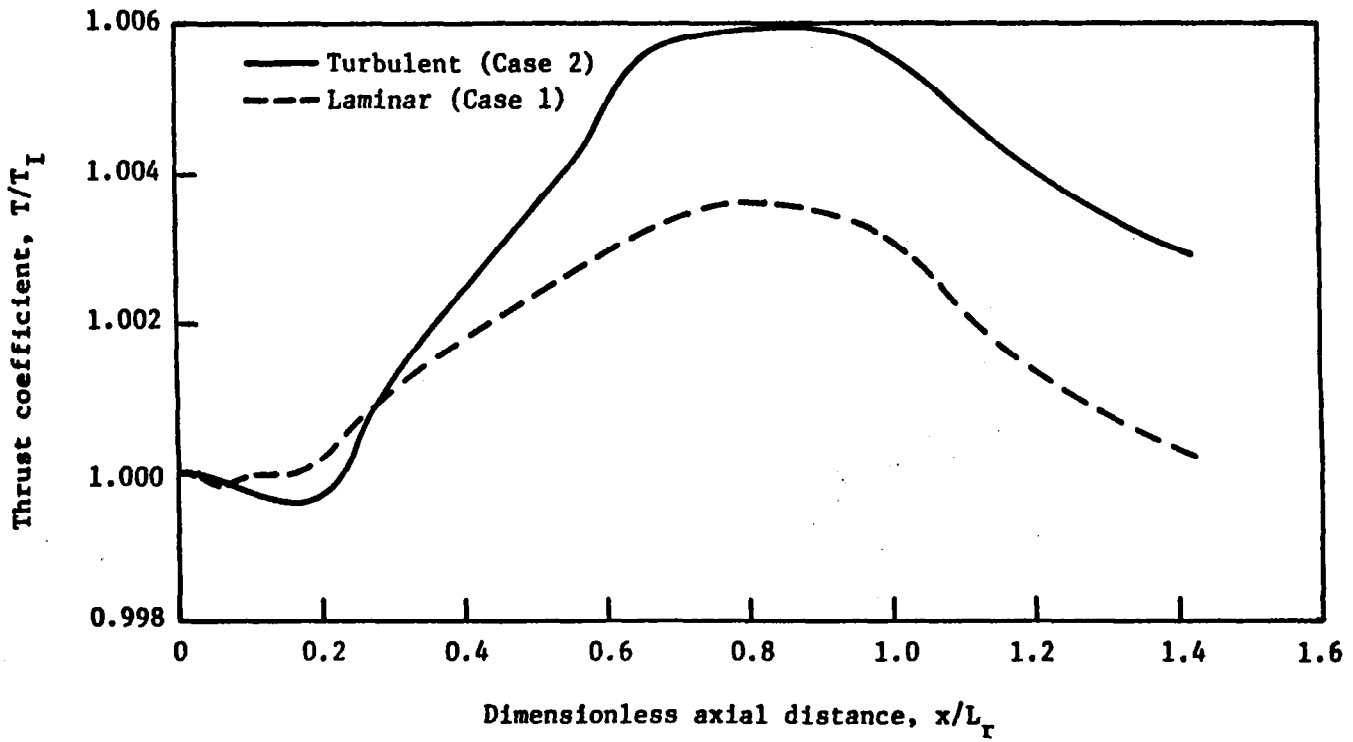

Figure 14. - Comparison of ideal thrust coefficient for laminar and turbulent flow in Geometry A.

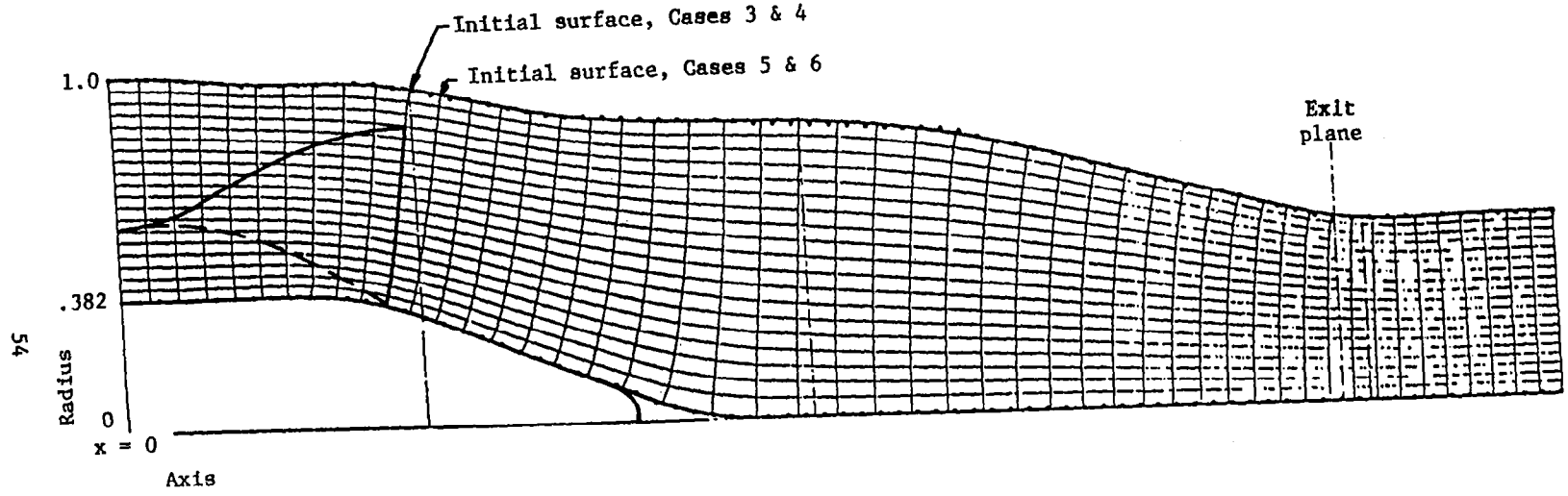

Figure 15. - Computed coordinate system for mixer Geometry B.

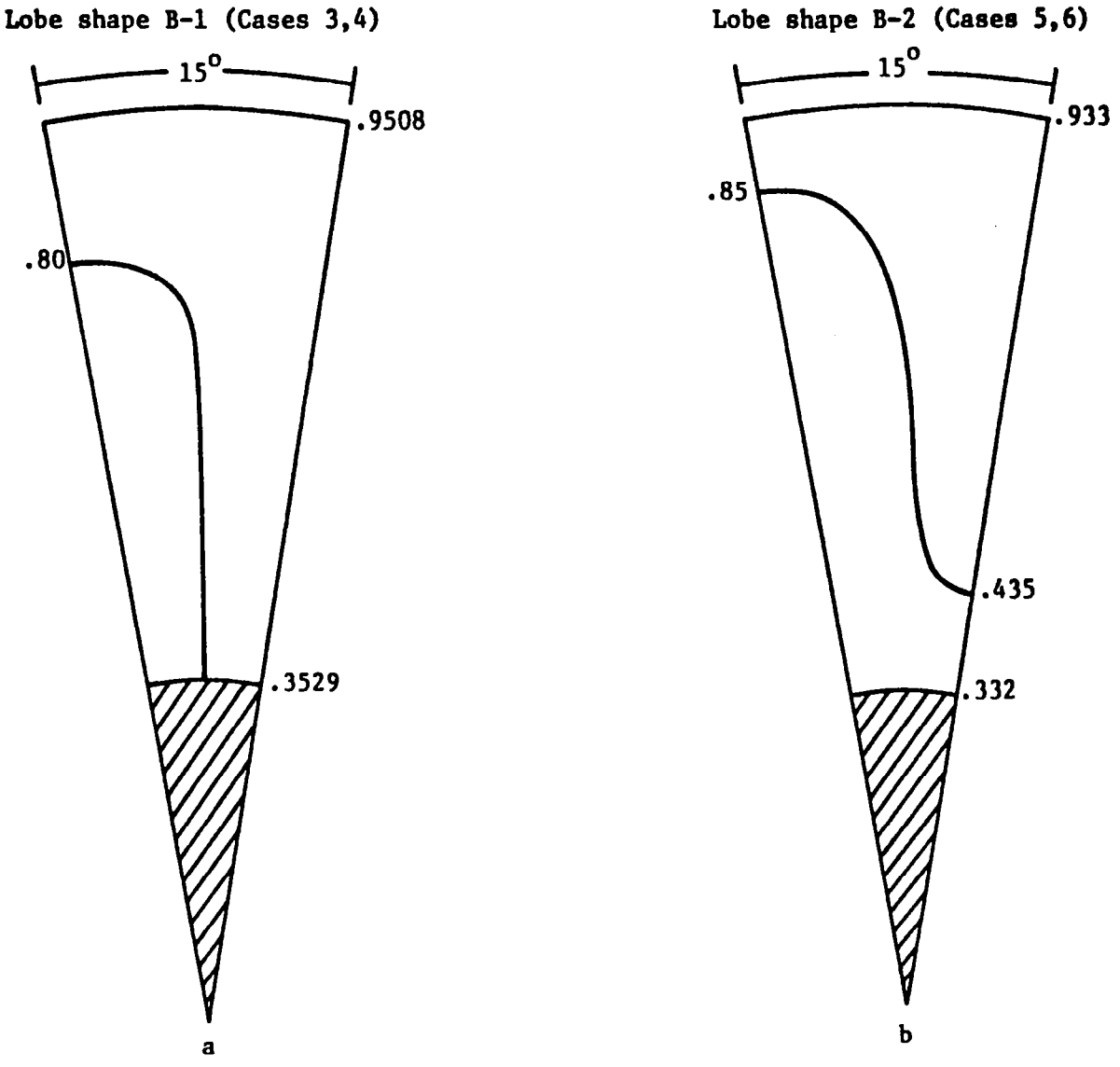

Figure 16. - Lobe shapes for Geometry B.

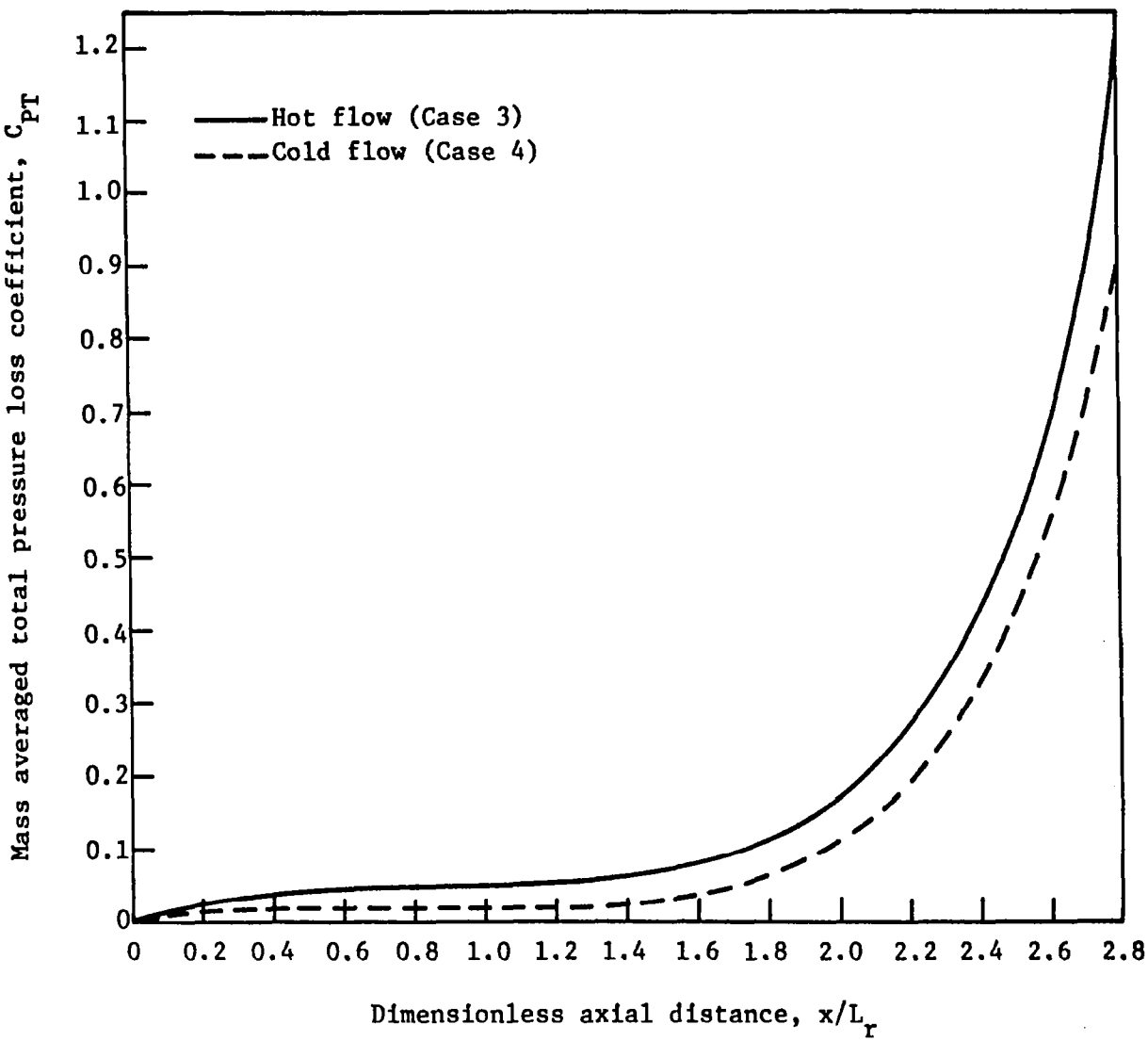

Figure 17. - Comparison of losses for hot and cold flow in mixer Geometry B.

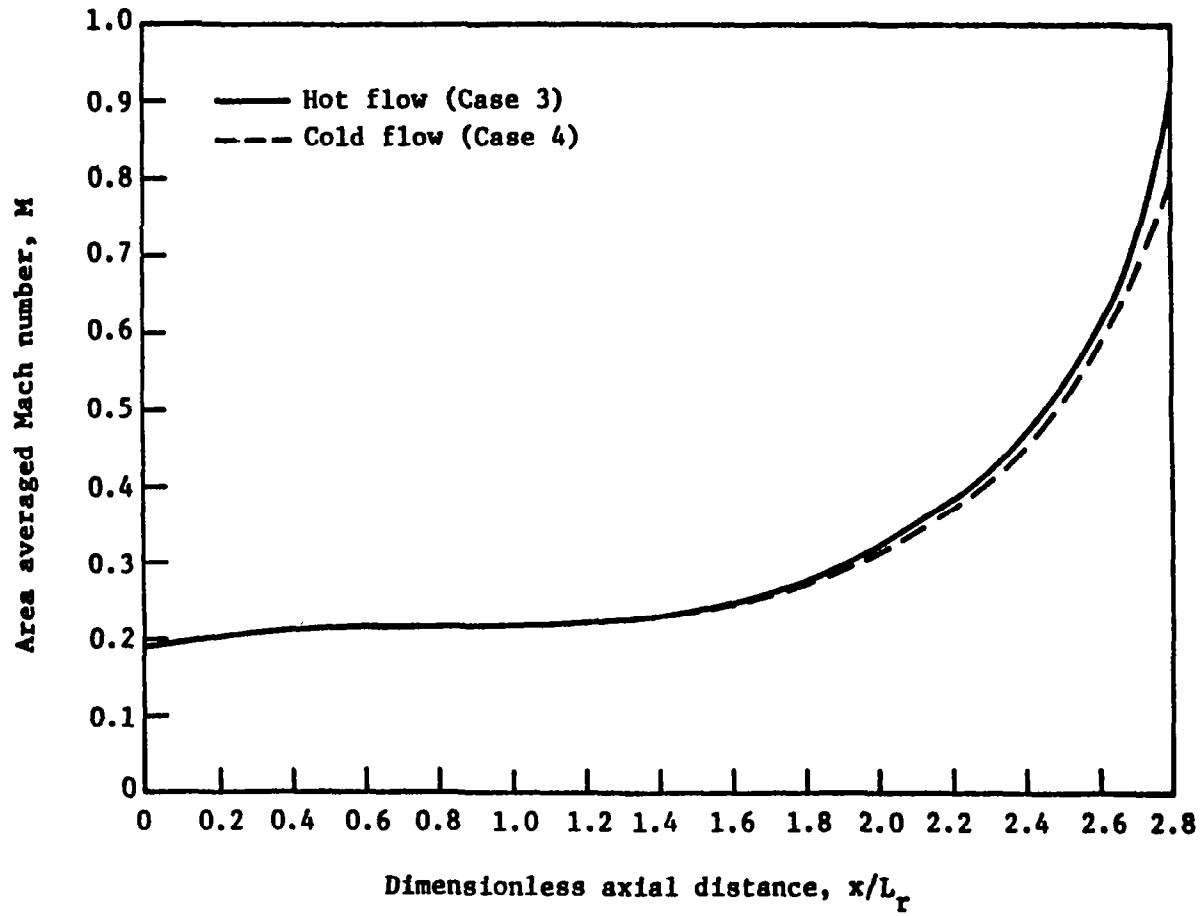

Figure 18. - Comparison of axial Mach number distributions for hot and cold flow in mixer Geometry B.

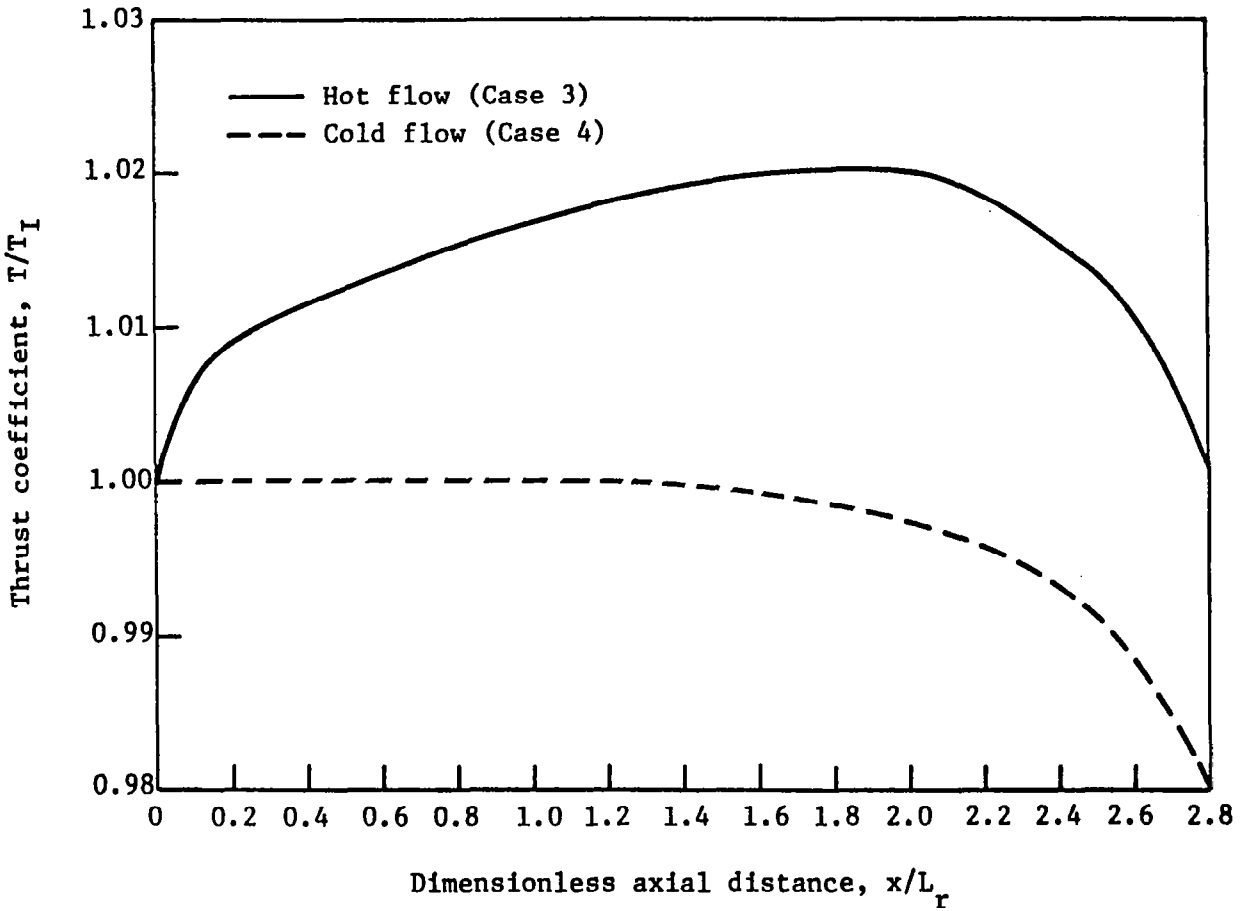

Figure 19. - Comparison of axial thrust development for hot and cold flow in mixer Geometry B.

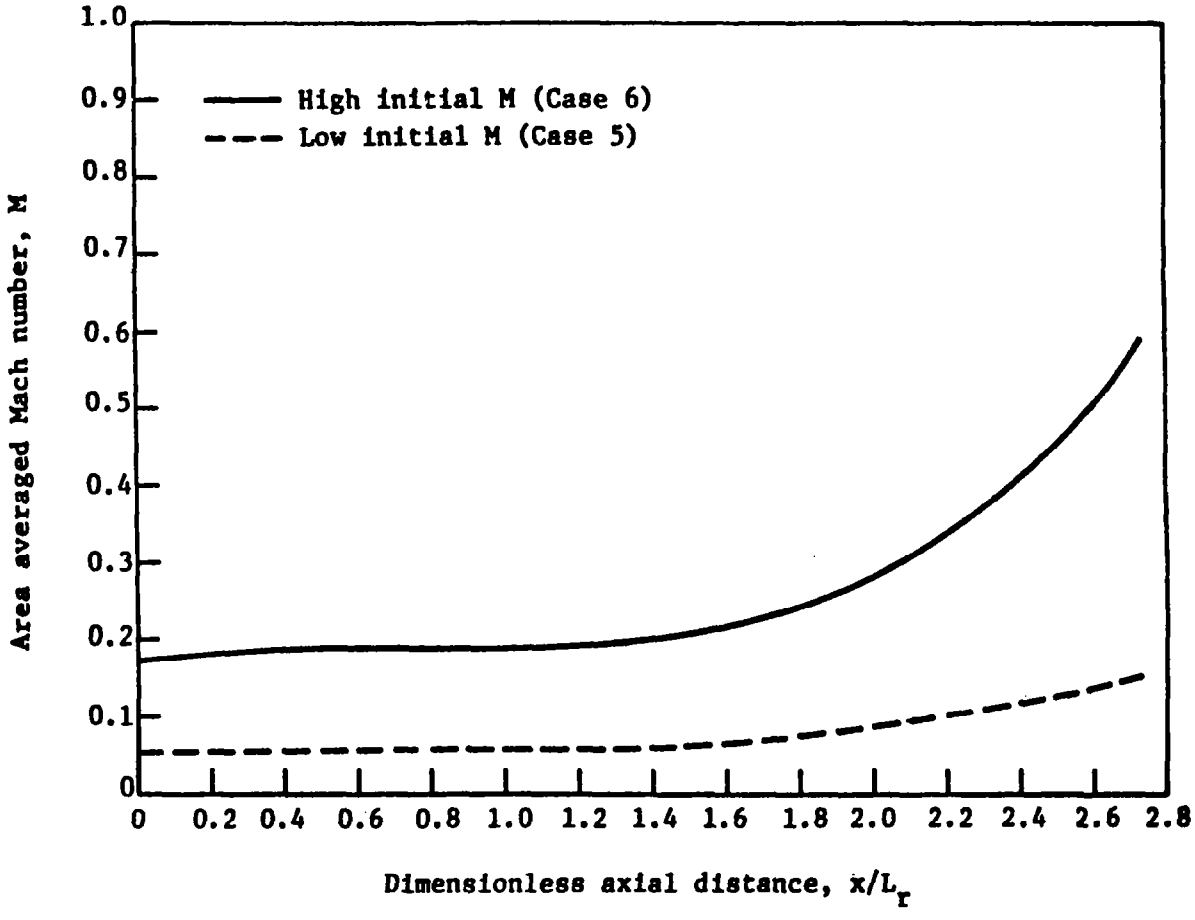

Figure 20. - Comparison of average Mach number variations for flows with mismatched initial Mach numbers.

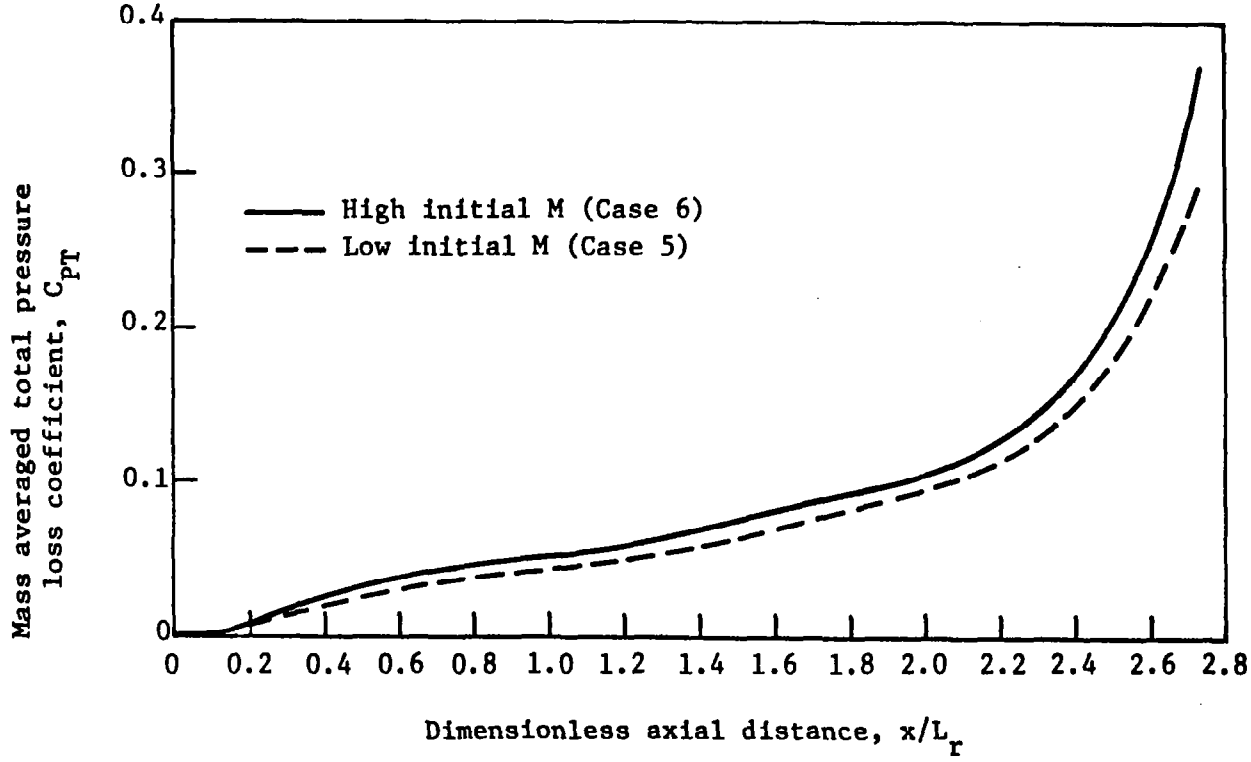

Figure 21. - Comparison of losses for flows with mismatched initial Mach numbers and different average initial Mach number.

APPENDIX-A

THE TURBULENT PRODUCTION TERM

The production term, P, in the turbulence kinetic energy and dissipation equations may be expressed as

$$P = \mu_T \left[2(e_{11}^2 + e_{22}^2 + e_{33}^2) + e_{31}^2 + e_{12}^2 + e_{23}^2 \right] \tag{A.1}$$

where

$$e_{11} = \frac{1}{h_1}\frac{\partial u}{\partial x} + \frac{v}{h_1 h_2}\frac{\partial h_1}{\partial y} + \frac{w}{h_1 h_3}\frac{\partial h_1}{\partial z} \tag{A.2}$$

$$e_{22} = \frac{1}{h_2}\frac{\partial v}{\partial y} + \frac{w}{h_2 h_3}\frac{\partial h_2}{\partial z} + \frac{u}{h_1 h_2}\frac{\partial h_2}{\partial x} \tag{A.3}$$

$$e_{33} = \frac{1}{h_3}\frac{\partial w}{\partial z} + \frac{u}{h_1 h_3}\frac{\partial h_3}{\partial x} + \frac{v}{h_2 h_3}\frac{\partial h_3}{\partial y} \tag{A.4}$$

$$e_{23} = \frac{h_3}{h_2}\frac{\partial}{\partial y}\left(\frac{w}{h_3}\right) + \frac{h_2}{h_3}\frac{\partial}{\partial z}\left(\frac{v}{h_2}\right) \tag{A.5}$$

$$e_{31} = \frac{h_1}{h_3}\frac{\partial}{\partial z}\left(\frac{u}{h_1}\right) + \frac{h_3}{h_1}\frac{\partial}{\partial x}\left(\frac{w}{h_3}\right) \tag{A.6}$$

$$e_{12} = \frac{h_1}{h_2}\frac{\partial}{\partial y}\left(\frac{u}{h_1}\right) + \frac{h_2}{h_1}\frac{\partial}{\partial x}\left(\frac{v}{h_2}\right) \tag{A.7}$$

The production term may be simplified considerably if it is first noted that in the present geometry the metric coefficients are not functions of z (the azimuthal coordinate). Furthermore, it may be assumed that the shear layers are thin, since the Reynolds number is high. Thus, if the flow is sheared in the y direction, v and $\partial/\partial y$ are assumed to be of order δ and

$1/\delta$, respectively. If the flow is sheared in the z direction, w and $\partial/\partial z$ are assumed of order δ and $1/\delta$. The quantity δ is taken to be representative of the shear layer thickness. Similarly, u, x and the metric coefficients are presumed to be of the order of unity. If the viscosity, μ_T, is assumed to be of the order δ^2 the relevant terms in P may be found by retaining only those terms which are of the order of unity in either of the two types of shear layer described above. As a result P is approximated as

$$P = \mu_T\left[\left(\frac{1}{h_2}\frac{\partial u}{\partial y}\right)^2 + \left(\frac{1}{h_2}\frac{\partial w}{\partial y}\right)^2 + \left(\frac{1}{h_3}\frac{\partial u}{\partial z}\right)^2 + \left(\frac{1}{h_3}\frac{\partial v}{\partial z}\right)^2\right] \qquad \text{(A.8)}$$

APPENDIX-B

USER'S MANUAL - SRA MIXER CODE

SUMMARY

The use of a finite-difference procedure for computing turbulent flow in lobe mixers is described. The procedure is based on the solution of an approximate set of governing equations derived from primary and secondary flow concepts. Heat transfer is accounted for through introduction of an energy equation. Turbulence is modeled using a two-equation model. The computer code may be used either in a mode in which starting conditions are generated by automated procedures or in a mode where sufficiently smooth and detailed experimental data may be used to specify the initial conditions. The manual describes the analysis upon which the code is based, input required and output. The manual also contains brief descriptions of the subroutines which comprise the code as well as a list of principal Fortran symbols. A flow chart of the overall program algorithm is also included.

INTRODUCTION

The lobe mixer is a device currently being used for thrust augmentation on a variety of turbofan engines. The forced mixer is designed to mix primary (turbine) and secondary (fan) flow streams before they enter the exhaust nozzle, thus providing the nozzle with air having a more uniform energy which results in a more uniform velocity at the nozzle exit. It has long been known that by mixing the fan and turbine exhaust streams of a turbofan engine in this manner prior to expansion through the exhaust nozzle, a small but significant performance gain may be realized. The level of these gains depends on trade-offs between the degree of mixing of the two streams and the viscous losses incurred in the mixing process.

To date, the performance of lobe mixers has been determined almost entirely through experiments. These experiments are sufficient to determine the relative merits of one mixer configuration as compared to another but they do not directly provide information as to the reasons why one given mixer configuration performs better than another. The overall mixer flow field consists of two major flow regions: (1) the flow upstream of the lobe exit plane (within the lobes) and (2) the flow downstream of the lobe exit plane where the mixing actually takes place. The present study concentrates upon the actual mixing process downstream of the lobe exit plane, through development of a computational procedure applicable in this region and capable of predicting the three-dimensional mixing process in detail.

Reference numbers and figure numbers mentioned in this appendix refer to the references and figures at the back of this appendix.

ANALYSIS

General

The calculation procedure described here is an application of the approach developed by Briley and McDonald [1] to lobe mixer flows. The procedure is based on a decomposition of the velocity field into primary and secondary flow velocities. Equations governing the streamwise development of the primary and secondary flow velocity fields are solved by an efficient algorithm using both block and scalar ADI methods derived from the Douglas-Gunn [2] splitting. Although the governing equations are solved by forward marching, elliptic effects due to curved geometries and area change are accounted for a priori through imposed pressure gradients determined from the potential flow in the geometry in question. Since the primary concern in the lobe mixer problem is thermal mixing of the fan and turbine stream to achieve thrust augmentation, an energy equation is introduced. Finally, turbulence is modeled using a two-equation k-ε model [3]. Since a detailed explanation of the analysis and of its application to the lobe mixer problem is available elsewhere [1,4], only a brief discussion is given here. A flow chart of the calculation procedure is shown in Fig. 1.

The Governing Equations and Solution Procedure

The solution procedure centers around the decomposition of the velocity into primary and secondary flow components

$$\bar{U} = \bar{U}_p + \bar{U}_s \tag{2.1}$$

It is assumed that in the orthogonal potential flow coordinate system used in the lobe mixer code, the primary flow velocity $\bar{U}_p$ is aligned with the potential flow streamlines (see Fig. 2). Similarly, the secondary velocity $\bar{U}_s$ is assumed to lie in the transverse coordinate surfaces which are normal to the streamlines. The equation governing development of the primary velocity component is thus approximated as [4]

$$\rho u h_2 h_3 \frac{\partial u}{\partial x} + \rho(v_s) h_1 h_3 \frac{\partial u}{\partial y} + \rho(w_s) h_1 h_2 \frac{\partial u}{\partial z}$$
$$+ \rho(v_s) u h_3 \frac{\partial h_1}{\partial y} - \rho(v_s)^2 h_3 \frac{\partial h_2}{\partial x}$$
$$- \rho(w_s)^2 h_2 \frac{\partial h_3}{\partial x} + h_2 h_3 \frac{\partial p_I}{\partial x} + h_2 h_3 \frac{dp_v(x)}{dx} \qquad (2.2)$$
$$= \frac{1}{Re} \frac{\partial}{\partial y}\left[\frac{(\mu+\mu_T) h_1 h_3}{h_2} \frac{\partial u}{\partial y}\right] + \frac{h_1 h_2}{Re h_3} \frac{\partial}{\partial z}\left[(\mu+\mu_T)\frac{\partial u}{\partial z}\right]$$

In Eq. (2.2) it is noted that the coordinate system is axisymmetric and thus the metric coefficients are not functions of the azimuthal coordinate, z. Additionally, in Eq. (2.2) u represents the sole component of $\bar{U}_p$, P_I is the imposed pressure and $P_v(x)$ represents the mean viscous pressure drop which is determined from the integral mass flux condition

$$\iint_A h_2 h_3 \rho u dy dz = C \qquad (2.3)$$

To account for thermal mixing between the fan and turbine streams, an energy equation is introduced in the form

$$\rho u h_2 h_3 \frac{\partial E}{\partial x} + \rho(v_s) h_1 h_3 \frac{\partial E}{\partial y} + \rho(w_s) h_1 h_2 \frac{\partial E}{\partial z}$$
$$= \frac{1}{Re} \frac{\partial}{\partial y}\left[\left(\frac{\mu}{Pr} + \frac{\mu_T}{Pr_T}\right)\frac{h_1 h_3}{h_2}\frac{\partial E}{\partial y} + \frac{h_1 h_3}{2h_2}\left(\mu + \mu_T - \frac{\mu}{Pr} - \frac{\mu_T}{Pr_T}\right)\frac{\partial}{\partial y}(\bar{u}^2 + \bar{w}_s^2)\right]$$
$$+ \frac{1}{Re} \frac{h_1 h_2}{h_3} \frac{\partial}{\partial z}\left[\left(\frac{\mu}{Pr} + \frac{\mu_T}{Pr_T}\right)\frac{\partial \bar{E}}{\partial z} + 1/2\left(\mu + \mu_T - \frac{\mu}{Pr} - \frac{\mu_T}{Pr_T}\right)\frac{\partial}{\partial z}(\bar{u}^2 + \bar{v}^2)\right] \qquad (2.4)$$

with the assumption that the laminar and turbulent Prandtl numbers are equal to 1.0.

The gas law is then introduced in the form

$$\frac{\partial}{\partial x}\left[\left(\frac{\gamma-1}{\gamma}\right)\rho\left(E - \frac{u^2}{2}\right)\right] = \frac{\partial P_I}{\partial x} + \frac{dP_v(x)}{dx} \qquad (2.5)$$

to relate the imposed and viscous pressure gradients to the other dependent variables.

At each axial station Eqs. (2.2) and (2.4) are solved initially using a block ADI scheme [5] with the convective coefficients lagged and with an assumed value for $dP_v(x)/dx$. The density is then updated using Eq. (2.5) and the integral mass flux is evaluated using Eq. (2.3). In general Eq. (2.3) will not be satisfied and Eq. (2.2) is thus solved assuming a new value for $dP_v(x)/dx$. This process is repeated using the standard secant method [6] to determine successive estimates for $P_v(x)$ until Eq. (2.3) is satisfied. At this point the primary flow velocity component u, the total energy E and the density ρ have been determined at the new axial station and the secondary flow velocities must be updated.

To determine the secondary flow velocity, $\bar{U}_s$ is presumed to consist of solenoidal (rotational) and irrotational components. The rotational components of $\bar{U}_s$ are determined from solution of a streamwise vorticity equation [7] written in the following form [4]

$$\frac{u}{Q}\left(\rho u\frac{\partial \xi}{\partial x}-\xi\frac{\partial \rho u}{\partial x}\right)+\frac{v_s}{Q}\frac{h_1}{h_2}\left(\rho u\frac{\partial \xi}{\partial y}-\xi\frac{\partial \rho u}{\partial y}\right)+\frac{w_s}{Q}\frac{h_1}{h_3}\left(\rho u\frac{\partial \xi}{\partial z}-\xi\frac{\partial \rho u}{\partial z}\right)$$
$$=-\frac{2}{h_2}\frac{\partial h_1}{\partial y}\rho u\frac{1}{h_3}\frac{\partial u}{\partial z}-\frac{h_1}{h_2h_3}\frac{1}{\rho}\left[\frac{\partial P}{\partial y}\frac{\partial \rho}{\partial z}-\frac{\partial \rho}{\partial y}\frac{\partial P}{\partial z}\right] \qquad (2.6)$$
$$+\frac{\rho}{Re}\left\{\frac{h_1}{h_2h_3}\frac{\partial}{\partial y}\left[\frac{h_3}{h_1h_2\rho}\frac{\partial h_1(\mu+\mu_T)\xi}{\partial y}\right]+\frac{h_1}{h_3^2}\frac{\partial}{\partial z}\left[\frac{1}{\rho}\frac{\partial(\mu+\mu_T)\xi}{\partial z}\right]\right\}$$

Here $Q^2 = u^2 + v_s^2 + w_s^2$ and the vorticity ξ is assumed to lie in the transverse coordinate surfaces and is related to the velocity by

$$\xi=\frac{1}{h_2h_3}\left(\frac{\partial h_3w_s}{\partial y}-\frac{\partial h_2v_s}{\partial z}\right) \qquad (2.7)$$

Eq. (2.6) is solved using the Douglas-Gunn splitting of the Crank-Nicolson scheme. Once a solution for ξ is obtained, a vector potential $\bar{\psi}_s$ is determined from the equation

$$\frac{1}{h_2h_3}\frac{\partial}{\partial y}\left[\left(\frac{h_3}{\rho h_1h_2}\right)\frac{\partial(h_1\psi_s)}{\partial y}\right]+\frac{1}{h_1h_3^2}\frac{\partial}{\partial z}\left[\left(\frac{1}{\rho}\right)\frac{\partial(h_1\psi_s)}{\partial z}\right]=-\xi \qquad (2.8)$$

which is solved using iterative ADI. The rotational components of the secondary flow are then determined from $\bar{\psi}_s$ as

$$v_\psi = \frac{1}{\rho h_1 h_3} \frac{\partial (h_1 \psi_s)}{\partial z} \tag{2.9a}$$

$$w_\psi = -\frac{1}{\rho h_1 h_2} \frac{\partial (h_1 \psi_s)}{\partial y} \tag{2.9b}$$

At this point the resulting velocity field satisfies integral continuity but not local continuity. This is corrected through introduction of a scalar potential governed by the equation

$$\frac{\partial}{\partial y}\left[\frac{\rho h_1 h_3}{h_2}\frac{\partial \phi_s}{\partial y}\right] + \frac{\partial}{\partial z}\left[\frac{\rho h_1 h_2}{h_3}\frac{\partial \phi_s}{\partial z}\right] = -\frac{\partial (h_2 h_3 \rho u)}{\partial x} \tag{2.10}$$

Upon solution of Eq. (2.10) by scalar ADI, the secondary velocity components v_ϕ and w_ϕ are found to be

$$v_\phi = \frac{1}{h_2}\frac{\partial \phi_s}{\partial y} \tag{2.11a}$$

$$w_\phi = \frac{1}{h_3}\frac{\partial \phi_s}{\partial z} \tag{2.11b}$$

and the secondary flow velocities are thus given by

$$v_s = v_\psi + v_\phi \tag{2.12a}$$

$$w_s = w_\psi + w_\phi \tag{2.12b}$$

The resulting velocity field

$$\bar{u} = \bar{i}_1 u_p + \bar{i}_2 v_s + \bar{i}_3 w_s \tag{2.13}$$

thus satisfies both differential and integral continuity.

The Turbulence Model

The foregoing discussion was limited to mean flow equations and their solution. For turbulent flows, the turbulent viscosity which appears in Eqs. (2.2), (2.4) and (2.6) must be determined. The turbulent viscosity is determined using the two-equation k-ε turbulence model as presented by Launder and Spalding [3]. In orthogonal coordinates and with the approximations required for forward marching solution [4], the equations governing the turbulence kinetic energy and dissipation are given by

$$\rho u h_2 h_3 \frac{\partial k}{\partial x} + \rho v_s h_1 h_3 \frac{\partial k}{\partial y} + \rho w_s h_1 h_2 \frac{\partial k}{\partial z}$$
$$= \frac{1}{Re}\left\{ \frac{\partial}{\partial y}\left[\frac{h_1 h_3}{h_2}\left(\mu + \frac{\mu_T}{\sigma_k}\right) \frac{\partial k}{\partial y}\right] \right. \tag{2.14}$$
$$\left. + \frac{h_1 h_2}{h_3} \frac{\partial}{\partial z}\left[\left(\mu + \frac{\mu_T}{\sigma_k}\right)\frac{\partial k}{\partial z}\right]\right\} - h_1 h_2 h_3 \rho \epsilon + p$$

$$\rho u h_2 h_3 \frac{\partial \epsilon}{\partial x} + \rho v_s h_1 h_3 \frac{\partial \epsilon}{\partial y} + \rho w_s h_1 h_2 \frac{\partial \epsilon}{\partial z}$$
$$= \frac{1}{Re}\left\{ \frac{\partial}{\partial y}\left[\frac{h_1 h_3}{h_2}\left(\mu + \frac{\mu_T}{\sigma_\epsilon}\right)\frac{\partial \epsilon}{\partial y}\right] + \frac{h_1 h_2}{h_3} \frac{\partial}{\partial z}\left[\left(\mu + \frac{\mu_T}{\sigma_\epsilon}\right)\frac{\partial \epsilon}{\partial z}\right]\right\} \tag{2.15}$$
$$- h_1 h_2 h_3 C_2 \rho \frac{\epsilon^2}{k} + C_1 \frac{\epsilon}{k} p$$

where k is the turbulence kinetic energy, ε is the turbulence dissipation and P represents the turbulence production given as

$$P = \mu_T\left[\left(\frac{1}{h_2}\frac{\partial u}{\partial y}\right)^2 + \left(\frac{1}{h_2}\frac{\partial w}{\partial y}\right)^2 + \left(\frac{1}{h_3}\frac{\partial u}{\partial z}\right)^2 + \left(\frac{1}{h_3}\frac{\partial v}{\partial z}\right)^2\right] \tag{2.16}$$

Eqs. (2.14) and (2.15) are solved independent of the fluids equations using a linearized block implicit (LBI) scheme. The turbulent viscosity is then determined from k and ε by the relationship

$$\mu_T = \frac{C_\mu \rho k^2}{\epsilon} Re \tag{2.17}$$

The constants appearing in Eqs. (2.14), (2.15) and (2.17) are assigned their usual values [3] of; $c_1 = 1.44$, $c_2 = 1.92$, $c_\mu = 0.09$, $\sigma_K = 1.0$ and $\sigma_\varepsilon = 1.3$.

It should be pointed out that the production term in the k and ε equations may be expressed computationally in several ways which may be selected by the user. The first option available to the user is to have the production terms expressed as in Eq. (2.16) with the turbulent viscosity lagged. In a second option, the production term in the dissipation equation is altered by substituting the relationship of Eq. (2.17) for μ_T. This simplifies the term representing production of dissipation and the resulting expression appears to be computationally advantageous. In the third option, the substitution for μ_T in the production term is made in both the k and ε equations. Computationally, the second option appears most attractive and is presently recommended.

If all the available two-equation turbulence model options are exhausted and a successful calculation is still not obtained due to turbulence model failures, the user may select a simpler wake turbulence model. The use of the wake model should provide a means of completing a given calculation under these circumstances

The Coordinate System and Specification of the Imposed Pressure Field

The coordinate system used in the present MIXER code is generated using the ADD code [8]. The ADD code generates a two-dimensional potential flow coordinate system, an example of which is shown in Fig. 2. The axisymmetric coordinate system for the lobe mixer calculation is then obtained by rotating this two-dimensional coordinate system about a centerline. Although the resulting coordinate system is suitable for the viscous flow calculation [4], the two-dimensional pressure field is not a suitable approximation to the axisymmetric pressure field. An a priori axisymmetric potential flow calculation is performed to obtain a suitable pressure field. The axisymmetric potential is obtained from the solution of the equation

$$\frac{h_2 h_3}{h_1}\frac{\partial^2 \phi}{\partial x^2} + \frac{\partial}{\partial x}\left[\frac{h_2 h_3}{h_1}\right]\frac{\partial \phi}{\partial x} + \frac{h_1 h_3}{h_2}\frac{\partial^2 \phi}{\partial y^2} + \frac{\partial}{\partial y}\left[\frac{h_1 h_3}{h_2}\right]\frac{\partial \phi}{\partial y} = 0 \quad (2.18)$$

using an iterative ADI scheme. The resulting inviscid axisymmetric velocity field $\bar{U}_I$ is then used to determine incompressible axisymmetric pressure gradients

$$\nabla\left(\frac{\bar{U}_I \cdot \bar{U}_I}{2}\right) - \bar{U}_I \times (\nabla \times \bar{U}_I) = -\frac{1}{\rho}\nabla P_{M=0} \tag{2.19}$$

The streamwise pressure gradient is then scaled for compressibility using the local Mach number, M_L, which is determined as part of the viscous flow calculation, to give the imposed pressure gradients

$$\frac{\partial P_I}{\partial x} = \frac{1}{\sqrt{1-M_L^2}}\frac{\partial P_{M=0}}{\partial x} \tag{2.20}$$

The maximum value of M_L used in Eq. (2.20) is limited to 0.7 in the computer code to avoid a singularity at $M_L = 1.0$, although local Mach numbers greater than 1.0 may appear in the flow field [4].

SPECIFICATION OF INITIAL CONDITIONS

The initial conditions for the lobe MIXER code are specified as input, with three possible starting procedures. The ICOAX=1 option is used for simple two-dimensional test cases. Under the ICOAX=1 option a confined coaxial jet initial profile is constructed assuming a cosine velocity profile for the shear layer between the primary and secondary streams (not to be confused with the primary and secondary flow) as shown in Fig. 3. The velocity and static temperature ratio between the two streams is specified as input by the user. A lobe of constant radius is specified, and the cosine shear layer velocity profile is centered about the lobe radius. The thickness of the shear layer is input as the variable DELMIX. Boundary layers may be specified at R_{MIN} and/or R_{MAX} (see Fig. 3) using the IHUB and/or ISHR options. Turbulence quantities are initialized by specification of a length scale which is assumed to be constant across the shear layer but which varies with distance from a wall if boundary layers are specified [4]. Additionally, free stream values of the turbulence kinetic energy are specified by the user. The user also has the option of initializing turbulence quantities by specifying constant turbulence kinetic energy throughout the flow field by using the IDIS option.

A second method of starting the calculation procedure is available to allow the user to perform calculations using automated starting profiles generated by the code itself. This starting procedure is used unless either the ICOAX option or IDATA option (to be discussed subsequently) is requested. In this mode, the user must specify a lobe shape, in terms of discrete data points, as indicated in Fig. 4, starting with the minimum r coordinate value. The lobe coordinates must be specified such that the lobe enters the computational domain through boundaries 1 or 4 and exits the domain through boundaries 2 or 3 as shown in Fig. 4. The user has the option of specifying boundary layers on the lobe, hub and shroud surfaces, or any combination thereof through use of the ILOBE, IHUB and ISHR options. The primary (turbine) and secondary (fan) streams are indicated in Fig. 4. The user may specify nominal velocity and static temperature ratios between the streams. Initial velocity profiles are constructed by assigning the appropriate values for velocity to each stream. The resulting uniform profiles are then corrected for radial pressure gradients present at the initial plane as determined from the potential flow calculation

and are also scaled by boundary layer profiles. Turbulence quantities are again initialized through specification of a length scale and free stream turbulence intensities. However, the user may specify whether the length scale in the region near the lobe varies with distance from the lobe or is constant across the lobe wake. Near the hub and shroud, the length scale will vary with distance from the wall if boundary layers are specified.

The third starting procedure is activated through the IDATA option. If IDATA is greater than zero, the program accepts card input to specify the velocity and temperature field at the initial plane. The data must be supplied for each grid point in the computational domain. A lobe shape is specified as before, and DELMIX is input as a number representative of the boundary layer thickness on the lobe. Boundary layers on the hub and/or shroud may be considered using the IHUB and ISHR options. If these options are elected, DELHUB and DELSHR must be input as representative values of the boundary layer thickness on the hub and shroud, respectively. Turbulence quantities are initialized as in the previously described starting method.

DESCRIPTION OF INPUT

Input to the MIXER code is accomplished by a combination of card input and information which is stored on auxiliary files. Metric information generated by the ADD code [8] and restart data sets are stored on separate auxiliary files. Program control is performed through card input, which is divided into three categories:

1) Plot file information for NASA-Lewis plotting package,
2) NAMELIST input, and
3) Experimental flow field input.

Format of the required input is as follows:

Plot File Input

CARD #	COLUMNS	VARIABLE	DESCRIPTION
Card 1	Col. 1-32	TITLE(I)	Plot title, format 5A6,A2. (May be left blank).
Card 2	Col. 1-2	ISYN	Twice the number of lobes in a 360^{o} cross section of the mixer geometry.
	Col. 3-12	SYSTEM	Indicates the type of coordinate system for plot routines. Format F10.0, Use SYSTEM=2.

Namelist Input

Namelist	Description
$IN1	
RG	Gas constant, ft lb_f/(slug ^{o}R), default 1716.3 (air).
CP	Constant pressure specific heat, ft lb_f/(slug ^{o}R), default is 6012.384 (air).
TZERO	Reference temperature, assumed to be nominal primary stream temperature in degrees Rankine.
UZERO	Reference velocity, assumed to be nominal primary stream velocity, ft/sec.
PZERO1	Reference static pressure, assumed to be nominal pressure at initial plane, lb_f/ft^2, default is 2116.8.
YZERO	Reference length, ft.

Namelist	Description
VISC1	Reference viscosity, slugs/(ft sec).
$END	
$IN2	
IAXI	=1, cylindrical coordinates.
	=2, rotated orthogonal coordinates (from ADD code) (default).
ICOMP	=-1, stop after input dump.
	=0, normal run (default).
	=1, stop after printing initial plane geometry.
	=2, stop after printing initial flow field.
IDATA	=0, automated start (default).
	=1, read initial velocity and temperature field data, use wall length scale near lobe.
	=2, read initial velocity and temperature field data, use wake length scale near lobe.
XENTR	Dimensionless distance from initial ADD code potential line to initial plane of lobe mixer calculation. Used only for IAXI=2. Determined from ADD code as XENTR=(JSTEP$_{XENTR}$-1)*DS where JSTEP$_{XENTR}$ is the number of the ADD code potential surface representing the MIXER code initial plane. See Fig. 2.
YS(I,J)	Dimensionless transverse limits of computations domain. YS(1,1)=r_{MIN}
	YS(2,1)=r_{MAX}
	YS(1,2)=θ_{MIN} (radians)
	YS(2,2)=θ_{MAX} (radians)
	See Fig. 2 for definition of YS(I,1) for mixer geometry.

Namelist	Description
NE(I)	NE(1) = number of radial grid points. For computations using ADD code geometry NE(1) must be equal to the number of ADD code streamlines. NE(2) = number of azimuthal grid points. Maximum values for NE(I) are 20.
IGRID(I)	IGRID=0, no grid stretching (default). =1, Roberts stretching at r_{MIN} or θ_{MIN}. =2, Roberts stretching at both r_{MIN} and r_{MAX} or θ_{MIN} and θ_{MAX}. =4, hyperbolic sine stretch about XCTR(I). I=1 for radial direction, I=2 for azimuthal direction.
EPS(I)	Used for IGRID(I)≠0 to control the grid stretch. If unequally spaced streamlines are used in the ADD code geometry, the value of EPS(1) must be specified from the ADD code. For Roberts stretching 0.0<EPS(I)<1.0. For hyperbolic sine 1.0<EPS(I)<5.0.
XCTR(I)	Used only with IGRID(I)=4 to specify the r(I=1) or θ(I=2) location about which points are concentrated.
NS	Number of axial stations to be computed. NS=1 is initial plane. Maximum value is 50.
AP	If AP is input .GT.0 a geometric streamwise grid is set up with $\Delta x(J)/\Delta x(J-1)$ = AP. If AP is input .LT.0 the user must specify the axial mesh. AP has a default of 1.05 but the AP.LT.0 option is recommended.
ILAP	ILAP=1 indicates that an axisymmetric potential solution is to be computed on the ADD code grid and the resulting pressure field used in the viscous flow calculation. ILAP has a default of 1. If IAXI is input as 1, ILAP is set to 0.
LX	LX is the number of potential lines generated by the ADD code. LX is used with ILAP=1. The maximum allowable value of LX is 50.

Namelist	Description
LY	LY is the number of streamlines generated by the ADD code. LY is used with ILAP=1. The maximum allowable value of LY is 20.
IPCOR	IPCOR is used with ILAP=1 to identify the potential surface whose average dimensionless velocity is 1.0 in the axisymmetric potential calculation. IPCOR should be input as IPCOR=$JSTEP_{XENTR}$ in general. See Fig. 2.
LSEC	LSEC is a secondary flow option. LSEC=1, solve streamwise vorticity equation. LSEC=0, do not solve streamwise vorticity. LSEC has a default value of 1.
ILAM	ILAM=0 for turbulent flow, default. ILAM=1 for laminar flow. ILAM=-1 wake turbulence model, requires specification of freestream turbulence for stream 1 and a length scale. The default value is 0. Only laminar flow may be considered using the automated starting routine without boundary layers.
ICOAX	ICOAX=0, default. ICOAX=1 activates the coaxial jet starting option.
X(JX)	X is an array which contains NS values of the streamwise mesh coordinate. If AP is input .GT.0 only X(1) and X(2) need be input. If AP is input .LT.0 NS values of X must be input. If IAXI=1, X is a physical but dimensionless distance. If IAXI=2 and ADD code geometry is used, X represents the dimensionless computational distance from the initial plane. The maximum allowable value of X is given as ($JSTEP_{MAX}$ - $JSTEP_{XENTR}$)*DS/USCALE where USCALE=YS(2,1)/(YS(2,1)-YS(1,1)). The maximum value of X should be slightly less than this value to avoid marching out of

Namelist	Description
	the ADD code geometry which will result in an error termination. See Fig. 2.
IKECUP	=0, μ_T lagged in turbulence model equations production terms.
	=1, μ_T treated implicitly in turbulence dissipation equation (default).
	=2, μ_T treated implicitly in both k & ϵ equations.
IDIF	=0, central difference radial convective terms in turbulence model equations.
	=1, use two-point one-sided differencing of radial convective terms in turbulence model equations (default).
IDIFBC	=0, use three-point one-sided normal gradient boundary condition weights.
	=1, use two-point one-sided normal gradient boundary condition weights (default).
IDIS	=1, specify uniform turbulence kinetic energy, at the turbine stream value throughout the initial flow field.
	=0, initial turbulence kinetic energy assumes turbulence production equal to dissipation.
	IDIS=0 by default. IDIS=1 should be used only with the constant length scale options thus if IDIS=1 and ILOBE is input as 1, ILOBE will be set to 2. If IDATA is input as 1, it will be set to 2.
$END	
$IN3	
IRSTIN	The number of the axial station to be read in for a restart. No restart if IRSTIN=0 (default).
IRSTOT	Increment for saving restart information. Restart files will be written every IRSTOT steps from starting value of JX, the axial station counter. Default assumes no restarts written.
JRSTIN	File number from which restart information is to be read. Default file number is 11.
JRSTOT	File number on to which restart information is to be written. Default file number is 11.

Namelist	Description
NFILE	Sequence number in file JRSTIN of the desired restart information.
NSAVED	The number of restart data blocks saved on file JRSTOT.
IPLOT	If IPLOT=1 a plot file must be assigned in the run stream and information will be written in this file for subsequent use in plotting. IPLOT=0 give no plot file. Default is IPLOT=0.
$END	
$IN4	
USTRM2	Ratio of secondary stream (fan) velocity to primary stream (turbine) velocity. For matched average inlet Mach numbers and total pressures USTRM2= $\sqrt{\text{TSTRM2}}$. Default value is USTRM2=.707.
TSTRM2	Ratio of secondary stream temperature to primary stream temperature. Default is TSTRM2=.5.
TUSTR1	Primary stream turbulence intensity. $T_{u_1} = \overline{u'^2}/u_1^2$ where u_1=UZERO.
TUSTR2	Secondary stream turbulence intensity. $T_{u_2} = \overline{u'^2}/u_2^2$ where u_2=UZEROxUSTRM2. If TUSTR2 is input as 0.0 the free stream turbulence in both streams ($k=3T_u^2/2$) is assumed equal to $3T_{u_1}^2/2$.
ALEN	Dimensionless free stream length scale ℓ_{ref}/YZERO. To be estimated by the user. As a guide, if IDATA or ICOAX is input .GT.0 ALEN should be on the order of 0.1xDELMIX. If the automated MIXER starting routine is used ALEN should be on the order of the displacement thickness specified.
AMEXIT	AMEXIT is an assumed exit plane Mach number which is used to specify the isentropic exit plane pressure for the thrust calculation. Default value is AMEXIT=0.9.
DELMIX	DELMIX is used in both the IDATA and ICOAX options. If IDATA is input .GT.0 DELMIX must be input as a dimensionless boundary layer thickness, δ/YZERO, presumed to be representative of the boundary layer on the lobe surfaces. If ICOAX is input .GT.0 DELMIX is the dimensionless thickness of the cosine shear layer. See Fig. 3.

Namelist	Description
DELHUB	DELHUB is input with IDATA .GT.0 as a dimensionless boundary layer thickness, δ/YZERO, representative of the hub boundary layer.
DELSHR	Similar to DELHUB but pertaining to the shroud boundary layer.
$END	
$IN5	
ILOBE	ILOBE is a flag used in the automated starting routine. ILOBE=0 indicates that no boundary layers are to be set up on the lobe surfaces. ILOBE=1 indicates that lobe boundary layers are to be set up and a wall-type length scale based on distance from the lobe is used to initialize turbulence quantities. ILOBE=2 is similar to =1 but the length scale is held constant across the lobe wake. If ILOBE is input .GT.0 the ILOBE=2 option is recommended. If IDIS is input as =1 and automated lobe boundary layers are to be constructed, ILOBE will be reset to 2.
IHUB	IHUB=0 indicates that hub boundary layers will not be present in the initial profile, regardless of other starting options. If IDATA is input .GT.0 and IHUB is input .GT.0 DELHUB must be input. If the IDATA option is not used, IHUB must be input equal to the number of points input to describe the hub boundary layer in the array BLHUB.
ISHR	ISHR is similar to IHUB except it pertains to the shroud boundary layer.
BLHUB(I,J)	If hub and/or shroud boundary layers are to be constructed using the automated starting routine (IDATA=0) the boundary layer displacement thickness and shape factor must be input as functions of θ along the hub and/or shroud surfaces. This is accomplished using the array BLHUB.

Namelist	Description
	BLHUB(I,1) contains the values of θ (in radians) where hub boundary layer parameters are specified. The θ values are arbitrary but must span the computational domain. The number of θ values specified must equal the input value of IHUB. A maximum of 20 values may be specified. BLHUB(I,2)=δ^*/YZERO, the dimensionless displacement thickness of the hub boundary layer at each specified θ location. BLHUB(I,2)=H, the shape factor at each θ location. BLHUB(I,4) is the shroud equivalent of BLHUB(I,1). ISHR values of θ must be loaded in BLHUB(I,4). BLHUB(I,5) and BLHUB(I,6) are similar to BLHUB(I,2) and BLHUB(I,3) except they pertain to the shroud boundary layer parameters. See Fig. 4.
NLOBE	NLOBE is the number of data points input to describe the lobe shape and lobe boundary layers.
YLOBE(I,J)	YLOBE is an array which contains the data needed to specify the lobe shape and lobe boundary layers. NLOBE values of each parameter in YLOBE must be read in. YLOBE(I,1) contains NLOBE dimensionless radial coordinates, R/YZERO, of the points used to describe the lobe shape, starting at the minimum radius. YLOBE(I,2) contains the corresponding θ coordinates in radians. YLOBE(I,3) contains NLOBE values of the dimensionless displacement thickness, δ^*/YZERO, at each coordinate point, for the primary stream lobe boundary layer. YLOBE(I,4) contains NLOBE values of the displacement thickness for the secondary stream. YLOBE(I,5) contains the distribution of the shape factors, H, at each coordinate point for the primary stream. Finally, YLOBE(I,6) contains the shape factor distribution for the secondary stream.

Namelist	Description
	YLOBE(I,3) through YLOBE(I,6) need not be specified if the IDATA or ICOAX option is specified, or if ILOBE=0. YLOBE(I,1) and YLOBE(I,2), the r-θ coordinates of the lobe, must be specified for all starting options. See Fig. 4.
IWAKE	If IWAKE=1 the slots for shape factor in BLHUB and YLOBE need not be input as an assumed value of the wake function in the boundary layer profile is assumed.
$END	
$IN6	
NBCON(I,J,K)	NBCON is a three-dimensional array which allows the user to select the desired boundary conditions for the streamwise velocity, the total enthalpy, the turbulence kinetic energy and the turbulence dissipation. It should be recalled that the momentum and energy equations are solved as a system of equations and the turbulence equations as a second system of equations. The third subscript, K, indicates which set of equations boundary conditions are being input for. K=1 for the momentum and energy equations. K=2 for the turbulence model equations. With K=1, I=1 indicates a boundary condition for u is to be specified. K=1 and I=2 is total enthalpy. K=2, I=1 is turbulence energy and K=2,I=2 is turbulence dissipation. The value of J ranges from 1 to 4 indicating the computational boundary considered. J=1 for the boundary at R_{MIN}, J=2 for R_{MAX}, J=3 for θ_{MIN} and J=4 for θ_{MAX}. NBCON(I,J,K)=0 specifies zero function value boundary condition. NBCON(I,J,K)=1 specifies zero normal gradient. NBCON(I,J,K)=2 specifies second derivative zero. NBCON(I,J,K)=4 specifies wall function boundary conditions. Default values are as follows: For streamwise velocity and energy symmetry (zero gradient) at θ_{MIN} and θ_{MAX} and zero second derivative at R_{MIN} and R_{MAX}. For turbulence variables, normal derivatives are specified zero on all surfaces.

Namelist	Description
	If a calculation is being performed with hub/or shroud boundary layers (using wall functions) the velocity boundary conditions at R_{MIN} and R_{MAX} should be specified as 4. Heat transfer at the wall is not considered in the MIXER code at present thus NBCON=1 should be specified at R_{MIN} and R_{MAX} for total enthalpy. Default values should be used for the turbulence energy (which is consistent with wall functions) and NBCON=4 should be specified at R_{MIN} and R_{MAX} for the turbulent dissipation. If hub and/or shroud boundary layers are not specified, the default values at R_{MIN} and/or R_{MAX} will suffice.
XCBC	XCBC is used in MIXER calculations to change boundary conditions as the flow moves down stream off the hub, where wall function boundary are applied, to a center line, where symmetry conditions are applied. The user must specify the value of XCBC by examination of the geometry from the ADD code. XCBC is computed as $XCBC=(JSTEP_{XCBC}-JSTEP_{XENTR})*DS$ where $JSTEP_{XCBC}$ is the number of the ADD code potential line where the plug degenerates to a center line and $JSTEP_{XENTR}$ is the number of the potential line representing the initial MIXER calculation plane. See Fig. 1. The default value causes no changes.
NBCONC(I,J,K)	NBCONC has the same function as NBCON but is used to specify which boundary conditions are to be changed for X>XCBC and what they are to be. Default value will cause no change in boundary conditions regardless of the value of XCBC. For a calculation with hub boundary layer, NBCONC is used to change from wall functions to symmetry conditions as the hub degenerated to a center line.
$END	
$IN7	
IPRN(I)	IPRN is an array which selects variables to be printed at each axial station. If IPRN(I)=1 variable "I" will be printed. If IPRN(I)=0 variable "I" will not be printed. The variables are numbered as follows:

Namelist	Description
	I= Variable
	1 u
	2 v
	3 w
	4 ρ
	5 E
	6 μ_T
	7 K
	8 ε
	9 ξ
	10 ψ
	11 M
	12 static temperature ratio T/T_r
	13 total temperature T^o/T^o_r
	14 pressure coefficient
	15 static pressure ratio P/P_r
	16 total pressure ratio P^o/P^o_r
	17 swirl angle, degrees
	18 $\overline{u'v'}$
	19 $\overline{u'w'}$
	20 $\overline{v'w'}$
ICON	ICON controls printer contour plots of the printed flow field variable.
	ICON=1 produces printer contour plots.
	ICON=0, no contour plots.
$END	

Experimental Flow Field Input

The following cards are needed only if starting profiles are to be read in (IDATA=1 or 2). Each card contains velocity components u, v, w in feet per second and static temperature, T, in degrees Rankine at each computational grid point. One card per grid point is required, thus a total of NE(1)*NE(2) data cards are needed. Format 4F10.0. The data is read for the grid point numbering shown in Fig. 5.

CARDS # $END+1 to $END+NE(1)*NE(2)

Col.	1-10	u - velocity component in the computational streamwise direction, ft/sec.
	11-20	v - velocity component in the computational radial direction, ft/sec.
	21-30	w - velocity component in the computational azimuthal direction, ft/sec.
	31-40	T - static temperature, ^{o}R.

Sample Run Stream

Listed in Fig. 6 is a sample UNIVAC 1110 run stream for a lobe mixer calculation. The run stream includes all file assignments required excluding a plot file, using default values of JRSTOT and JRSTIN. The input data will reproduce the Case 6 results presented in [4] and will duplicate the sample output contained in this manual.

The first card in the run stream assigns file 9. File 9 is a temporary file which is used to store out of core flow field variables. File PDATA5(2) is the file which contains geometric information. It is created using the ADD code [8] and must be a FASTRAN format file. The USE card which follows the assignment specifies the internal unit number used in the MIXER code for the geometry file. PEPR3 is the restart file and must be cataloged as a word addressable file before the run. The USE card which follows specifies the unit number which is used in the MIXER code for the restart file. Note that this must be the same as the value of JRSTOT. If JRSTOT≠JRSTIN an additional file must be assigned with a USE card specifying the unit number as JRSTIN. Files 12 through 14 are temporary files. The remainder of the input has been described previously.

DESCRIPTION OF THE OUTPUT

The output of the MIXER code can be divided into two categories. The first includes output associated with initiation or restart of a calculation. The second category of output is controlled by the user and consists of summary tables of integral properties, skin friction coefficients, and flow field printouts at each marching station. Sample output, typical of that obtained when initiating a calculation using the automated starting procedure is shown in Figs. 7-13.

The output for any case begins with the printed message ***INPUT NAMELIST DUMP*** which is then followed by a dump of namelists IN1 through IN7. This provides the user with a record of the namelist input used to run a given case. It should be noted that the values of XENTR and XCBC printed here may differ from the input values since they have been divided by the metric scale factor for consistency with the MIXER coordinates. After the namelist dump, the message ****SUMMARY OF INPUT DATA**** is printed. This summary data is shown in Fig. 8 and includes the R-θ coordinates which describe the lobe shape, input which describes the mixing duct including the computed value of the metric scale factor, the primary or turbine stream, reference conditions, the velocity, temperature and total pressure ratios between streams, free stream turbulence intensities and length scale, and a list of computational options either specified or set by default. Following the list of computational options, information pertaining to the computational coordinates is printed. This information includes NS values of the axial mesh distribution, the transverse grid limits and grid stretching information. The message **TRANSVERSE GRID AND DIFFERENCE WEIGHTS** is then printed followed by a table as shown in Fig. 9. In this table, the first column contains the grid point indices for the y or radial direction, followed by the z or azimuthal direction. The second column lists the computational location of each grid point. The third through fifth columns list the first-derivative difference weights and columns 6 through 8 list second-derivative weights. If the case is a restart, a restart message will be printed at this point and the calculation will proceed. If the case is an initial calculation and if the IAXI=2 option with the ILAP=1 option is specified, the message **POTENTIAL FLOW SOLUTION** will appear next, followed by an ADI convergence message. The next LX columns of information printed is the axisymmetric potential flow solution followed by

LX columns of information which represent the incompressible potential flow pressure coefficients. The potential flow solution will not be printed if IAXI=1, if IAXI=2 and ILAP=0, or if IRSTIN>0. The potential flow printout is shown in Fig. 10.

If IAXI=2, metric information will follow the potential flow solution (if it has been printed) or restart message. This metric information is shown in Fig. 11. JSTEP indicates the number of the potential surface from the ADD code just upstream of the current axial location. DSTEP is the MIXER equivalent of the ADD code DS divided by the metric scale factor. SQ1 is the value of the axial coordinate at the JSTEP+1 potential surface and SQ2 is the axial coordinate value at the JSTEP potential surface. SQ12 is the value of the axial coordinate of the transverse computational plane for which the metric information is needed. The variable FRACT is the fraction of the distance between SQ1 and SQ2 of SQ12, FRACT=(SQ12-SQ2)/(SQ2-SQ1). In the table which follows, YPHYS and XPHYS are dimensionless radial and axial coordinates in physical space, respectively. H1, H2 and H3 are the metric coefficients, DH1/DY, etc., are derivatives of the metrics and PRESS is 1/2 of the inviscid pressure coefficient. If this is the first geometry printout of a new case or restart, two tables of this metric information are printed. The first corresponds to the initial or restart location and the second corresponds to the following axial station.

If the run is a new case having IDATA>0, for which initial profile data is read in, the message ****UNPROCESSED INPUT DATA**** will be printed followed by flow field prints of normalized specified input profiles. If automated starting procedures are used, this printout is omitted. The next item printed is the message ****AREA INTEGRALS**** followed by a summary table of area-weighted or averaged quantities. This summary table is shown in Fig. 12 and may be repeated several times to trace the history of the iteration of the mean pressure drop. The last table printed contains the values associated with the converged solution. The table contains, in dimensionless form, the following:

AREA - cross-sectional flow area.

MASS FLUX - self explanatory.

VELOCITY FLUX - the area-averaged streamwise velocity.

AVE RU - the area-averaged value of ρu.

AREA RATIO - the ratio of the local area to the inlet area.

MASS ERROR - the error in the mass flux from the mean pressure drop iteration.

MASS AVE CPT - a mass-averaged total pressure loss (cf. [4]).

IDEAL THRUST COEF - a ratio of the local value of the thrust obtainable to the value at the mixer inlet (cf. [4]).

THRUS - the dimensionless thrust, $T/(\rho_r u_r^2 y_o^2)$.

THARAT - an area ratio of the required exit area to the exit area required at the initial plane. This also implies losses as it rises above 1.0.

THAREA - the exit area used in the thrust calculation (cf. [4]).

AVE MACH NO - the area-averaged value of the Mach number.

AVE PT RATIO - the area-averaged total pressure ratio.

AVE T TOTAL RATIO - the area-averaged total temperature ratio.

AVE CP - the area-averaged pressure coefficient.

BLOCKAGE - a local reference quantity.

Following this summary table, the message ****PROCESSED STARTING PROFILES**** is printed as shown in Fig. 13 followed by flow field prints of the initial conditions after some preprocessing to be compatible with continuity. From this point onward, the form of the program output is independent of the mode of operation. With the exception of the first computational station, a table of geometric information is printed if IAXI=2. This is followed by the area integral tables. Following the area integrals, an ADI convergence message is printed indicating the convergence of the vector potential equation, Eq. (2.8). A second ADI convergence message is printed indicating convergence of the scalar potential equation, Eq. (2.10). A tabulation of skin friction coefficients is then printed if hub and/or shroud boundary layers are specified. Following the skin friction coefficients, the detailed flow field variables specified by the user are printed. The columns labeled R and Z (see Fig. 13) contain the dimensionless radial and axial location of each grid point in physical space. There is no azimuthal (θ) variation of these coordinates due to the axisymmetric coordinate system. After the flow variables are printed, the output sequence is repeated for subsequent axial steps.

TEMPORARY AND PERMANENT STORAGE REQUIREMENTS

With the MIXER code dimensioned for a 20x20 grid in the transverse plane and 50 axial stations, the core requirement on a UNIVAC 1110 computer is about 68000 words. Four temporary file assignments are required. These files are assigned as word-addressable files on the UNIVAC 1110 as follows:

Unit 9	50,000 words
Unit 12	5,000 words
Unit 13	5,000 words
Unit 14	5,000 words

If a plot file is to be written, a permanent file must be created prior to the run. This file should be FASTRAN-formatted and must be given a local file name of Unit 8. The actual size of the file will depend on the computational grid used but approximately 14xNE(1)*NE(2)+5 words are written on this file for each axial step. If restarts are generated, a permanent word-addressable file must be created and a local file name consistent with JRSTOT must be used (unit 11 by default). Again, the actual length of this file will depend on the number of restarts written but approximately 22000 words per restart will be written with the deck dimensioned as stated above.

ERROR CONDITIONS

Certain types of error conditions may cause program termination. Those conditions which are known to represent possible modes of error termination are discussed below.

If both ICOAX and IDATA are greater than zero, the computer code will produce the message ***INPUT FOR IDATA AND ICOAX IS INCONSISTENT*** and the run will be terminated. The user should correct the input.

Several error terminations may occur in subroutine GEOTRB. The first of these errors terminates the run with a RETURN 0 CALL FROM GEOTRB and is associated with the inability of the computer program to find the position in the geometry file which corresponds to the current axial location to be computed. Error termination also occurs if the value of the axial coordinate is greater than the extent of the geometry generated by the ADD code. Both of these errors occur only for IAXI=2 and are caused by improper specification of the axial grid. The user should examine the grid being used and correct it as necessary. Error termination may also occur in GEOTRB if the geometry file is improperly assigned.

Although no error termination occurs, it is possible that the ADI routine used to solve the vector potential equation or the scalar potential equation, Eqs. (2.8) and (2.10), may fail to satisfy certain convergence criteria. When this happens, it usually indicates a failure to meet the convergence requirement within the allotted number of iteration, which is set at 50, rather than indicating divergence of the solution. Should this situation occur, the message ***ADI FAILS TO CONVERGE*** is printed followed by the message

ITERS,PHIMAX,RHSMAX,EPS1-2=XX .XXX .XXX .XXX .XXX

where the X's indicate numbers. The first number is the maximum number of iterations. The following two numbers represent maximum normalized errors in the solution. If the first of these two numbers is less than 1.0 and the second number is not greater than about 10., the message may be ignored although if repeated failure occurs, the secondary flow velocities should be examined carefully. If both of these numbers are significantly greater than 1.0, it may indicate divergence of the solution, although this has not been encountered as of this writing. Should such a failure occur, the user should carefully examine all input to determine if a problem exists elsewhere. The ADI messages

appear just after the area integral summary tables. The first ADI message corresponds to the vector potential; the second corresponds to the scalar potential.

Another error message is generated by the code (but does not terminate the run) if the iteration for the mean viscous pressure drop fails to converge within 5 iterations. If this occurs, the message WARNING-MASS FLUX ITERATION DID NOT CONVERGE--CHECK RESULTS CAREFULLY appears. If this message appears, the user should check the mass error printed in the area integral summary tables and decide whether the solution is acceptable.

If the flow chokes upstream of the last exit plane, the warning message discussed above may appear at the axial station before the flow chokes. At the axial station where the flow actually chokes the calculation procedure may break down completely and an error termination may occur in the square-root routine during the iteration for the mean pressure drop. Under these conditions, the user should adjust the inlet mass flux to allow the calculation to proceed to the exit plane without choking.

Program execution will also be terminated on a restart case if the input value of IRSTIN and NFILE are not consistent. The program will print the message RESTART REQUESTED AT STATION XX BUT STORED INFORMATION AT SEQUENCE XX IS AT STATION XX and the run will terminate with STOP RESTAR. The user should correct the value of IRSTIN or NFILE and rerun the case.

DESCRIPTION OF SUBROUTINES

Subroutine Name	Description
ADI	ADI is a general purpose scalar ADI solver.
ADICUP	ADICUP is a control routine which specifies the calling sequence of routines which set up the difference equations for the streamwise momentum, thermal energy, turbulence kinetic energy and turbulence dissipation equations, specify boundary conditions and invert the coefficient matrices.
BCONB	BCONB controls and manipulates boundary conditions placing them in the desired computational form.
BCONW	BCONW performs the actual specification of the boundary condition for the streamwise momentum, energy and turbulence model equations.
COEFT	COEFT sets up the finite difference approximations for the streamwise momentum and energy equations at interior grid points.
COEFT1	COEFT1 performs a function similar to COEFT but for the turbulence model equations.
CON	CON creates printed contour plots of flow variables, if called for.
COPY	COPY reads (writes) the required information for a restart from (to) a restart file.
CROSEC	CROSEC performs numerous functions associated with a transverse computational plane. The IROTE option over writes the n level solution with the n+1 level solution prior to computation of the next axial step. The IOPT1 option is used to compute area integrals. The IOPT2 option updates the turbulent viscosity. The IOPT3 option sets up the secondary flow stream function and vorticity equations. The IOPT4 option writes plot files. The IOPT5 option computes the imposed pressure gradients and updates the secondary flow velocities. The IOPT6 option sets up the scalar potential equation.
DMAT1	DMAT1 interfaces coefficient generation subroutines with the block matrix inverter, MGAUSS.

Subroutine Name	Description
DYF	DYF computes linearized difference coefficients of terms composed of the derivative of the product of a known function and the derivative of a flow variable.
DYZA	DYZA computes linearized difference coefficients of a transverse derivative of a flow variable.
GAUSS	GAUSS is a scalar tridiagonal matrix solver.
GEOTRB	GEOTRB reads the ADD code geometry file and loads the FG array with metric information.
HINVRS	HINVRS is a matrix inversion routine used by BCONB.
IFACE	IFACE interfaces forward marching subroutines with the axisymmetric potential flow solver.
INPUTS	INPUTS reads the input for a case and performs preliminary set up.
LAPLAC	LAPLAC performs the axisymmetric potential flow solution.
LENGTH	LENGTH initializes the turbulence quantities and updates the turbulent viscosity, as the calculation proceeds, given values of k and ϵ.
MAIN	MAIN is the main program. It controls the case set up, the iteration on the mean viscous pressure drop and output.
MGAUSS	MGAUSS is a block tridiagonal matrix solver.
MINVRS	MINVRS computes the inverse of a square matrix.
MMULT	MMULT performs matrix multiplication.
MSUBT	MSUBT performs matrix subtraction.
MTPROF	MTPROF sets up initial profiles from data or using automated procedures.
NTRANA NTRANB	NTRANA and NTRANB transfer dependent variables to and from mass stroage devices and reorders in-core storage of the dependent variables as required by the solution procedure.
OUTPUT	OUTPUT controls the printing of flow field variables in transverse planes.
PRINT1	PRINT1 performs the actual printing of flow field variables.

Subroutine Name	Description
PROFT	PROFT sets up the boundary layer scaling when using the automated starting routines.
READZ	READZ reads dependent variables from mass storage devices and loads them into two-dimensional arrays for printing.
RESTAR	RESTAR controls the reading and writing of restart files.
ROBTS	ROBTS sets up the transverse computational grid.
SECANT	SECANT is a general secant iteration scheme.
SECFLO	SECFLO controls the solution of the secondary flow equations.
SHEAR	SHEAR computes the friction velocity compatible with the log law velocity profile used in the wall function boundary conditions.
STATUS	STATUS returns control to the program after an NTRAN read or write providing there is not an NTRAN error. If an NTRAN error is detected, an error termination is performed.
TAU	TAU computes the velocity gradients appearing in the turbulence model production terms.
TPLOT	TPLOT creates printer plots of the axial variation of specific variables at a particular transverse grid location.
VISC	VISC computes the laminar viscosity. Currently only the constant viscosity option is available.
WALFUN	WALFUN is an auxiliary routine called from BCONW when wall function boundary conditions are required.

PRINCIPAL FORTRAN SYMBOLS

NPOINT	Maximum number of grid points in y direction.
NZ	Maximum number of grid points in z direction, must be .LE. NPOINT.
NX	Maximum number of streamwise computational steps or maximum number of potential lines in geometry file.
MZVAR	The number of different variables stored in the z array.
NIN	The maximum number of lines of data for a transverse plane which may be in core at one time.
MLEVEL	The number of levels of the dependent variables which are stored in the z array.
NGEOMV	The number of different geometric variables stored in the FG array at each y direction grid point.
CMUT	The constant c_μ in the turbulent viscosity relationship.
CCON1	The constant, c_1 in the turbulence dissipation equation.
CCON2	The constant c_2 in the turbulence dissipation equation.
SIGK	The constant σ_K in the turbulence kinetic energy equation.
SIGE	The constant σ_ϵ in the turbulence dissipation equation.
I2EQMD	Flag indicating use of the two-equation turbulence model.
MUT	z array index for turbulent viscosity.
MU	z array index for laminar viscosity.
NTAU	z array index for the velocity gradient term appearing in the turbulence equations production term.

NLEN	z array index for local length scale.
NRHO	z array index for density.
NV1	z array index for streamwise component of velocity.
NV2	z array index for viscous v velocity (=0.).
NV3	z array index for viscous w velocity (=0.).
NENG	z array index for total enthalpy difference.
NTKE	z array index for turbulnece kinetic energy.
NDIS	z array index for turbulence dissipation.
NVOR	z array index for streamwise vorticity.
NSTR	z array index for secondary flow stream function.
NUI	z array index for inviscid u velocity
NVI	z array index for secondary flow velocity, v_s.
NWI	z array index for secondary flow velocity, w_s.
NCPI	z array index for imposed pressure coefficient.
NPHI	z array index for scalar potential.
NH1	FG array index for h_1.
NH2	FG array index for h_2.
NH3	FG array index for h_3.
NPI	FG array index for inviscid pressure coefficient.
NH12	FG array index for $\partial h_1/\partial y$.
NH21	FG array index for $\partial h_2/\partial x$.
NH31	FG array index for $\partial h_3/\partial x$.
NH32	FG array index for $\partial h_3/\partial y$.
Y(NPOINT,2)	An array containing the distance between transverse grid points in physical space.
X(NX)	An array containing the computational axial location of transverse planes.

AP	Ratio of successive axial spacing for geometric progression axial grid.
YZERO	Reference length.
RREF	Reference radius, equal to YZERO.
UE(NX)	Value of u at NE(1)/2,NE(2)/2 stored for axial plot.
VE(NX)	Value of v_g at NE(1)/2,NE(2)/2 stored for axial plot.
RE(NX)	Value of ρ at NE(1)/2,NE(2)/2 stored for axial plot.
WE(NX)	Value of w_g at NE(1)/2,NE(2)/2 stored for axial plot.
JX	Index for axial station.
NE(2)	An array containing the number of grid points in each transverse direction.
NS	The total number of streamwise steps to be marched.
UZERO	Reference velocity.
RZERO	Reference density.
TZERO	Reference static temperature.
XENTR	Distance from ADD code initial plane to mixer code initial plane.
ILAM	Laminar turbulent flow flag.
ICDIF	A preset wall function boundary condition difference weight flag.
ILAP	A potential flow solver flag.
LX	The number of axial stations in the potential flow solution.
LY	The number of transverse grid points in the potential flow solution.
LSEC	Secondary flow option flag.
NLOBE	The number of points input to describe the lobe shape and boundary layers.
YLOBE(I,J)	An array containing the lobe shape and boundary layer data points.

BLHUB(I,J)	An array containing the hub and shroud boundary layer data points.
IHUB	The number of hub boundary layer data points.
ISHR	The number of shroud boundary layer data points.
ILOBE	A flag used to indicate whether lobe boundary layers are to be considered.
IWAKE	A flag controlling iteration for a wake parameter in the initial boundary layer profiles.
A(MREW,MCOL,NPOINT)	An array containing the block matrix coefficients of the difference equations.
Z(MZVAR,MLEVEL,NPOINT,NIN)	An array containing the in-core values of dependent variables.
AG(NPOINT,9,2)	An array containing the transverse direction difference weights.
AG7	$1./\Delta x$.
AG8	$-1./\Delta x$.
YS(2,2)	An array containing the transverse grid limits.
B	A coefficient in the dimensionless form of the gas law.
AB	A coefficient in the dimensionless form of the gas law.
RM1	The inverse of the Reynolds number.
IJ	A transverse grid index.
PRL	The laminar Prandtl number.
PRT	The turbulent Prandtl number.
ABENG	A coefficient in the energy-temperature relationship.
EZERO	Reference total energy.
GAMCON	The quantity $\gamma/\gamma-1$, where γ = the ratio of specific heats.
CMACH	A reference Mach number.

ZE(MROW,MROW,2) ZF(MROW,MROW,2) ZG(MROW,MROW,2) ZH(MROW,MROW,2)	Dummy arrays used in setting up boundary conditions for coupled systems of equations.
NHIGH	Maximum of NE(1) or NE(2) depending on ADI sweep.
EPS(2)	Grid stretching parameters.
IPLOT	Plot flag.
RG	Gas constant.
CP	Specific heat.
VISCOS	Reference kinematic viscosity.
TSTAG	Reference stagnation temperature.
GAMMA	Ratio of specific heats.
DWT(MROW,4)	Boundary condition coefficient array.
DW	Boundary condition source term.
NCS	Variable indicator in boundary condition routines.
NBCON(MROW,4,NSETS)	Boundary condition specification array.
NBCONC(MROW,4,NSETS)	Boundary condition specification array.
IWALLF	Wall function flag.
XCBC	Axial location where a change in boundary conditions occurs.
ITCNT	Viscous pressure drop iteration index.
ITMAX	Maximum number of pressure-drop iterations allowed.
RUFLUX	Reference mass flux.
FG(NGEOMV,2,NPOINT)	An array containing the needed metric information at the current axial location.
YSAVE(NPOINT,2)	An array containing the computational locations of the transverse grid points.
PEXIT	Pressure used in the thrust calculation.

ZVAR(100,4)	Dummy array used in axial plots.
IRSTIN	Restart flag.
IRSTOT	Restart dump flag.
JRSTIN	Restart file unit number.
JRSTOT	Restart dump file unit number.
NFILE	Sequence number of restart data.
NSAVED	The number of restarts saved on file JRSTOT.
COOR(NPOINT,4)	An array containing the physical locations of the grid points.
COORA(NPOINT)	An array containing the physical value of the axial coordinate at the previous axial step.
USTAR(NPOINT,4)	An array containing the dimensionless friction velocity.
VKC	von Karman's constant.
PCORR(NPOINT)	A dummy array.
IPCOR	Potential flow normalization index.
IAXI	Geometry option flag.
DELMIX	Shear layer thickness.
YCL(NPOINT)	Dummy array used in setting up lobe shape.
USTRM1	Dimensionless velocity of the primary (turbine) stream.
USTRM2	Dimensionless velocity of the secondary (fan) stream.
ESTRM1	Total energy of the primary stream.
ESTRM2	Total energy of the secondary stream.
TU1	Turbulence intensity of the primary stream.
TU2	Turbulence intensity of the secondary stream.
ALEN	Free stream length scale.

USCALE	Metric scale factor.
ICOMP	Run mode flag.
UCOMP(NPOINT)	A dummy array.
IDATA	Starting option flag.
DELHUB	Hub shear layer thickness.
DELSHR	Shroud shear layer thickness.
ICOAX	Starting option flag.
IKECUP	Turbulence model coupling option flag.
IDIS	Turbulence starting option.
IPRN(20)	A 20 bite binary output word.
ICON	Printer contour plot option.
DISTL(2,NPOINT,NPOINT)	An array containing the distance to a surface and the appropriate boundary layer thickness, used in starting.
ATS(NATS,NPOINT)	A dummy array.

CODE ADAPTABILITY

The current MIXER code was written in a form which readily provides a means for adapting the code to changing needs. For example, the interface with the ADD code is performed in subroutine IFACE for the axisymmetric potential solver and in GEOTRB for the basic MIXER calculation. Thus other sources of coordinate generation could be used with the MIXER code through proper modification of these subroutines. Similarly, subroutine MTPROF controls the means of setting initial conditions and can be modified to provide additional starting options and capabilities.

With regard to adapting the MIXER code to a machine other than a UNIVAC 1110, it is noted that the systems routine NTRAN is used to perform most of the reading and writing on mass storage. If the code is to be used on a machine which does not have this system routine, either the routine must be replaced or a subroutine which mimics NTRAN can be written using available system resources. Additionally, PARAMETER and INCLUDE statements are used in many areas of the code to specify dimensions and to access commons. If these statements cannot be used, they must be changed to suit the contemplated machine.

REFERENCES

B-1. Briley, W. R. and H. McDonald: Analysis and Computation of Viscous Subsonic Primary and Secondary Flows. AIAA Paper No. 79-1453, July 1979.

B-2. Douglas, J. and J. E. Gunn: A General Formulation of Alternating Direction Methods, Part I. Parabolic and Hyperbolic Problems. Numerische Mathematik, Vol. 6, 1964, p. 428.

B-3. Launder, B. E. and D. B. Spalding: The Numerical Computation of Turbulent Flows. Computer Methods in Applied Mechanics and Engineering, Vol. 3, 1974, p. 269.

B-4. Kreskovsky, J. P., W. R. Briley and H. McDonald: Development of a Method for Computing Three-Dimensional Subsonic Turbulent Flows in Turbofan Lobe MIXERS. SRA Report R79-300006-8, November 1979.

B-5. McDonald, H. and W. R. Briley: Computational Aspects of Internal Flows. AIAA Paper No. 79-1445, 1979.

B-6. Ralston, A.: A First Course in Numerical Analysis. (McGraw-Hill), 1965, p. 323.

B-7. Lakshminarayana, B. and J. H. Horlock: Generalized Expressions for Secondary Vorticity Using Intrinsic Coordinates. J. Fluid Mech., Vol. 59, 1973, p. 97.

B-8. Anderson, O. L.: User's Manual for a Finite-Difference Calculation of Turbulent Swirling Compressible Flow in Axisymmetric Ducts with Struts and Slot Cooled Walls. USAAMRDL-TR-74-50, Vol. I, 1974.

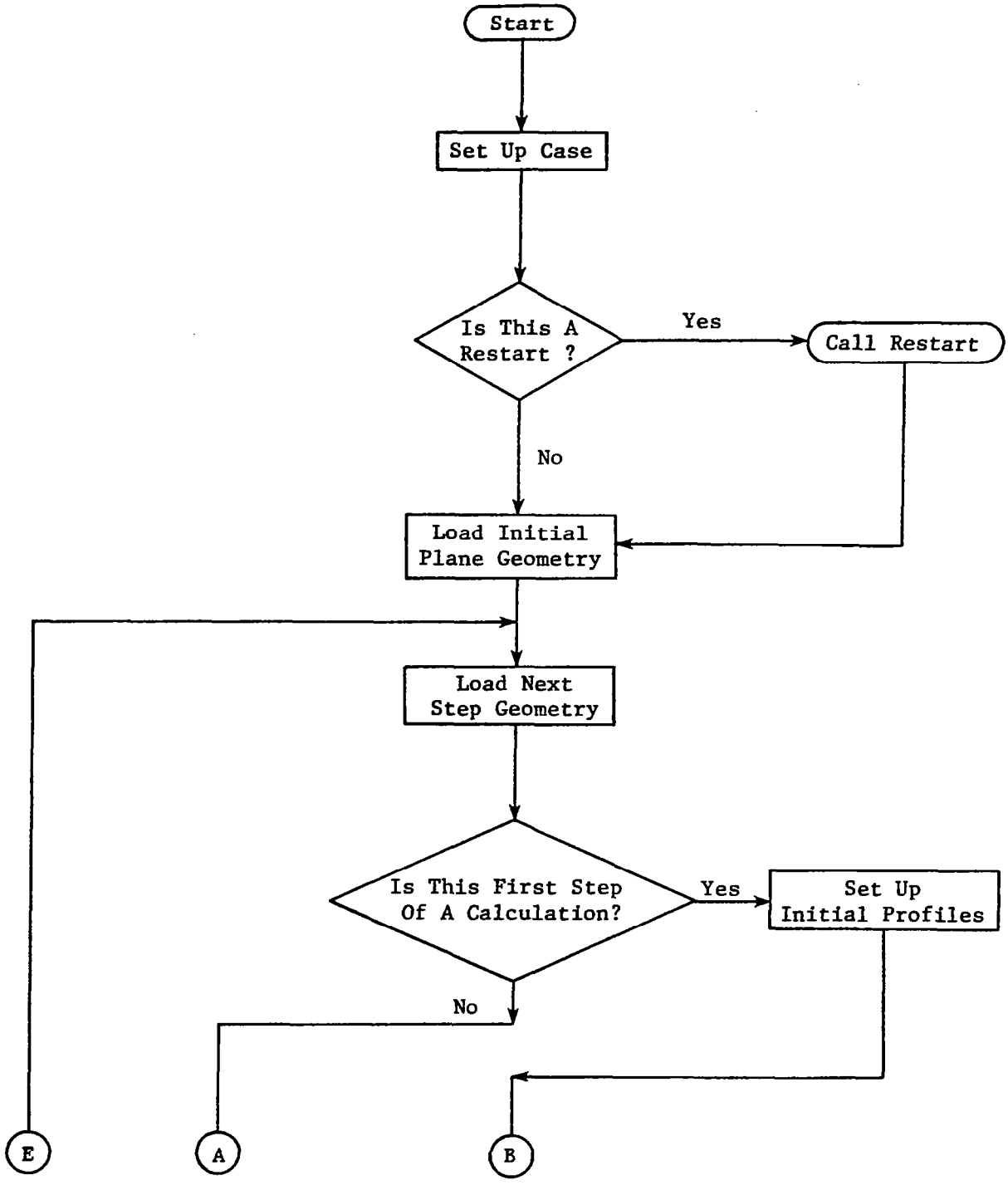

Figure B1.- Flow chart of the Mixer code calculation procedure.

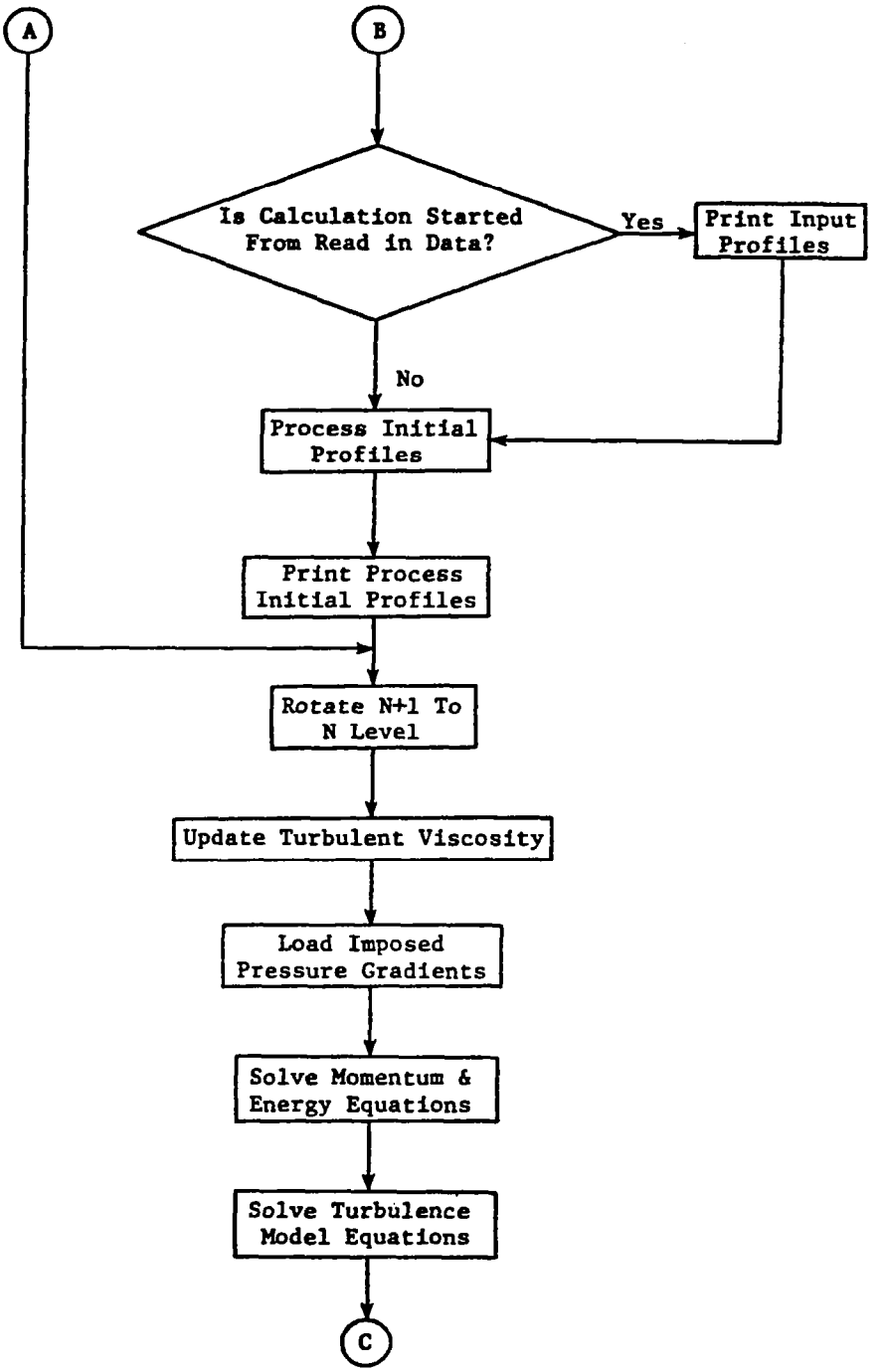

Figure B1. - Continued.

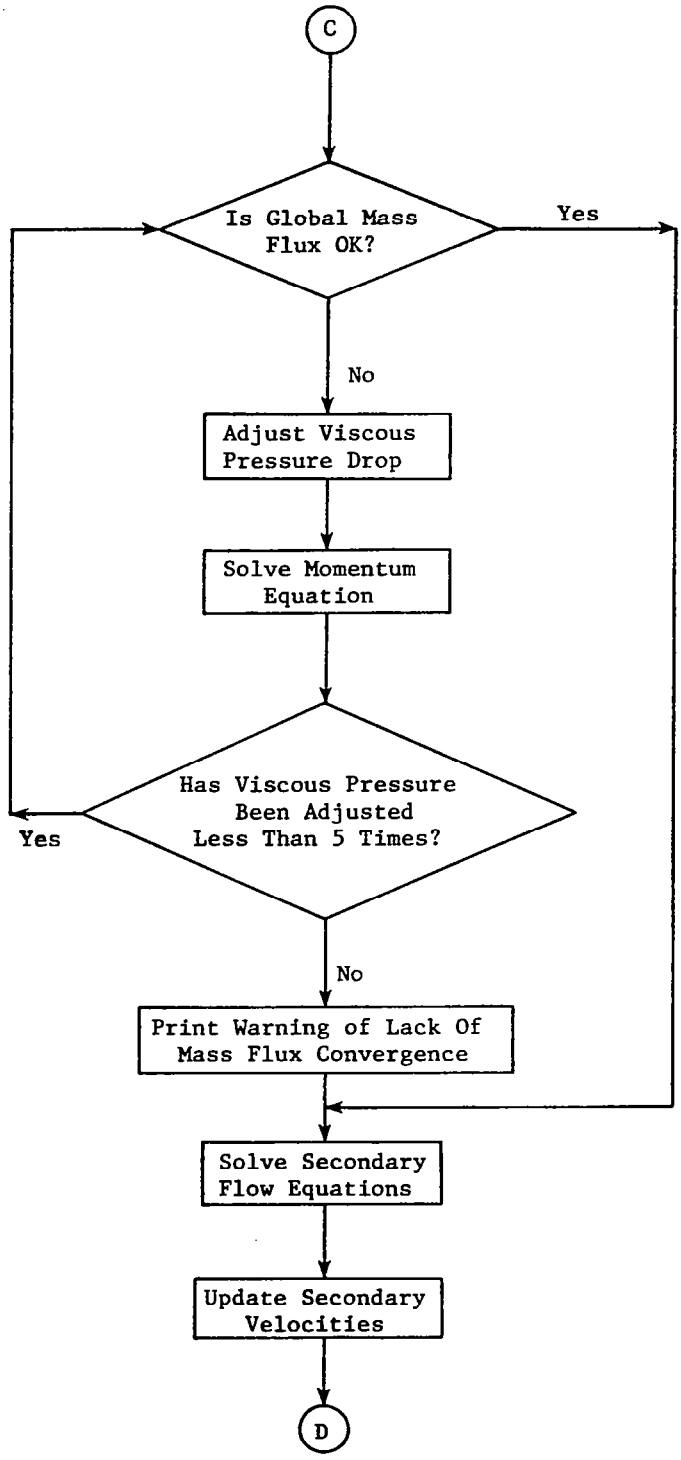

Figure B1.- Continued.

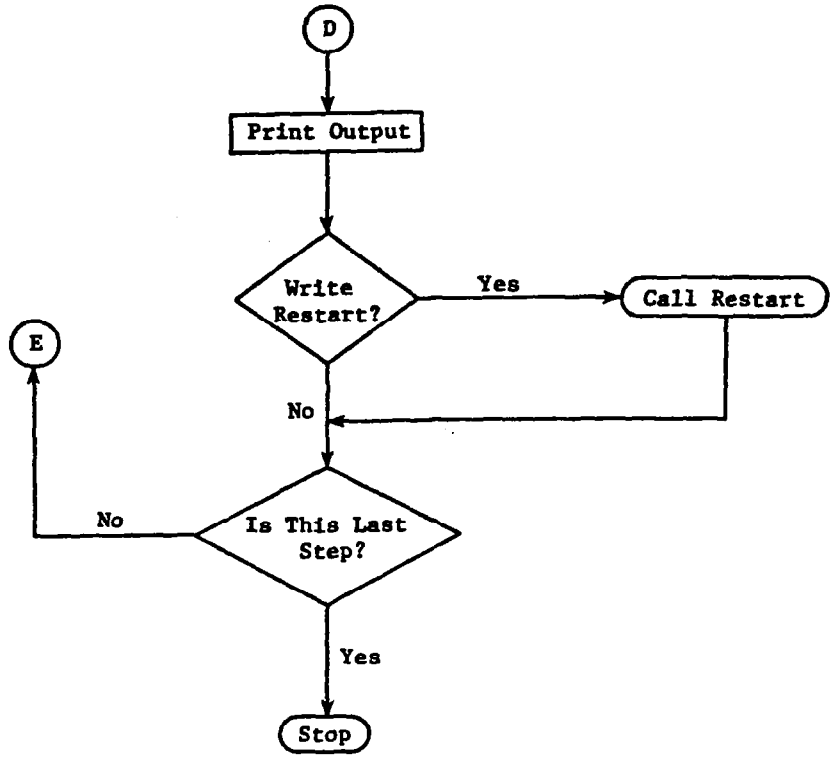

Figure B1.- Concluded.

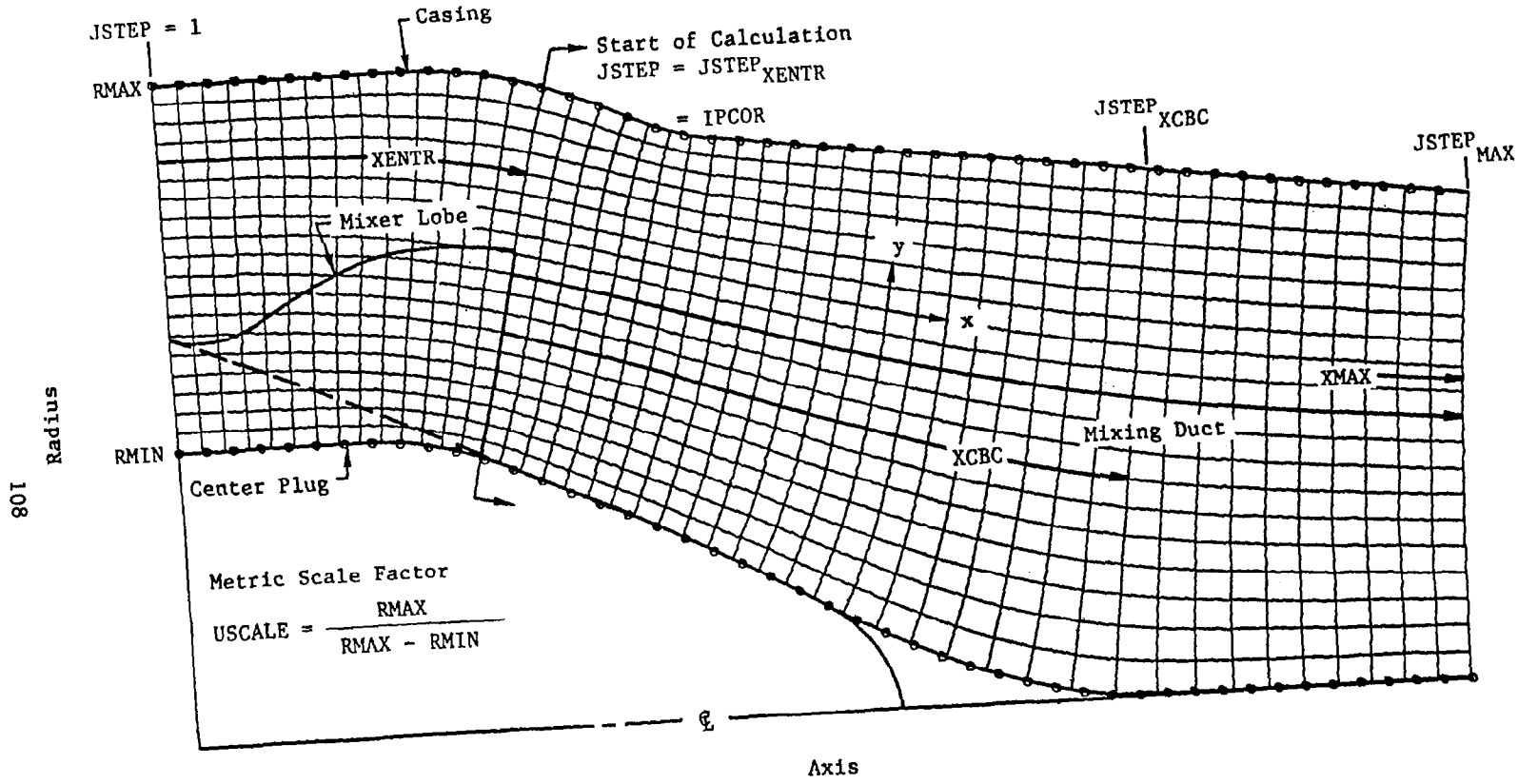

Figure B2.- Typical coordinate system and definition of input parameters.

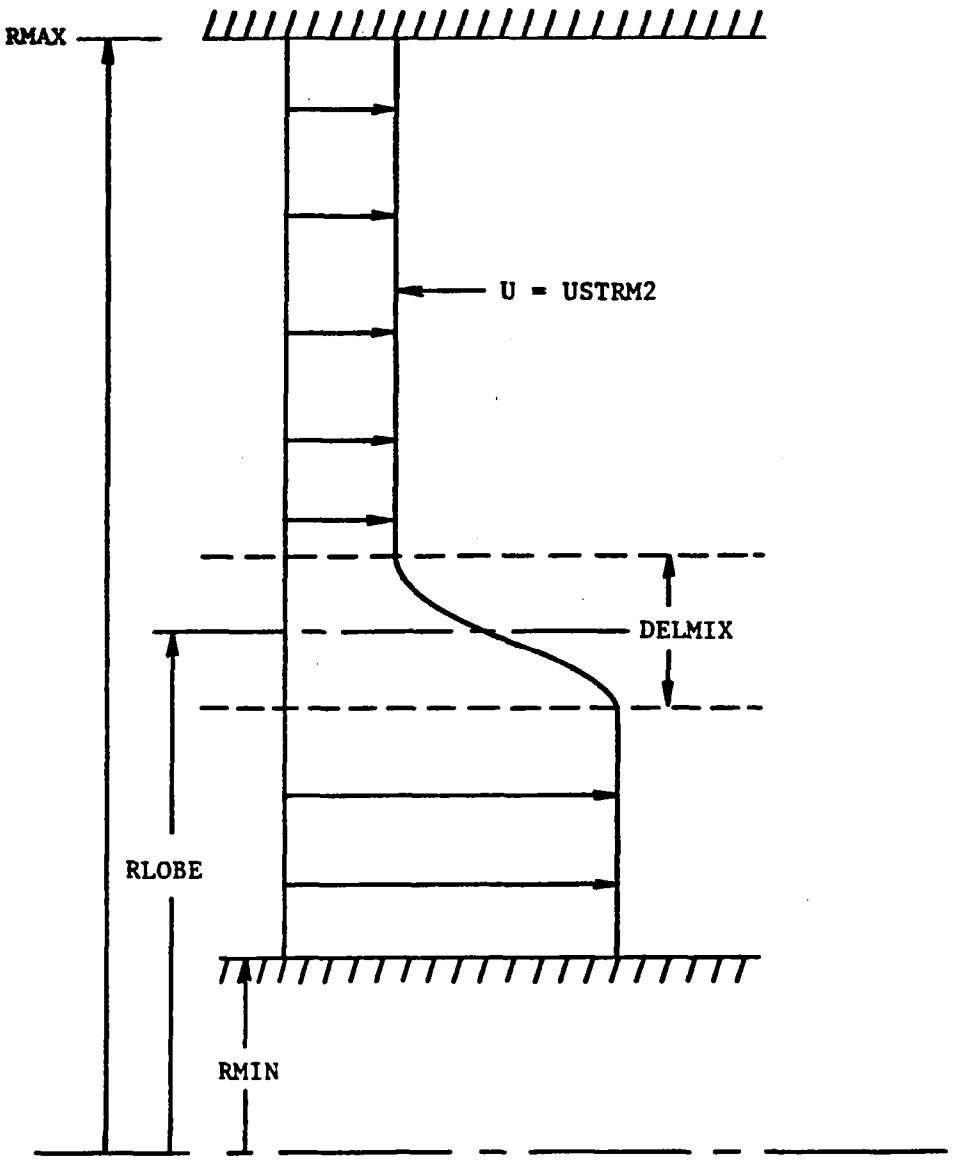

Figure B3.- Definition of input parameters for the ICOAX option.

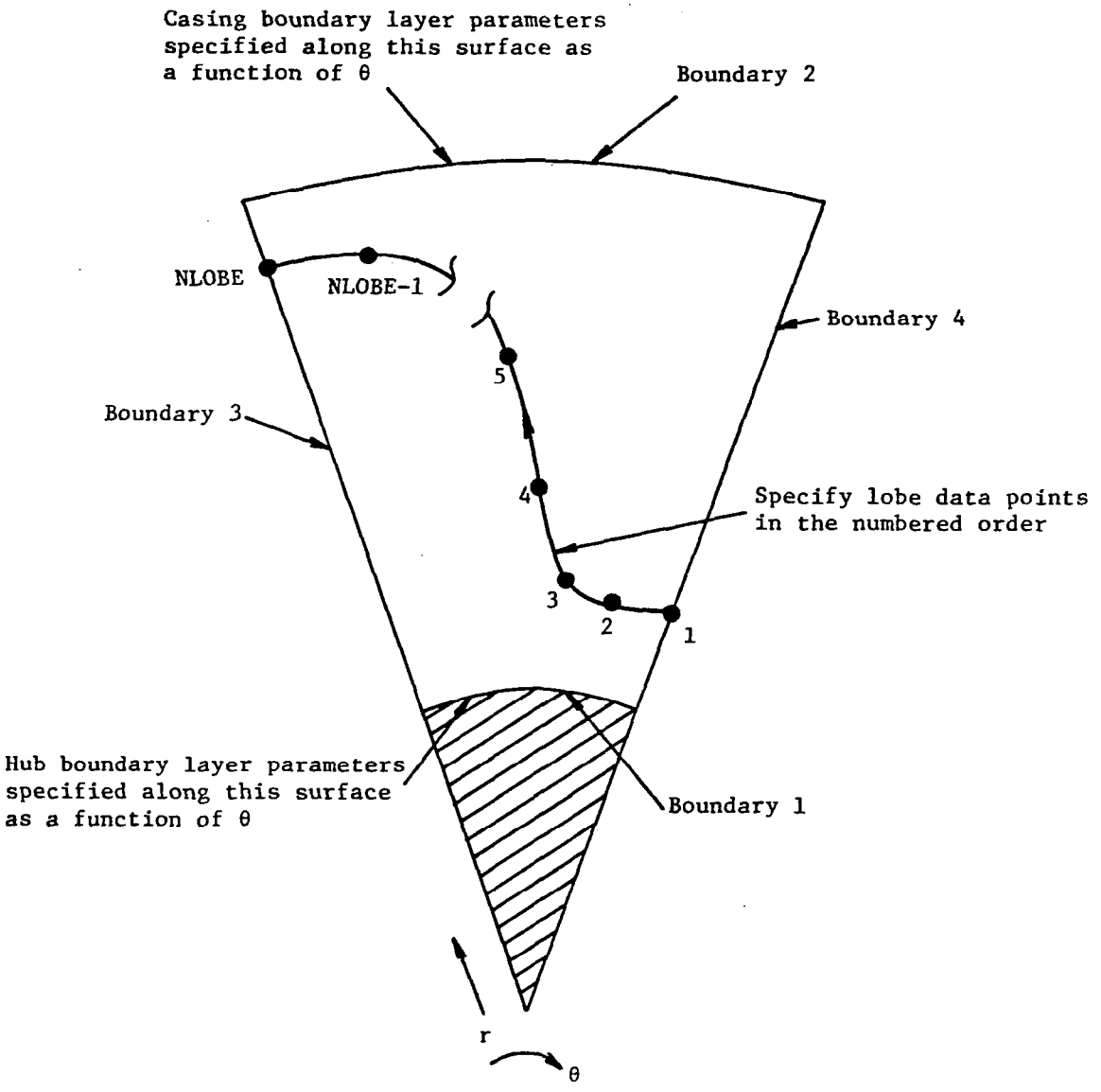

Figure B4.- Specification of the lobe shape and hub and casing boundary layers.

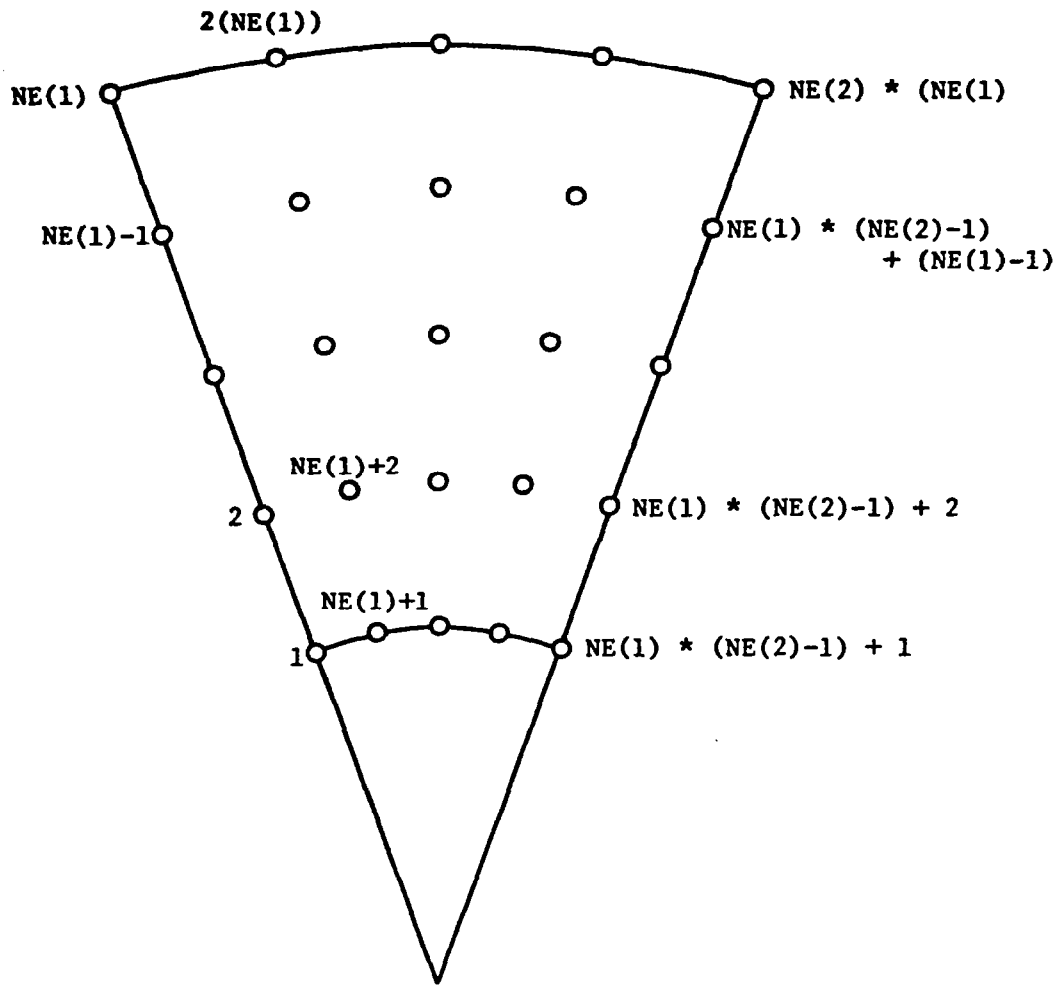

Figure B5. - Ordering of grid points for IDATA option.

```
1       @PRT,S XQTEXA
2       @ASG,T 9,D/50000/TRK/50000
3       @ASG,A A060JK*PDATA5(2),
4       @USE 10,A060JK*PDATA5(2),
5       @ASG,A A060WR*PEPR3,
6       @USE 11,A060WR*PEPR3,
7       @ASG,T 12,D/5000/TRK/5000
8       @ASG,T 13,D/5000/TRK/5000
9       @ASG,T 14,D/5000/TRK/5000
10      @XQT ABS
11          TEST COLD FLOW
12      24   2.
13       $IN1
14         TZERO = 520., UZERO = 325., PZERO1 = 5220., YZERO = .3, VISC1 = .369E-6,
15       $END
16       $IN2
17         ICOMP = 0, XENTR = 1.52361, YS = .382, 1., 0., .2618, NE = 20, 10,
18         NS=2, AP=-1., ILAP=1, LX=50, LY=20, IPCOR=12,IDIS=1,
19         X = 0., .06, .13, .19, .27, .36, .46, .57, .68, .8, .95, 1.1, 1.25,
20        1.4, 1.55, 1.7, 1.85, 2., 2.15, 2.3944,
21       $END
22       $IN3
23         IRSTIN = 00, IRSTOT = 99, NFILE = 0, NSAVED = 0, IPLOT = 0,
24       $END
25       $IN4
26         USTRM2 = .5, TSTRM2 = 1., AMEXIT = .9, TUSTR1 = .05, TUSTR2 = .00
27         ALEN = .006,
28       $END
29       $IN5
30         NLOBE = 5,
31            YLOBE = .435, .445, .72, .843, .85, 45*0.,
32                    .2618, .19635, .1309, .06545, 46*0.,
33         100*.003, 100*1.4,
34         ILOBE = 2, IHUB = 2, ISHR = 2,
35         BLHUB = -.0001, .2619, 18*0., 2*.006, 18*0., 2*1.4, 18*0.,
36        -.0001, .2619, 18*0., 2*.008, 18*0., 2*1.5, 18*0.,
37       $END
38       $IN6
39         NBCON(1,1,1) = 4, NBCON(1,2,1) = 4, NBCON(1,3,1) = 1,
40         NBCON(1,4,1) = 1, NBCON(2,1,1) = 1, NBCON(2,2,1) = 1,
41         NBCON(2,3,1) = 1, NBCON(2,4,1) = 1,
42         NBCON(2,1,2) = 4, NBCON(2,2,2) = 4,
43         NBCONC(1,1,1) = 1, NBCONC(2,1,2) = 1,
44         XCRC = 1.3A,
45       $END
46       $IN7
47         IPRN = 1,1,1,0,0,1,1,1,0,6*0,0,4*0,
48         ICON = 0,
49       $END
```

Figure B6. - Sample UNIVAC 1110 run stream.

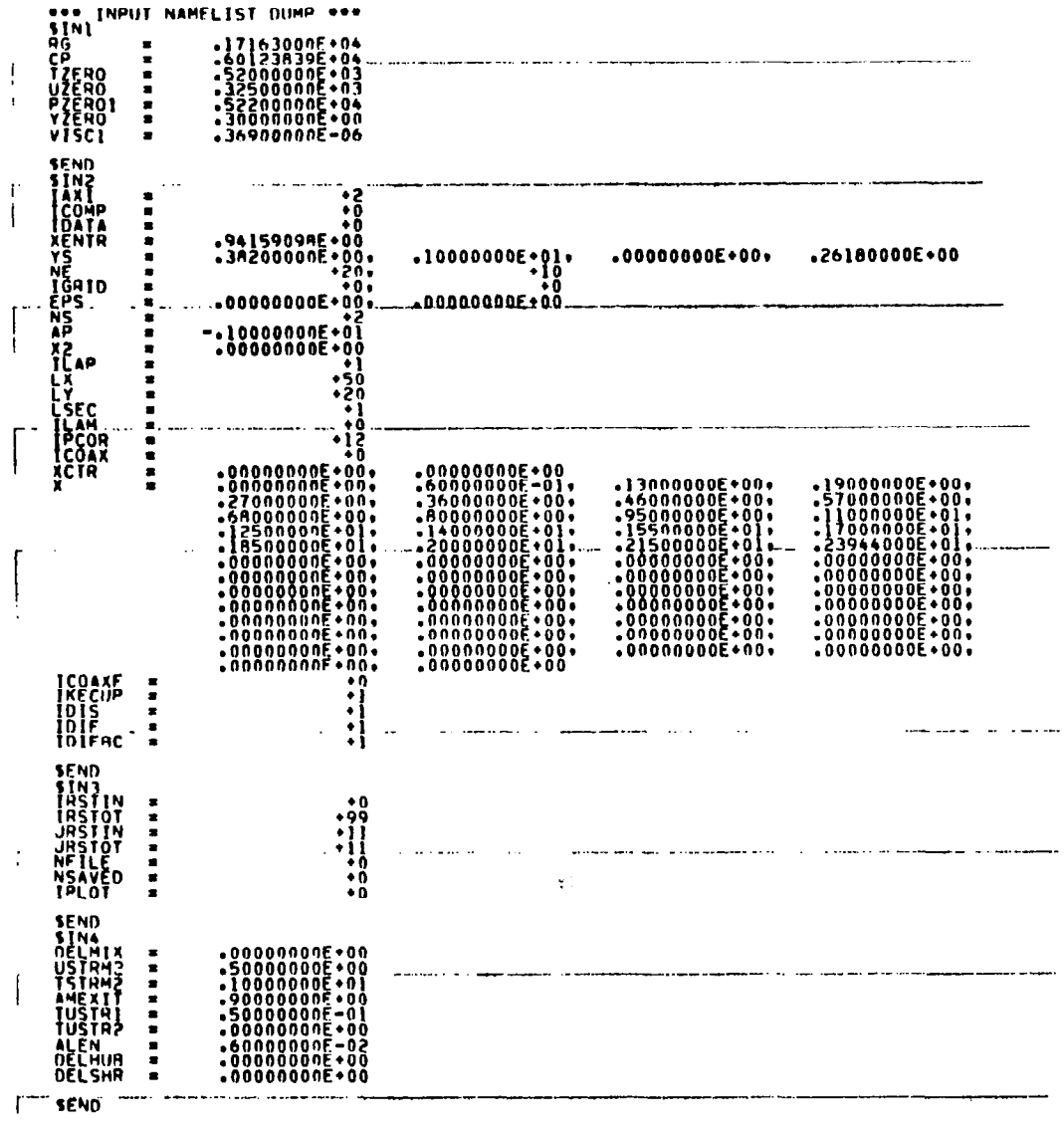

```
*** INPUT NAMELIST DUMP ***
$IN1
RG      =      .17163000E+04
CP      =      .60123839E+04
TZERO   =      .52000000E+03
UZERO   =      .32500000E+03
PZERO1  =      .52200000E+04
YZERO   =      .30000000E+00
VISC1   =      .36900000E-06

$END
$IN2
IAXI    =                 +2
ICOMP   =                 +0
IDATA   =                 +0
XENTR   =      .94159098E+00
YS      =      .38200000E+00,    .10000000E+01,    .00000000E+00,    .26180000E+00
NF      =                +20,              +10
IGRID   =                 +0,               +0
EPS     =      .00000000E+00,    .00000000E+00
NS      =                 +2
AP      =     -.10000000E+01
X2      =      .00000000E+00
ILAP    =                 +1
LX      =                +50
LY      =                +20
LSEC    =                 +1
ILAM    =                 +0
IPCOR   =                +12
ICOAX   =                 +0
XCTR    =      .00000000E+00,    .00000000E+00
X       =      .00000000E+00,    .60000000E-01,    .13000000E+00,    .19000000E+00,
               .27000000E+00,    .36000000E+00,    .46000000E+00,    .57000000E+00,
               .68000000E+00,    .80000000E+00,    .95000000E+00,    .11000000E+01,
               .12500000E+01,    .14000000E+01,    .15500000E+01,    .17000000E+01,
               .18500000E+01,    .20000000E+01,    .21500000E+01,    .23944000E+01,
               .00000000E+00,    .00000000E+00,    .00000000E+00,    .00000000E+00,
               .00000000E+00,    .00000000E+00,    .00000000E+00,    .00000000E+00,
               .00000000E+00,    .00000000E+00,    .00000000E+00,    .00000000E+00,
               .00000000E+00,    .00000000E+00,    .00000000E+00,    .00000000E+00,
               .00000000E+00,    .00000000E+00,    .00000000E+00,    .00000000E+00,
               .00000000E+00,    .00000000E+00,    .00000000E+00,    .00000000E+00,
               .00000000E+00,    .00000000E+00
ICOAXF  =                 +0
IRECUP  =                 +1
IDIS    =                 +1
IDIF    =                 +1
IDIFAC  =                 +1

$END
$IN3
IRSTIN  =                 +0
IRSTOT  =                +99
JRSTIN  =                +11
JRSTOT  =                +11
NFILE   =                 +0
NSAVED  =                 +0
IPLOT   =                 +0

$END
$IN4
DELMIX  =      .00000000E+00
USTRM2  =      .50000000E+00
TSTRM2  =      .10000000E+01
AMEXIT  =      .90000000E+00
IUSTR1  =      .50000000E-01
IUSTR2  =      .00000000E+00
ALEN    =      .60000000E-02
DELMUB  =      .00000000E+00
DELSHR  =      .00000000E+00

$END
```

Figure B7. - Output dump of NAMELIST input.

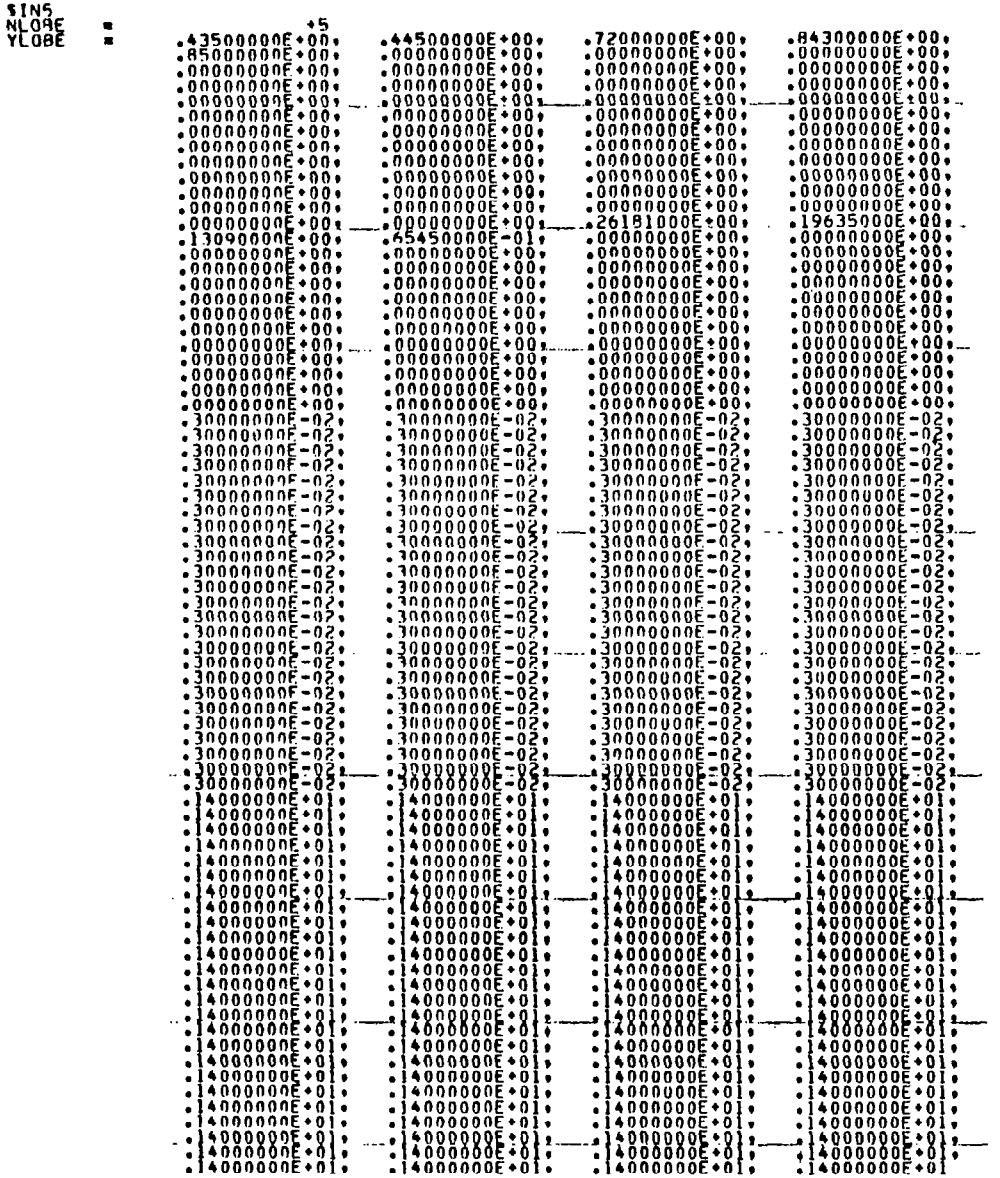

Figure B7. - Continued.

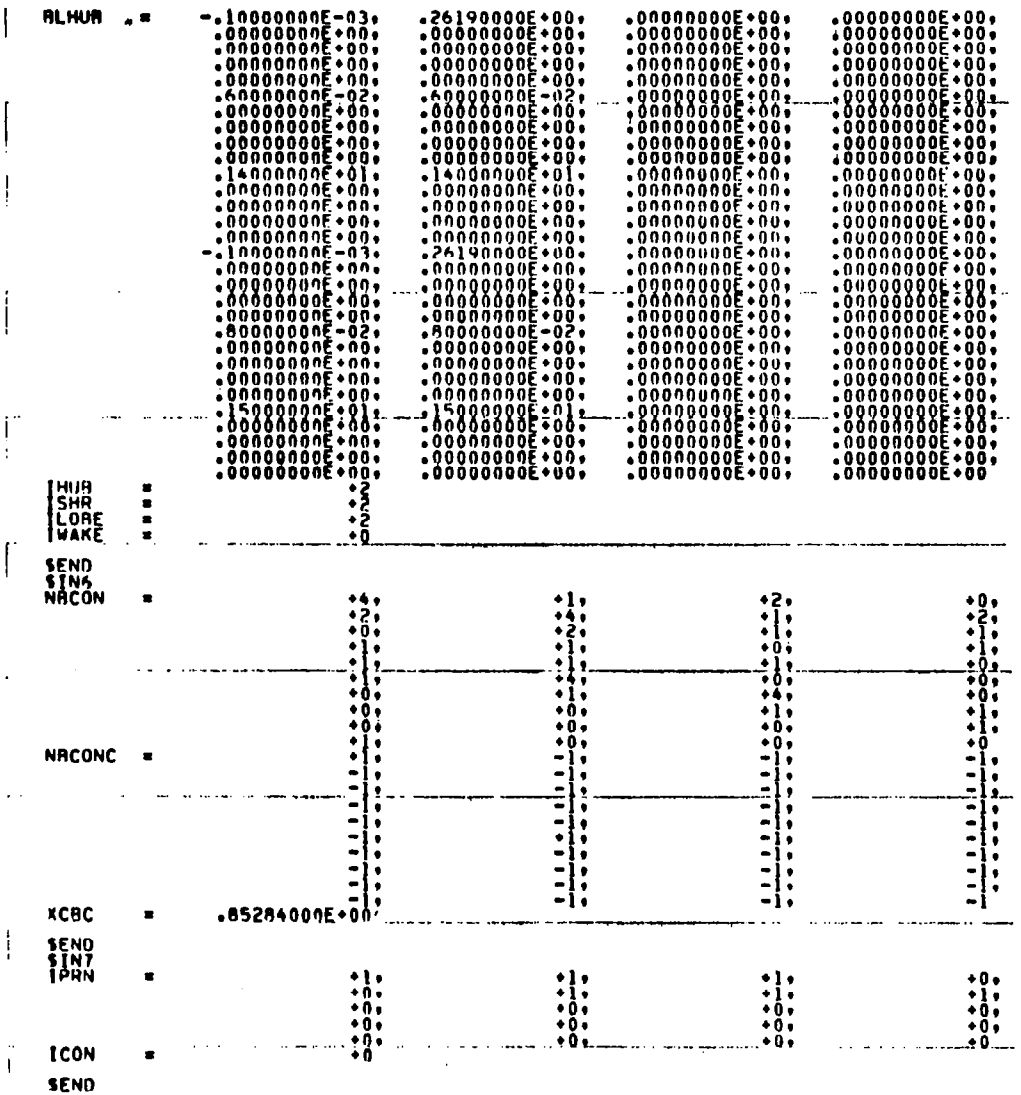

Figure B7. - Concluded.

```
**** SUMMARY OF INPUT DATA ****

*** LOBE AND MIXING DUCT DESCRIPTION ***

** INPUT COORDINATES OF LOBE, R-THETA **
  RADIUS, (DIMENSIONLESS) =    .53500+00   THETA, (RADIANS) =    .25181+00
  RADIUS, (DIMENSIONLESS) =    .49500+00   THETA, (RADIANS) =    .13635+00
  RADIUS, (DIMENSIONLESS) =    .72000+00   THETA, (RADIANS) =    .13090+00
  RADIUS, (DIMENSIONLESS) =    .94300+00   THETA, (RADIANS) =    .65450-01
  RADIUS, (DIMENSIONLESS) =    .85000+00   THETA, (RADIANS) =    .00000

** INPUT DESCRIBING MIXING DUCT **

INITIAL MIXING DUCT OUTER RADIUS (DIMENSIONLESS) =    .10000+01
INITIAL PLUG RADIUS (DIMENSIONLESS) =    .38200+00
DISTANCE FROM MIXING DUCT INLET TO MIXER DUMP PLANE, XENTR (DIMENSIONLESS) =    .94159+00
METRIC SCALE FACTOR =    .16181+01

*** REFERENCE FLOW CONDITIONS ***

REF VELOCITY, VZERO (FT/SEC) =    .32500+03
REF STATIC PRESSURE, PZERO) (LBF/FT**2)=    .52200+04
REF STATIC TEMPERATURE, TZERO (DEG-R) =    .52000+03
REF DENSITY, RZERO (SLUGS/FT**3) =    .58689-02
REF VISCOSITY, VISC) (SLUGS/FT-SEC) =    .36900-06
REF MACH NO =    .29080+00
REYNOLDS NO =    .15454+07
REF LENGTH, VZERO (FT) =    .30000+00
REF STAGNATION PRESSURE (LBF/FT**2) =    .55355+04
REF STAGNATION TEMPERATURE (DEG-R) =    .52478+03

*** INLET FLOW AND TURBULENCE PARAMETERS ***

VELOCITY RATIO =    .50000+00
TEMPERATURE RATIO =    .10000+01
TOTAL PRESSURE RATIO =    .95703+00
TURBULENCE INTENSITIES, STREAM 1=    .50000-01 STREAM 2=    .00000
FREE STREAM LENGTH SCALE =    .60000-02
NOTE- IF STREAM 2 TURB INTENSITY IS 0. , BOTH STREAMS ARE ASSIGNED THE STREAM 1 VALUE.

*** COMPUTATIONAL OPTIONS ***
IAXI =  2
IDATA =  0
ICOMP =  0
LSEC =  1
ILAM =  0
ILAP =  1 WITH LX = 50  LY = 20 AND IPCOR= 12
IHUB=  2
ISHR=  2
ILOBE=  2
IWAKE=  0
ICOAX=  0
IKECUP=  1
IDIS=  1
IDIF=  1
IDIFBC=  1
```

Figure B8. - Input data summary table.

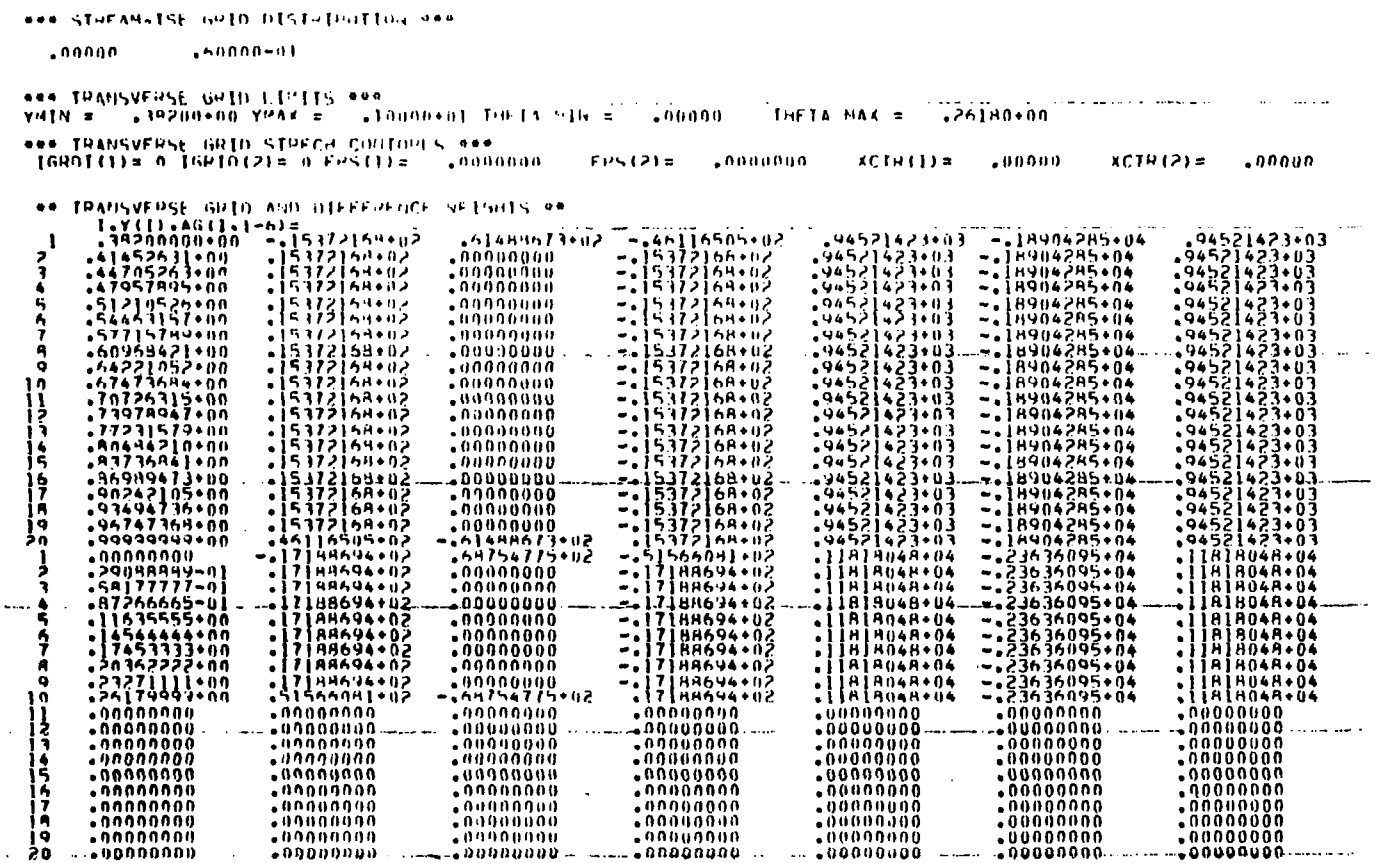

```
*** STREAMWISE GRID DISTRIBUTION ***

  .00000       .50000-01

*** TRANSVERSE GRID LIMITS ***
YMIN =   .19200+00 YMAX =   .10000+01 THETA MIN =   .00000    THETA MAX =   .26180+00

*** TRANSVERSE GRID SPACE CONTROLS ***
 IGRD1(1)= 0 IGRID(2)= 0 EPS(1)=   .0000000    EPS(2)=   .0000000    XCTR(1)=   .00000    XCTR(2)=   .00000

 ** TRANSVERSE GRID AND DIFFERENCE WEIGHTS **
     I,Y(I),AG(I),1-G)=
  1   .39200000+00  -.15372168+02   .61488673+02  -.46116505+02   .94521423+03  -.18904285+04   .94521423+03
  2   .41652631+00   .15372168+02   .00000000  -.15372168+02   .94521423+03  -.18904285+04   .94521423+03
  3   .44105263+00   .15372168+02   .00000000  -.15372168+02   .94521423+03  -.18904285+04   .94521423+03
  4   .47957895+00   .15372168+02   .00000000  -.15372168+02   .94521423+03  -.18904285+04   .94521423+03
  5   .51210526+00   .15372168+02   .00000000  -.15372168+02   .94521423+03  -.18904285+04   .94521423+03
  6   .54463157+00   .15372168+02   .00000000  -.15372168+02   .94521423+03  -.18904285+04   .94521423+03
  7   .57715789+00   .15372168+02   .00000000  -.15372168+02   .94521423+03  -.18904285+04   .94521423+03
  8   .60959421+00   .15372168+02   .00000000  -.15372168+02   .94521423+03  -.18904285+04   .94521423+03
  9   .64221052+00   .15372168+02   .00000000  -.15372168+02   .94521423+03  -.18904285+04   .94521423+03
 10   .67473684+00   .15372168+02   .00000000  -.15372168+02   .94521423+03  -.18904285+04   .94521423+03
 11   .70726315+00   .15372168+02   .00000000  -.15372168+02   .94521423+03  -.18904285+04   .94521423+03
 12   .73978947+00   .15372168+02   .00000000  -.15372168+02   .94521423+03  -.18904285+04   .94521423+03
 13   .77231579+00   .15372168+02   .00000000  -.15372168+02   .94521423+03  -.18904285+04   .94521423+03
 14   .80484210+00   .15372168+02   .00000000  -.15372168+02   .94521423+03  -.18904285+04   .94521423+03
 15   .83736841+00   .15372168+02   .00000000  -.15372168+02   .94521423+03  -.18904285+04   .94521423+03
 16   .86989473+00   .15372168+02   .00000000  -.15372168+02   .94521423+03  -.18904285+04   .94521423+03
 17   .90242105+00   .15372168+02   .00000000  -.15372168+02   .94521423+03  -.18904285+04   .94521423+03
 18   .93494736+00   .15372168+02   .00000000  -.15372168+02   .94521423+03  -.18904285+04   .94521423+03
 19   .96747368+00   .15372168+02   .00000000  -.15372168+02   .94521423+03  -.18904285+04   .94521423+03
 20   .99999999+00   .46116505+02  -.61488673+02   .15372168+02   .94521423+03  -.18904285+04   .94521423+03
  1   .00000000  -.17188694+02   .68754775+02  -.51566081+02   .11818048+04  -.23636095+04   .11818048+04
  2   .29098899-01   .17188694+02   .00000000  -.17188694+02   .11818048+04  -.23636095+04   .11818048+04
  3   .58177777-01   .17188694+02   .00000000  -.17188694+02   .11818048+04  -.23636095+04   .11818048+04
  4   .87266665-01   .17188694+02   .00000000  -.17188694+02   .11818048+04  -.23636095+04   .11818048+04
  5   .11635555+00   .17188694+02   .00000000  -.17188694+02   .11818048+04  -.23636095+04   .11818048+04
  6   .14544444+00   .17188694+02   .00000000  -.17188694+02   .11818048+04  -.23636095+04   .11818048+04
  7   .17453333+00   .17188694+02   .00000000  -.17188694+02   .11818048+04  -.23636095+04   .11818048+04
  8   .20362222+00   .17188694+02   .00000000  -.17188694+02   .11818048+04  -.23636095+04   .11818048+04
  9   .23271111+00   .17188694+02   .00000000  -.17188694+02   .11818048+04  -.23636095+04   .11818048+04
 10   .26179999+00   .51566081+02  -.68754775+02   .17188694+02   .11818048+04  -.23636095+04   .11818048+04
 11   .00000000   .00000000   .00000000   .00000000   .00000000   .00000000   .00000000
 12   .00000000   .00000000   .00000000   .00000000   .00000000   .00000000   .00000000
 13   .00000000   .00000000   .00000000   .00000000   .00000000   .00000000   .00000000
 14   .00000000   .00000000   .00000000   .00000000   .00000000   .00000000   .00000000
 15   .00000000   .00000000   .00000000   .00000000   .00000000   .00000000   .00000000
 16   .00000000   .00000000   .00000000   .00000000   .00000000   .00000000   .00000000
 17   .00000000   .00000000   .00000000   .00000000   .00000000   .00000000   .00000000
 18   .00000000   .00000000   .00000000   .00000000   .00000000   .00000000   .00000000
 19   .00000000   .00000000   .00000000   .00000000   .00000000   .00000000   .00000000
 20   .00000000   .00000000   .00000000   .00000000   .00000000   .00000000   .00000000
```

Figure B9. - Output table of grid and difference weights.

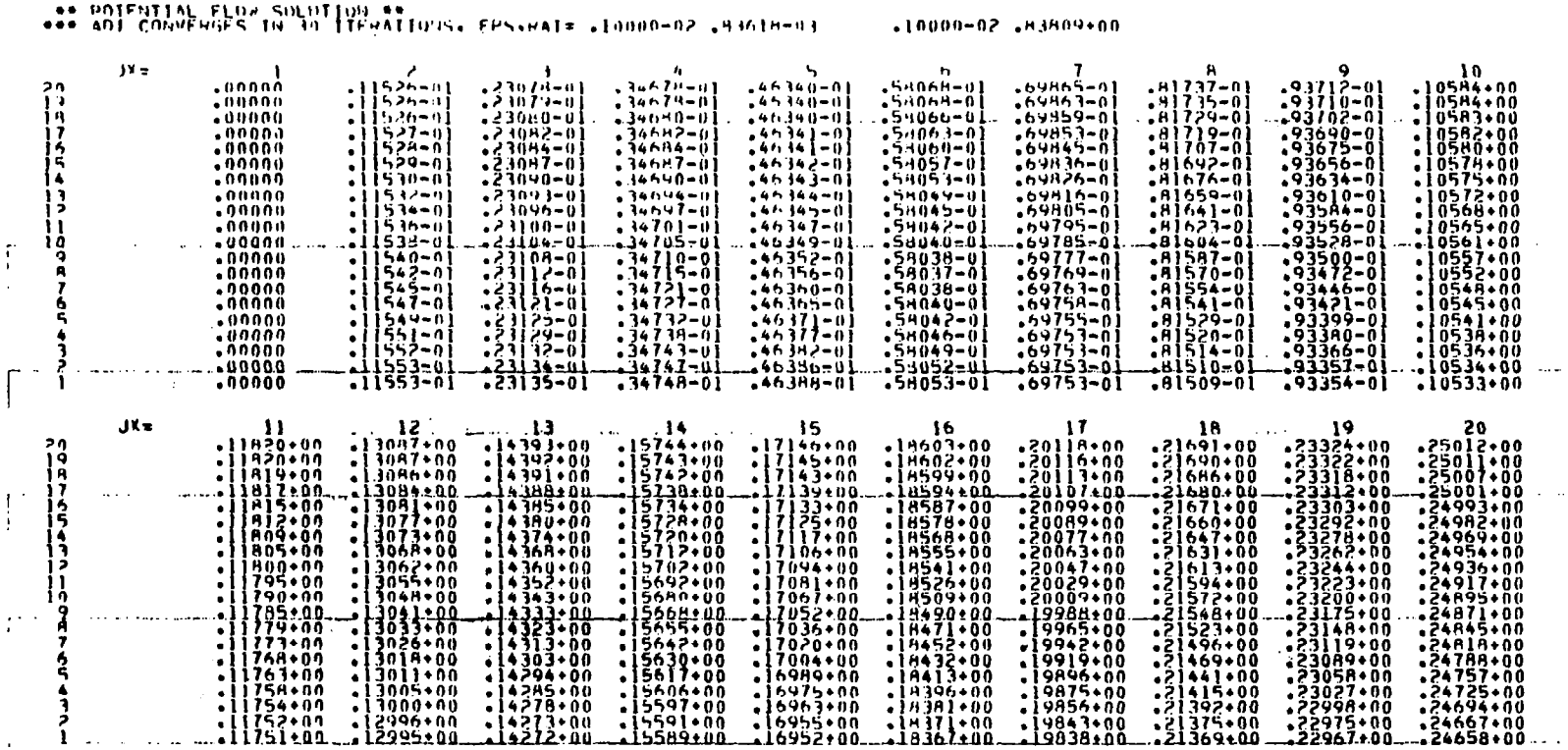

```
 ** POTENTIAL FLOW SOLUTION **
*** ADJ CONVERGES IN 10 ITERATIONS. EPS,MAX= .10000-02 .94618-03      .10000-02 .83809+00

     JK=        1          2          3          4          5          6          7          8          9         10
20           .00000     .11526-01  .23074-01  .34678-01  .46340-01  .58068-01  .69865-01  .81737-01  .93712-01  .10584+00
19           .00000     .11526-01  .23073-01  .34679-01  .46340-01  .58068-01  .69863-01  .81735-01  .93710-01  .10584+00
18           .00000     .11526-01  .23080-01  .34680-01  .46340-01  .58066-01  .69859-01  .81729-01  .93702-01  .10583+00
17           .00000     .11527-01  .23082-01  .34682-01  .46341-01  .58063-01  .69853-01  .81719-01  .93690-01  .10582+00
16           .00000     .11528-01  .23084-01  .34684-01  .46341-01  .58060-01  .69845-01  .81707-01  .93675-01  .10580+00
15           .00000     .11529-01  .23087-01  .34687-01  .46342-01  .58057-01  .69836-01  .81692-01  .93656-01  .10578+00
14           .00000     .11530-01  .23090-01  .34690-01  .46343-01  .58053-01  .69826-01  .81676-01  .93634-01  .10575+00
13           .00000     .11532-01  .23093-01  .34694-01  .46344-01  .58049-01  .69816-01  .81659-01  .93610-01  .10572+00
12           .00000     .11534-01  .23096-01  .34697-01  .46345-01  .58045-01  .69805-01  .81641-01  .93584-01  .10568+00
11           .00000     .11536-01  .23100-01  .34701-01  .46347-01  .58042-01  .69795-01  .81623-01  .93556-01  .10565+00
10           .00000     .11538-01  .23104-01  .34705-01  .46349-01  .58040-01  .69785-01  .81604-01  .93528-01  .10561+00
 9           .00000     .11540-01  .23108-01  .34710-01  .46352-01  .58038-01  .69777-01  .81587-01  .93500-01  .10557+00
 8           .00000     .11542-01  .23112-01  .34715-01  .46356-01  .58037-01  .69769-01  .81570-01  .93472-01  .10552+00
 7           .00000     .11545-01  .23116-01  .34721-01  .46360-01  .58038-01  .69763-01  .81554-01  .93446-01  .10548+00
 6           .00000     .11547-01  .23121-01  .34727-01  .46365-01  .58040-01  .69758-01  .81541-01  .93421-01  .10545+00
 5           .00000     .11549-01  .23125-01  .34732-01  .46371-01  .58042-01  .69755-01  .81529-01  .93399-01  .10541+00
 4           .00000     .11551-01  .23129-01  .34738-01  .46377-01  .58046-01  .69753-01  .81520-01  .93380-01  .10538+00
 3           .00000     .11552-01  .23132-01  .34743-01  .46382-01  .58049-01  .69753-01  .81514-01  .93366-01  .10536+00
 2           .00000     .11553-01  .23134-01  .34747-01  .46386-01  .58052-01  .69753-01  .81510-01  .93357-01  .10534+00
 1           .00000     .11553-01  .23135-01  .34748-01  .46388-01  .58053-01  .69753-01  .81509-01  .93354-01  .10533+00

     JK=        11         12         13         14         15         16         17         18         19         20
20           .11820+00  .13087+00  .14393+00  .15744+00  .17146+00  .18603+00  .20118+00  .21691+00  .23324+00  .25012+00
19           .11820+00  .13087+00  .14392+00  .15743+00  .17145+00  .18602+00  .20116+00  .21690+00  .23322+00  .25011+00
18           .11819+00  .13086+00  .14391+00  .15742+00  .17143+00  .18599+00  .20113+00  .21686+00  .23318+00  .25007+00
17           .11817+00  .13084+00  .14388+00  .15738+00  .17139+00  .18594+00  .20107+00  .21680+00  .23312+00  .25001+00
16           .11815+00  .13081+00  .14385+00  .15734+00  .17133+00  .18587+00  .20099+00  .21671+00  .23303+00  .24993+00
15           .11812+00  .13077+00  .14380+00  .15728+00  .17125+00  .18578+00  .20089+00  .21660+00  .23292+00  .24982+00
14           .11809+00  .13073+00  .14374+00  .15720+00  .17117+00  .18568+00  .20077+00  .21647+00  .23278+00  .24969+00
13           .11805+00  .13068+00  .14368+00  .15712+00  .17106+00  .18555+00  .20063+00  .21631+00  .23262+00  .24954+00
12           .11800+00  .13062+00  .14360+00  .15702+00  .17094+00  .18541+00  .20047+00  .21613+00  .23244+00  .24936+00
11           .11795+00  .13055+00  .14352+00  .15692+00  .17081+00  .18526+00  .20029+00  .21594+00  .23223+00  .24917+00
10           .11790+00  .13048+00  .14343+00  .15680+00  .17067+00  .18509+00  .20009+00  .21572+00  .23200+00  .24895+00
 9           .11785+00  .13041+00  .14333+00  .15668+00  .17052+00  .18490+00  .19988+00  .21548+00  .23175+00  .24871+00
 8           .11779+00  .13033+00  .14323+00  .15655+00  .17036+00  .18471+00  .19965+00  .21523+00  .23148+00  .24845+00
 7           .11773+00  .13026+00  .14313+00  .15642+00  .17020+00  .18452+00  .19942+00  .21496+00  .23119+00  .24818+00
 6           .11768+00  .13018+00  .14303+00  .15630+00  .17004+00  .18432+00  .19919+00  .21469+00  .23089+00  .24788+00
 5           .11763+00  .13011+00  .14294+00  .15617+00  .16989+00  .18413+00  .19896+00  .21441+00  .23058+00  .24757+00
 4           .11758+00  .13005+00  .14285+00  .15606+00  .16975+00  .18396+00  .19875+00  .21415+00  .23027+00  .24725+00
 3           .11754+00  .13000+00  .14278+00  .15597+00  .16963+00  .18381+00  .19856+00  .21392+00  .22998+00  .24694+00
 2           .11752+00  .12996+00  .14273+00  .15591+00  .16955+00  .18371+00  .19843+00  .21375+00  .22975+00  .24667+00
 1           .11751+00  .12995+00  .14272+00  .15589+00  .16952+00  .18367+00  .19838+00  .21369+00  .22967+00  .24658+00
```

Figure B10. - Potential flow solution print out.

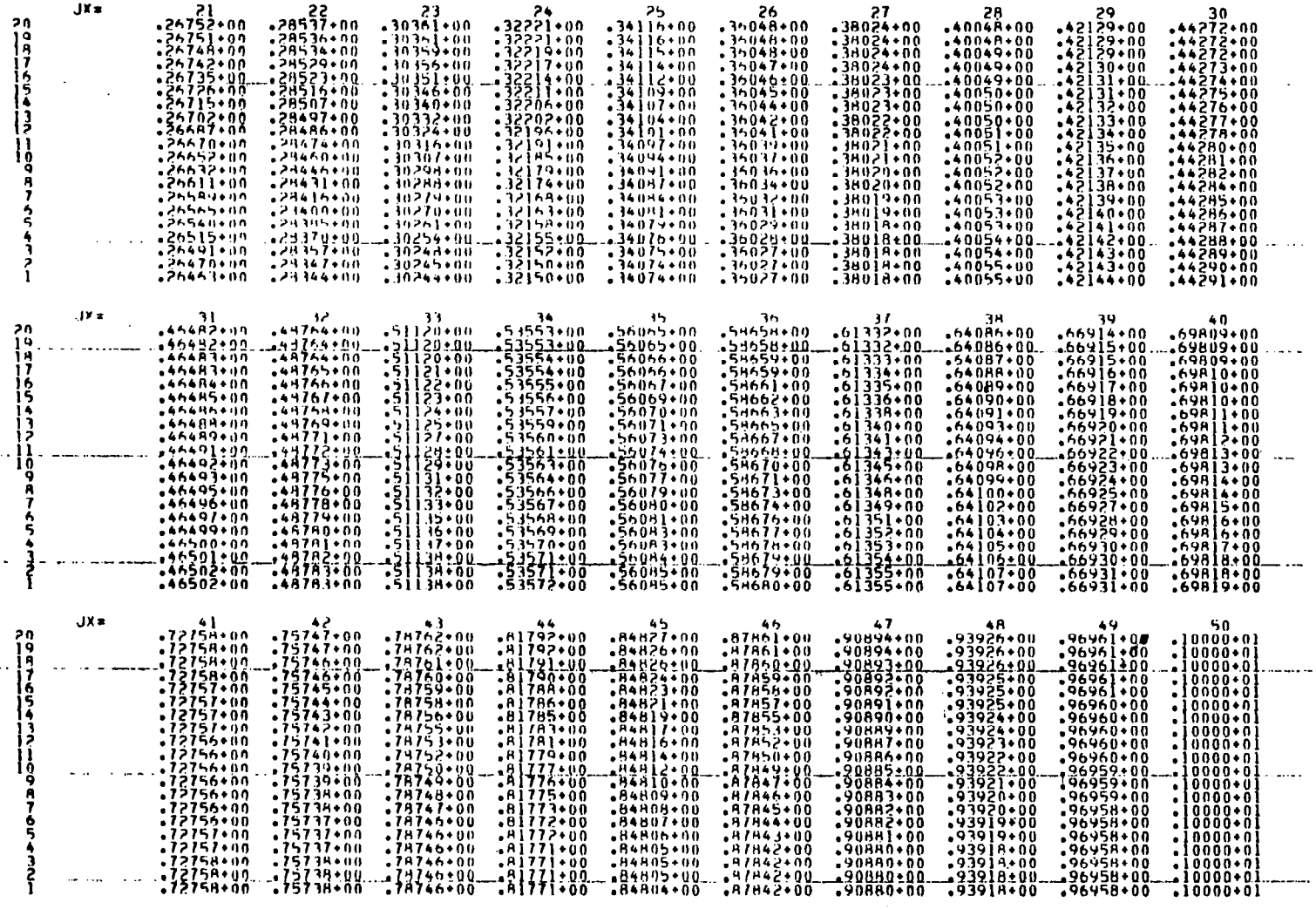

JX=	21	22	23	24	25	26	27	28	29	30
20	.26752+00	.28537+00	.30361+00	.32221+00	.34116+00	.36048+00	.38024+00	.40048+00	.42129+00	.44272+00
19	.26751+00	.28536+00	.30361+00	.32221+00	.34116+00	.36048+00	.38024+00	.40048+00	.42129+00	.44272+00
18	.26748+00	.28534+00	.30359+00	.32219+00	.34115+00	.36048+00	.38024+00	.40049+00	.42129+00	.44272+00
17	.26742+00	.28529+00	.30356+00	.32217+00	.34114+00	.36047+00	.38024+00	.40049+00	.42130+00	.44273+00
16	.26735+00	.28523+00	.30351+00	.32214+00	.34112+00	.36046+00	.38023+00	.40049+00	.42131+00	.44274+00
15	.26726+00	.28516+00	.30346+00	.32211+00	.34109+00	.36045+00	.38023+00	.40050+00	.42131+00	.44275+00
14	.26715+00	.28507+00	.30340+00	.32206+00	.34107+00	.36044+00	.38023+00	.40050+00	.42132+00	.44276+00
13	.26702+00	.28497+00	.30332+00	.32202+00	.34104+00	.36042+00	.38022+00	.40050+00	.42133+00	.44277+00
12	.26687+00	.28486+00	.30324+00	.32196+00	.34101+00	.36041+00	.38022+00	.40051+00	.42134+00	.44278+00
11	.26670+00	.28474+00	.30316+00	.32191+00	.34097+00	.36039+00	.38021+00	.40051+00	.42135+00	.44280+00
10	.26652+00	.28460+00	.30307+00	.32185+00	.34094+00	.36037+00	.38021+00	.40052+00	.42136+00	.44281+00
9	.26632+00	.28446+00	.30298+00	.32179+00	.34091+00	.36036+00	.38020+00	.40052+00	.42137+00	.44282+00
8	.26611+00	.28431+00	.30288+00	.32174+00	.34087+00	.36034+00	.38020+00	.40052+00	.42138+00	.44284+00
7	.26589+00	.28416+00	.30279+00	.32168+00	.34084+00	.36032+00	.38019+00	.40053+00	.42139+00	.44285+00
6	.26565+00	.28400+00	.30270+00	.32163+00	.34081+00	.36031+00	.38019+00	.40053+00	.42140+00	.44286+00
5	.26540+00	.28385+00	.30261+00	.32158+00	.34077+00	.36029+00	.38018+00	.40053+00	.42141+00	.44287+00
4	.26515+00	.28370+00	.30254+00	.32155+00	.34076+00	.36028+00	.38018+00	.40054+00	.42142+00	.44288+00
3	.26491+00	.28357+00	.30248+00	.32152+00	.34075+00	.36027+00	.38018+00	.40054+00	.42143+00	.44289+00
2	.26470+00	.28347+00	.30245+00	.32150+00	.34074+00	.36027+00	.38018+00	.40055+00	.42143+00	.44290+00
1	.26453+00	.28344+00	.30244+00	.32150+00	.34074+00	.36027+00	.38018+00	.40055+00	.42144+00	.44291+00

JX=	31	32	33	34	35	36	37	38	39	40
20	.46482+00	.48764+00	.51120+00	.53553+00	.56065+00	.58658+00	.61332+00	.64086+00	.66914+00	.69809+00
19	.46482+00	.48764+00	.51120+00	.53553+00	.56065+00	.58658+00	.61332+00	.64086+00	.66915+00	.69809+00
18	.46483+00	.48764+00	.51120+00	.53554+00	.56066+00	.58659+00	.61333+00	.64087+00	.66915+00	.69809+00
17	.46483+00	.48765+00	.51121+00	.53554+00	.56066+00	.58659+00	.61334+00	.64088+00	.66916+00	.69810+00
16	.46484+00	.48766+00	.51122+00	.53555+00	.56067+00	.58661+00	.61335+00	.64089+00	.66917+00	.69810+00
15	.46485+00	.48767+00	.51123+00	.53556+00	.56069+00	.58662+00	.61336+00	.64090+00	.66918+00	.69810+00
14	.46486+00	.48768+00	.51124+00	.53557+00	.56070+00	.58663+00	.61338+00	.64091+00	.66919+00	.69811+00
13	.46488+00	.48769+00	.51125+00	.53559+00	.56071+00	.58665+00	.61340+00	.64093+00	.66920+00	.69811+00
12	.46489+00	.48771+00	.51127+00	.53560+00	.56073+00	.58667+00	.61341+00	.64094+00	.66921+00	.69812+00
11	.46491+00	.48772+00	.51128+00	.53561+00	.56074+00	.58668+00	.61343+00	.64096+00	.66922+00	.69813+00
10	.46492+00	.48773+00	.51129+00	.53563+00	.56076+00	.58670+00	.61345+00	.64098+00	.66923+00	.69813+00
9	.46493+00	.48775+00	.51131+00	.53564+00	.56077+00	.58671+00	.61346+00	.64099+00	.66924+00	.69814+00
8	.46495+00	.48776+00	.51132+00	.53566+00	.56079+00	.58673+00	.61348+00	.64100+00	.66925+00	.69814+00
7	.46496+00	.48778+00	.51133+00	.53567+00	.56080+00	.58674+00	.61349+00	.64102+00	.66927+00	.69815+00
6	.46497+00	.48779+00	.51135+00	.53568+00	.56081+00	.58676+00	.61351+00	.64103+00	.66928+00	.69816+00
5	.46499+00	.48780+00	.51136+00	.53569+00	.56083+00	.58677+00	.61352+00	.64104+00	.66929+00	.69816+00
4	.46500+00	.48781+00	.51137+00	.53570+00	.56083+00	.58678+00	.61353+00	.64105+00	.66930+00	.69817+00
3	.46501+00	.48782+00	.51138+00	.53571+00	.56084+00	.58679+00	.61354+00	.64106+00	.66930+00	.69818+00
2	.46502+00	.48783+00	.51138+00	.53571+00	.56085+00	.58679+00	.61355+00	.64107+00	.66931+00	.69818+00
1	.46502+00	.48783+00	.51138+00	.53572+00	.56085+00	.58680+00	.61355+00	.64107+00	.66931+00	.69819+00

JX=	41	42	43	44	45	46	47	48	49	50
20	.72758+00	.75747+00	.78762+00	.81792+00	.84827+00	.87861+00	.90894+00	.93926+00	.96961+00	.10000+01
19	.72758+00	.75747+00	.78762+00	.81792+00	.84826+00	.87861+00	.90894+00	.93926+00	.96961+00	.10000+01
18	.72758+00	.75746+00	.78761+00	.81791+00	.84826+00	.87860+00	.90893+00	.93926+00	.96961+00	.10000+01
17	.72758+00	.75746+00	.78760+00	.81790+00	.84824+00	.87859+00	.90892+00	.93925+00	.96961+00	.10000+01
16	.72757+00	.75745+00	.78759+00	.81788+00	.84823+00	.87858+00	.90892+00	.93925+00	.96961+00	.10000+01
15	.72757+00	.75744+00	.78758+00	.81786+00	.84821+00	.87857+00	.90891+00	.93925+00	.96960+00	.10000+01
14	.72757+00	.75743+00	.78756+00	.81785+00	.84819+00	.87855+00	.90890+00	.93924+00	.96960+00	.10000+01
13	.72757+00	.75742+00	.78755+00	.81783+00	.84817+00	.87853+00	.90889+00	.93924+00	.96960+00	.10000+01
12	.72756+00	.75741+00	.78753+00	.81781+00	.84816+00	.87852+00	.90887+00	.93923+00	.96960+00	.10000+01
11	.72756+00	.75740+00	.78752+00	.81779+00	.84814+00	.87850+00	.90886+00	.93922+00	.96960+00	.10000+01
10	.72756+00	.75739+00	.78750+00	.81777+00	.84812+00	.87849+00	.90885+00	.93922+00	.96959+00	.10000+01
9	.72756+00	.75739+00	.78749+00	.81776+00	.84810+00	.87847+00	.90884+00	.93921+00	.96959+00	.10000+01
8	.72756+00	.75738+00	.78748+00	.81775+00	.84809+00	.87846+00	.90883+00	.93920+00	.96959+00	.10000+01
7	.72756+00	.75738+00	.78747+00	.81773+00	.84808+00	.87845+00	.90882+00	.93920+00	.96958+00	.10000+01
6	.72756+00	.75737+00	.78746+00	.81772+00	.84807+00	.87844+00	.90882+00	.93919+00	.96958+00	.10000+01
5	.72757+00	.75737+00	.78746+00	.81772+00	.84806+00	.87843+00	.90881+00	.93919+00	.96958+00	.10000+01
4	.72757+00	.75737+00	.78746+00	.81771+00	.84805+00	.87842+00	.90880+00	.93918+00	.96958+00	.10000+01
3	.72758+00	.75738+00	.78746+00	.81771+00	.84805+00	.87842+00	.90880+00	.93918+00	.96958+00	.10000+01
2	.72758+00	.75738+00	.78746+00	.81771+00	.84805+00	.87842+00	.90880+00	.93918+00	.96958+00	.10000+01
1	.72758+00	.75738+00	.78746+00	.81771+00	.84804+00	.87842+00	.90880+00	.93918+00	.96958+00	.10000+01

Figure B10. - Continued.

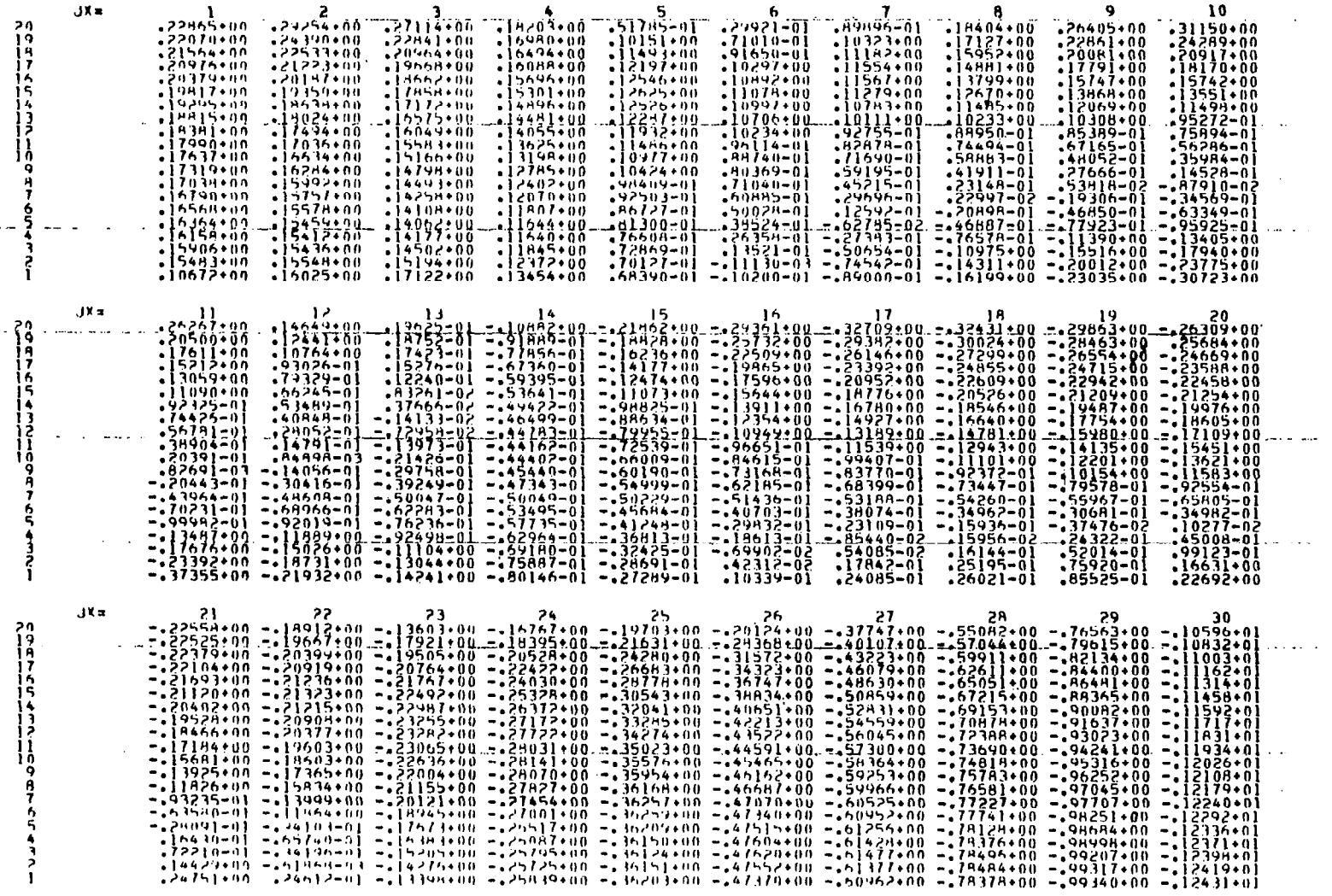

JX=	1	2	3	4	5	6	7	8	9	10
20	.22865+00	.24254+00	.27114+00	.18203+00	.51785-01	.29921-01	.89096-01	.18404+00	.26405+00	.31150+00
19	.22070+00	.24300+00	.22841+00	.16980+00	.10151+00	.71010-01	.10323+00	.17127+00	.22861+00	.24289+00
18	.21564+00	.22533+00	.20964+00	.16494+00	.11493+00	.91650-01	.11182+00	.15952+00	.20081+00	.20917+00
17	.20975+00	.21223+00	.19668+00	.16088+00	.12197+00	.10297+00	.11554+00	.14881+00	.17791+00	.18170+00
16	.20379+00	.20147+00	.18662+00	.15696+00	.12546+00	.10892+00	.11567+00	.13799+00	.15747+00	.15742+00
15	.19817+00	.19159+00	.17858+00	.15301+00	.12625+00	.11078+00	.11279+00	.12670+00	.13868+00	.13551+00
14	.19295+00	.18534+00	.17172+00	.14896+00	.12526+00	.10997+00	.10783+00	.11485+00	.12069+00	.11498+00
13	.18815+00	.18024+00	.16575+00	.14481+00	.12247+00	.10706+00	.10111+00	.10233+00	.10308+00	.95272-01
12	.18381+00	.17494+00	.16049+00	.14055+00	.11932+00	.10234+00	.92755-01	.88950-01	.85389-01	.75894-01
11	.17990+00	.17036+00	.15583+00	.13625+00	.11466+00	.96114-01	.82878-01	.74494-01	.67165-01	.56286-01
10	.17637+00	.16634+00	.15166+00	.13198+00	.10977+00	.88740-01	.71690-01	.58883-01	.48052-01	.35984-01
9	.17319+00	.16244+00	.14798+00	.12785+00	.10424+00	.80369-01	.59195-01	.41911-01	.27666-01	.14528-01
8	.17034+00	.15902+00	.14443+00	.12402+00	.98409-01	.71040-01	.45215-01	.23148-01	.53818-02	-.87910-02
7	.16790+00	.15757+00	.14258+00	.12070+00	.92503-01	.60885-01	.29696-01	.22997-02	-.19306-01	-.34569-01
6	.16568+00	.15578+00	.14108+00	.11807+00	.86727-01	.50028-01	.12592-01	-.20898-01	-.46850-01	-.63349-01
5	.16364+00	.15454+00	.14002+00	.11644+00	.81300-01	.38524-01	-.62785-02	-.46887-01	-.77923-01	-.95925-01
4	.16158+00	.15412+00	.14177+00	.11440+00	.76604-01	.26358-01	-.27343-01	-.76578-01	-.11390+00	-.13405+00
3	.15906+00	.15436+00	.14502+00	.11845+00	.72869-01	.13521-01	-.50654-01	-.10975+00	-.15516+00	-.17940+00
2	.15483+00	.15548+00	.15194+00	.12372+00	.70127-01	-.11130-03	-.74542-01	-.14311+00	-.20012+00	-.23775+00
1	.10672+00	.16025+00	.17122+00	.13454+00	.68390-01	-.10200-01	-.89000-01	-.16199+00	-.23035+00	-.30723+00

JX=	11	12	13	14	15	16	17	18	19	20
20	.26267+00	.14649+00	.19625-01	-.10882+00	-.21862+00	-.29361+00	-.32709+00	-.32431+00	-.29863+00	-.26309+00
19	.20500+00	.12441+00	.18752-01	-.91889-01	-.18828+00	-.25732+00	-.29342+00	-.30024+00	-.28463+00	-.25684+00
18	.17611+00	.10764+00	.17423-01	-.77856-01	-.16236+00	-.22509+00	-.26146+00	-.27299+00	-.26554+00	-.24669+00
17	.15212+00	.93026-01	.15276-01	-.67360-01	-.14177+00	-.19865+00	-.23392+00	-.24855+00	-.24715+00	-.23588+00
16	.13059+00	.79329-01	.12240-01	-.59395-01	-.12474+00	-.17596+00	-.20952+00	-.22609+00	-.22942+00	-.22458+00
15	.11090+00	.66245-01	.83261-02	-.53641-01	-.11073+00	-.15644+00	-.18776+00	-.20526+00	-.21209+00	-.21254+00
14	.92325-01	.53489-01	.37664-02	-.49422-01	-.98825-01	-.13911+00	-.16780+00	-.18546+00	-.19487+00	-.19976+00
13	.74425-01	.40848-01	-.14133-02	-.46499-01	-.88634-01	-.12354+00	-.14927+00	-.16640+00	-.17754+00	-.18605+00
12	.56781-01	.28052-01	-.72958-02	-.44783-01	-.79955-01	-.10949+00	-.13189+00	-.14781+00	-.15980+00	-.17109+00
11	.38904-01	.14781-01	-.13973-01	-.44162-01	-.72539-01	-.96651-01	-.11539+00	-.12943+00	-.14135+00	-.15451+00
10	.20391-01	.84898-03	-.21426-01	-.44402-01	-.66009-01	-.84615-01	-.99407-01	-.11101+00	-.12201+00	-.13621+00
9	.82691-03	-.14056-01	-.29758-01	-.45440-01	-.60190-01	-.73168-01	-.83770-01	-.92372-01	-.10154+00	-.11583+00
8	-.20443-01	-.30416-01	-.39249-01	-.47343-01	-.54999-01	-.62185-01	-.68399-01	-.73447-01	-.79578-01	-.92554-01
7	-.43964-01	-.48608-01	-.50047-01	-.50049-01	-.50229-01	-.51436-01	-.53188-01	-.54260-01	-.55967-01	-.65805-01
6	-.70231-01	-.68966-01	-.62283-01	-.53495-01	-.45684-01	-.40703-01	-.38074-01	-.34962-01	-.30681-01	-.34982-01
5	-.99982-01	-.92019-01	-.76236-01	-.57735-01	-.41248-01	-.29832-01	-.23109-01	-.15934-01	-.37476-02	.10277-02
4	-.13487+00	-.11889+00	-.92498-01	-.62964-01	-.36813-01	-.18613-01	-.85440-02	.15956-02	.24322-01	.45008-01
3	-.17676+00	-.15026+00	-.11104+00	-.69180-01	-.32425-01	-.69902-02	.54085-02	.16144-01	.52014-01	.99123-01
2	-.23392+00	-.18731+00	-.13044+00	-.75887-01	-.28691-01	.42312-02	.17842-01	.25195-01	.75920-01	.16631+00
1	-.37355+00	-.21932+00	-.14241+00	-.80146-01	-.27289-01	.10339-01	.24085-01	.26021-01	.85525-01	.22692+00

JX=	21	22	23	24	25	26	27	28	29	30
20	-.22558+00	-.18912+00	-.13603+00	-.16767+00	-.19703+00	-.20124+00	-.37747+00	-.55082+00	-.76563+00	-.10596+01
19	-.22525+00	-.19647+00	-.17921+00	-.18395+00	-.21631+00	-.24368+00	-.40107+00	-.57044+00	-.79615+00	-.10832+01
18	-.22379+00	-.20399+00	-.19505+00	-.20528+00	-.24280+00	-.31572+00	-.43223+00	-.59911+00	-.82134+00	-.11003+01
17	-.22104+00	-.20919+00	-.20764+00	-.22422+00	-.26683+00	-.34323+00	-.46079+00	-.62611+00	-.84600+00	-.11162+01
16	-.21693+00	-.21236+00	-.21767+00	-.24030+00	-.28778+00	-.36747+00	-.48630+00	-.65051+00	-.86841+00	-.11314+01
15	-.21120+00	-.21323+00	-.22492+00	-.25328+00	-.30543+00	-.38834+00	-.50859+00	-.67215+00	-.88365+00	-.11458+01
14	-.20402+00	-.21215+00	-.22987+00	-.26372+00	-.32041+00	-.40651+00	-.52831+00	-.69153+00	-.90082+00	-.11592+01
13	-.19528+00	-.20904+00	-.23255+00	-.27172+00	-.33285+00	-.42213+00	-.54559+00	-.70878+00	-.91637+00	-.11717+01
12	-.18466+00	-.20377+00	-.23282+00	-.27722+00	-.34274+00	-.43522+00	-.56045+00	-.72388+00	-.93023+00	-.11831+01
11	-.17184+00	-.19603+00	-.23065+00	-.28031+00	-.35023+00	-.44591+00	-.57300+00	-.73690+00	-.94241+00	-.11934+01
10	-.15681+00	-.18583+00	-.22636+00	-.28141+00	-.35576+00	-.45465+00	-.58364+00	-.74818+00	-.95316+00	-.12026+01
9	-.13925+00	-.17365+00	-.22004+00	-.28070+00	-.35954+00	-.46162+00	-.59253+00	-.75783+00	-.96252+00	-.12108+01
8	-.11826+00	-.15834+00	-.21155+00	-.27827+00	-.36168+00	-.46687+00	-.59966+00	-.76581+00	-.97045+00	-.12179+01
7	-.93235-01	-.13909+00	-.20121+00	-.27454+00	-.36257+00	-.47070+00	-.60525+00	-.77227+00	-.97707+00	-.12240+01
6	-.63580-01	-.11464+00	-.18945+00	-.27001+00	-.36257+00	-.47340+00	-.60952+00	-.77741+00	-.98251+00	-.12292+01
5	-.28091-01	-.84101-01	-.17673+00	-.26517+00	-.36207+00	-.47515+00	-.61256+00	-.78128+00	-.98684+00	-.12336+01
4	.16430-01	-.55740-01	-.16384+00	-.26087+00	-.36150+00	-.47604+00	-.61428+00	-.78376+00	-.98998+00	-.12371+01
3	.72210-01	-.41136-01	-.15207+00	-.25795+00	-.36124+00	-.47620+00	-.61477+00	-.78495+00	-.99207+00	-.12394+01
2	.14429+00	-.41464-01	-.14276+00	-.25725+00	-.36151+00	-.47552+00	-.61377+00	-.78484+00	-.99317+00	-.12419+01
1	.24751+00	.24612-01	-.13398+00	-.25839+00	-.36203+00	-.47370+00	-.60962+00	-.78378+00	-.99340+00	-.12431+01

Figure B10. - Continued.

JX=	31	32	33	34	35	36	37	38	39	40
20	-.14192+01	-.13120+01	-.22424+01	-.27234+01	-.32817+01	-.39768+01	-.48986+01	-.59124+01	-.69597+01	-.81196+01
19	-.14249+01	-.13120+01	-.22416+01	-.27245+01	-.32843+01	-.39793+01	-.48806+01	-.58403+01	-.68708+01	-.78914+01
18	-.14326+01	-.13131+01	-.22408+01	-.27257+01	-.32916+01	-.39709+01	-.47886+01	-.57290+01	-.67046+01	-.76042+01
17	-.14411+01	-.13154+01	-.22411+01	-.27269+01	-.32897+01	-.39562+01	-.47397+01	-.56227+01	-.65328+01	-.73580+01
16	-.14501+01	-.13197+01	-.22420+01	-.27252+01	-.32846+01	-.39377+01	-.46914+01	-.55254+01	-.63768+01	-.71474+01
15	-.14592+01	-.13243+01	-.22433+01	-.27236+01	-.32773+01	-.39168+01	-.46442+01	-.54375+01	-.62404+01	-.69684+01
14	-.14684+01	-.13291+01	-.22447+01	-.27214+01	-.32688+01	-.38952+01	-.45989+01	-.53574+01	-.61197+01	-.68126+01
13	-.14770+01	-.13341+01	-.22462+01	-.27188+01	-.32595+01	-.38734+01	-.45561+01	-.52847+01	-.60130+01	-.66767+01
12	-.14852+01	-.13390+01	-.22475+01	-.27160+01	-.32499+01	-.38522+01	-.45163+01	-.52195+01	-.59195+01	-.65593+01
11	-.14929+01	-.13436+01	-.22489+01	-.27131+01	-.32404+01	-.38320+01	-.44798+01	-.51616+01	-.58382+01	-.64582+01
10	-.14999+01	-.13479+01	-.22501+01	-.27102+01	-.32313+01	-.38131+01	-.44466+01	-.51100+01	-.57668+01	-.63704+01
9	-.15062+01	-.13514+01	-.22512+01	-.27074+01	-.32227+01	-.37957+01	-.44169+01	-.50644+01	-.57045+01	-.62943+01
8	-.15119+01	-.13554+01	-.22522+01	-.27048+01	-.32149+01	-.37802+01	-.43905+01	-.50250+01	-.56514+01	-.62299+01
7	-.15169+01	-.13589+01	-.22532+01	-.27025+01	-.32079+01	-.37665+01	-.43678+01	-.49914+01	-.56065+01	-.61759+01
6	-.15212+01	-.13618+01	-.22541+01	-.27006+01	-.32019+01	-.37546+01	-.43483+01	-.49629+01	-.55688+01	-.61308+01
5	-.15251+01	-.13646+01	-.22551+01	-.26990+01	-.31967+01	-.37446+01	-.43320+01	-.49393+01	-.55379+01	-.60960+01
4	-.15284+01	-.13670+01	-.22561+01	-.26979+01	-.31927+01	-.37367+01	-.43193+01	-.49211+01	-.55143+01	-.60662+01
3	-.15312+01	-.13694+01	-.22573+01	-.26973+01	-.31897+01	-.37308+01	-.43098+01	-.49077+01	-.54972+01	-.60461+01
2	-.15338+01	-.13717+01	-.22587+01	-.26971+01	-.31876+01	-.37265+01	-.43033+01	-.48989+01	-.54861+01	-.60333+01
1	-.15357+01	-.13734+01	-.22602+01	-.26973+01	-.31865+01	-.37245+01	-.43005+01	-.48953+01	-.54817+01	-.60281+01

JX=	41	42	43	44	45	46	47	48	49	50
20	-.96022+01	-.89679+01	-.88216+01	-.85983+01	-.80281+01	-.75610+01	-.73353+01	-.72641+01	-.74057+01	-.75611+01
19	-.86653+01	-.83041+01	-.87188+01	-.84579+01	-.79928+01	-.75941+01	-.73713+01	-.73166+01	-.74398+01	-.75642+01
18	-.82603+01	-.85417+01	-.85310+01	-.83075+01	-.79573+01	-.76341+01	-.74334+01	-.73871+01	-.74711+01	-.75715+01
17	-.79712+01	-.82919+01	-.83394+01	-.81824+01	-.79183+01	-.76597+01	-.74895+01	-.74442+01	-.74993+01	-.75816+01
16	-.77337+01	-.80720+01	-.81660+01	-.80720+01	-.78765+01	-.76725+01	-.75319+01	-.74883+01	-.75252+01	-.75931+01
15	-.75342+01	-.78832+01	-.80143+01	-.79731+01	-.78335+01	-.76750+01	-.75608+01	-.75214+01	-.75478+01	-.76049+01
14	-.73614+01	-.77145+01	-.78800+01	-.78831+01	-.77906+01	-.76711+01	-.75805+01	-.75471+01	-.75673+01	-.76163+01
13	-.72113+01	-.75746+01	-.77612+01	-.78013+01	-.77487+01	-.76630+01	-.75934+01	-.75666+01	-.75838+01	-.76270+01
12	-.70820+01	-.74501+01	-.76571+01	-.77279+01	-.77086+01	-.76514+01	-.76004+01	-.75810+01	-.75974+01	-.76367+01
11	-.69712+01	-.73429+01	-.75665+01	-.76625+01	-.76709+01	-.76379+01	-.76032+01	-.75912+01	-.76083+01	-.76452+01
10	-.68751+01	-.72497+01	-.74870+01	-.76041+01	-.76359+01	-.76236+01	-.76034+01	-.75985+01	-.76171+01	-.76528+01
9	-.67921+01	-.71691+01	-.74177+01	-.75524+01	-.75934+01	-.76092+01	-.76017+01	-.76035+01	-.76241+01	-.76592+01
8	-.67221+01	-.71009+01	-.73587+01	-.75078+01	-.75755+01	-.75955+01	-.75987+01	-.76066+01	-.76295+01	-.76647+01
7	-.66634+01	-.70438+01	-.73090+01	-.74698+01	-.75504+01	-.75830+01	-.75952+01	-.76085+01	-.76337+01	-.76693+01
6	-.66146+01	-.69962+01	-.72675+01	-.74378+01	-.75297+01	-.75718+01	-.75917+01	-.76095+01	-.76369+01	-.76731+01
5	-.65750+01	-.69576+01	-.72338+01	-.74117+01	-.75123+01	-.75625+01	-.75884+01	-.76100+01	-.76392+01	-.76762+01
4	-.65451+01	-.69286+01	-.72085+01	-.73922+01	-.74992+01	-.75553+01	-.75857+01	-.76100+01	-.76409+01	-.76786+01
3	-.65238+01	-.69081+01	-.71908+01	-.73786+01	-.74902+01	-.75506+01	-.75840+01	-.76099+01	-.76420+01	-.76805+01
2	-.65104+01	-.68957+01	-.71803+01	-.73706+01	-.74851+01	-.75483+01	-.75833+01	-.76095+01	-.76426+01	-.76817+01
1	-.65049+01	-.68917+01	-.71769+01	-.73679+01	-.74845+01	-.75484+01	-.75855+01	-.76091+01	-.76428+01	-.76821+01

Figure B10. - Concluded.

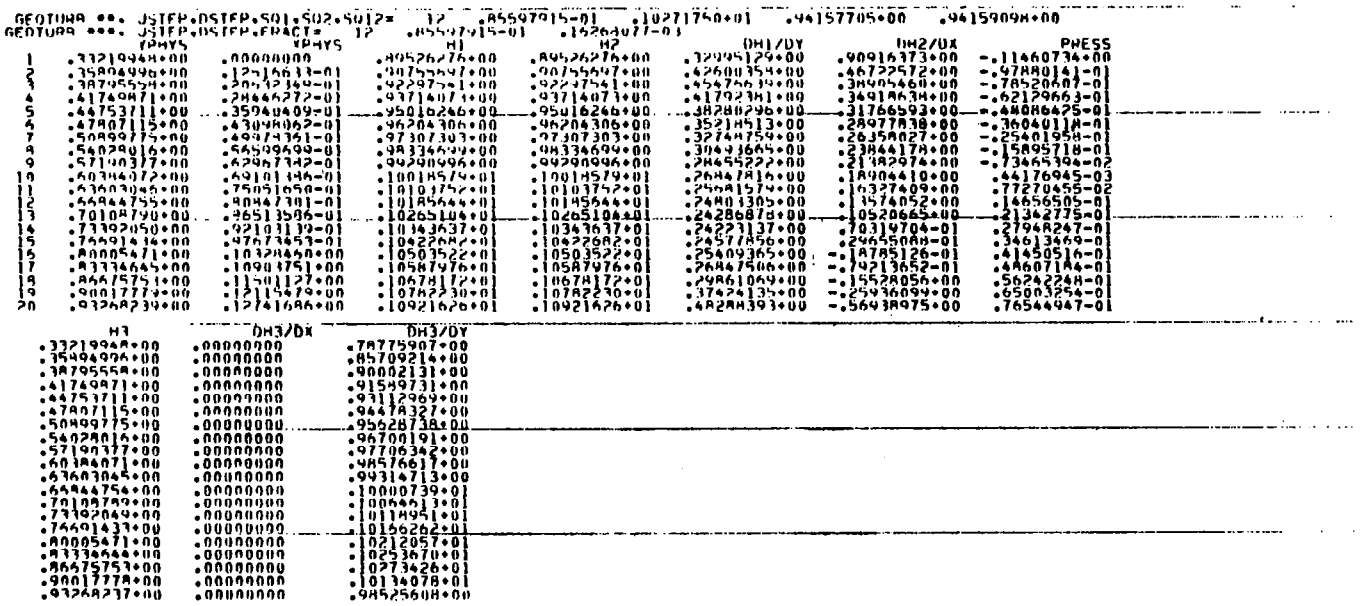

```
 GEOTURB **. JSTEP,DSTEP,SQ1,SQ2,SQ12=    12    .8559791E-01    .1027175E+01    .9415770E+00    .9415909E+00
 GEOTURB ***. JSTEP,DSTEP,FRACT=    12    .8559791E-01    .1426447E-01
          YPHYS          YPHYS          H1          H2          DH1/DY          DH2/DX          PHESS
   1   .3321994E+00    .0000000E+00    .8952627E+00    .8952627E+00    .3299513E+00    .9091637E+00   -.1146073E+00
   2   .3549499E+00    .1271561E-01    .9075599E+00    .9075599E+00    .4260035E+00    .4672257E+00   -.9788014E-01
   3   .3879555E+00    .2941234E-01    .9229754E+00    .9229754E+00    .4547663E+00    .3490546E+00   -.7852060E-01
   4   .4176987E+00    .2866527E-01    .9371407E+00    .9371407E+00    .4179233E+00    .3491863E+00   -.6212966E-01
   5   .4475371E+00    .3594049E-01    .9501626E+00    .9501626E+00    .3828029E+00    .3176659E+00   -.4808642E-01
   6   .4790711E+00    .4304806E-01    .9620430E+00    .9620430E+00    .3521845E+00    .2897783E+00   -.3604011E-01
   7   .5089977E+00    .4994736E-01    .9730730E+00    .9730730E+00    .3274475E+00    .2635802E+00   -.2540195E-01
   8   .5402801E+00    .5659949E-01    .9833466E+00    .9833466E+00    .3049366E+00    .2384417E+00   -.1589571E-01
   9   .5719037E+00    .6298679E-01    .9929099E+00    .9929099E+00    .2845522E+00    .2138297E+00   -.7346539E-02
  10   .6037443E+00    .6910144E-01    .1001857E+01    .1001857E+01    .2664781E+00    .1890441E+00    .4417694E-03
  11   .6360304E+00    .7505165E-01    .1010375E+01    .1010375E+01    .2508815E+00    .1632740E+00    .7727045E-02
  12   .6684475E+00    .8084473E-01    .1018544E+01    .1018544E+01    .2378043E+00    .1367405E+00    .1465650E-01
  13   .7010847E+00    .8651350E-01    .1026514E+01    .1026514E+01    .2272887E+00    .1052066E+00    .2136277E-01
  14   .7339205E+00    .9210113E-01    .1034363E+01    .1034363E+01    .2192313E+00    .7031970E-01    .2794826E-01
  15   .7669134E+00    .9763653E-01    .1042208E+01    .1042208E+01    .2137856E+00    .3465508E-01    .3461366E-01
  16   .8000547E+00    .1032846E+00    .1050352E+01    .1050352E+01    .2109365E+00   -.1478512E-01    .4145051E-01
  17   .8333664E+00    .1090475E+00    .1058797E+01    .1058797E+01    .2106475E+00   -.7021365E-01    .4860718E-01
  18   .8667575E+00    .1150112E+00    .1067817E+01    .1067817E+01    .2129610E+00   -.1552805E+00    .5624224E-01
  19   .9001777E+00    .1211547E+00    .1078223E+01    .1078223E+01    .2182413E+00   -.2593609E+00    .6500325E-01
  20   .9336823E+00    .1274168E+00    .1092162E+01    .1092162E+01    .2282883E+00   -.3693897E+00    .7654494E-01

          H3          DH3/DX          DH3/DY
   .3321994E+00    .0000000E+00    .7877590E+00
   .3549499E+00    .0000000E+00    .8570921E+00
   .3879555E+00    .0000000E+00    .9000213E+00
   .4176987E+00    .0000000E+00    .9158973E+00
   .4475371E+00    .0000000E+00    .9311236E+00
   .4790711E+00    .0000000E+00    .9447832E+00
   .5089977E+00    .0000000E+00    .9562873E+00
   .5402801E+00    .0000000E+00    .9670019E+00
   .5719037E+00    .0000000E+00    .9770634E+00
   .6036804E+00    .0000000E+00    .9857661E+00
   .6360304E+00    .0000000E+00    .9931471E+00
   .6684475E+00    .0000000E+00    .1000074E+01
   .7010847E+00    .0000000E+00    .1006691E+01
   .7339205E+00    .0000000E+00    .1011495E+01
   .7669134E+00    .0000000E+00    .1016626E+01
   .8000547E+00    .0000000E+00    .1021206E+01
   .8333664E+00    .0000000E+00    .1025367E+01
   .8667575E+00    .0000000E+00    .1027342E+01
   .9001777E+00    .0000000E+00    .1013407E+01
   .9336823E+00    .0000000E+00    .9452560E+00
```

Figure B11. - Sample printout of metric information.

```
**** AREA INTEGRALS ****

 AREA=   .1009+00  MASS FLUX=   .6324-01  VEL FLUX=   .6346-01  AVE RU =   .6265+00  AREA RATIO=   .9848+00  MASS ERROR=  -.6505-01

 MASS AVE CPT (LOSS=+) =   .45233+00  IDEAL THRUST COEF=   .10633+01  THRUST=   .17845+00  THARAT=   .10667+01  THAREA=   .31382-01

  AVE MACH NO= .183+00  AVE PT RATIO=   .96822+00  AVE T TOTAL RATIO=   .99343+00  AVE CP=  -.60061-02  BLOCKAGE=   .39597+00
SECANT - P-1.P.P+1.E-1.E.RUREF.RU=
       1        .00000      -.20331-03   -.21347-03    .00000       .38624-02    .59376-01    .63239-01

**** AREA INTEGRALS ****

 AREA=   .1009+00  MASS FLUX=   .6324-01  VEL FLUX=   .6346-01  AVE RU =   .6265+00  AREA RATIO=   .9848+00  MASS ERROR=  -.6505-01

 MASS AVE CPT (LOSS=+) =   .45233+00  IDEAL THRUST COEF=   .10633+01  THRUST=   .17845+00  THARAT=   .10667+01  THAREA=   .31382-01

  AVE MACH NO= .183+00  AVE PT RATIO=   .96822+00  AVE T TOTAL RATIO=   .99343+00  AVE CP=  -.60073-02  BLOCKAGE=   .39597+00
SECANT - P-1.P.P+1.E-1.E.RUREF.RU=
       2       -.20331-03   -.21347-03    .29668+00    .38624-02    .38625-02    .59376-01    .63239-01

**** AREA INTEGRALS ****

 AREA=   .1009+00  MASS FLUX=   .5943-01  VEL FLUX=   .5956-01  AVE RU =   .5887+00  AREA RATIO=   .9848+00  MASS ERROR=  -.9299-03

 MASS AVE CPT (LOSS=+) =   .43416+00  IDEAL THRUST COEF=   .10001+01  THRUST=   .16786+00  THARAT=   .10017+01  THAREA=   .29468-01

  AVE MACH NO= .171+00  AVE PT RATIO=   .96805+00  AVE T TOTAL RATIO=   .99343+00  AVE CP=   .29620-01  BLOCKAGE=   .42382+00
SECANT - P-1.P.P+1.E-1.E.RUREF.RU=
       3       -.21347-03    .29668+00    .30099+00    .38625-02    .55215-04    .59376-01    .59432-01

**** AREA INTEGRALS ****

 AREA=   .1009+00  MASS FLUX=   .5938-01  VEL FLUX=   .5951-01  AVE RU =   .5882+00  AREA RATIO=   .9848+00  MASS ERROR=  -.1088-05

 MASS AVE CPT (LOSS=+) =   .43791+00  IDEAL THRUST COEF=   .99923+00  THRUST=   .16771+00  THARAT=   .10007+01  THAREA=   .29441-01

  AVE MACH NO= .171+00  AVE PT RATIO=   .96805+00  AVE T TOTAL RATIO=   .99343+00  AVE CP=   .30137-01  BLOCKAGE=   .42423+00
SECANT - P-1.P.P+1.E-1.E.RUREF.RU=
       4        .29668+00    .30099+00    .30098+00    .55215-04   -.63796-07    .59376-01    .59376-01
*** ADI CONVERGES IN  5 ITERATIONS. FPS.RAT= .10000-02 .00000       .10000-02 .00000
SECFLO - GRNA.GRNS=    .10435+00   -.30699-02
*** ADI CONVERGES IN 25 ITERATIONS. FPS.RAT= .10000-02 .16031-01       .10000-02 .85186+00

**** AREA INTEGRALS ****

 AREA=   .1025+00  MASS FLUX=   .5938-01  VEL FLUX=   .5956-01  AVE RU =   .5792+00  AREA RATIO=   .1000+01  MASS ERROR=   .0000

 MASS AVE CPT (LOSS=+) =   .41431+00  IDEAL THRUST COEF=   .10000+01  THRUST=   .17051+00  THARAT=   .10000+01  THAREA=   .29875-01

  AVE MACH NO= .171+00  AVE PT RATIO=   .96837+00  AVE T TOTAL RATIO=   .99335+00  AVE CP=   .21851-01  BLOCKAGE=   .44455+00
```

Figure B12. - Area integral summary.

**** PROCESSED STARTING PROFILES ****

JX= 2, VARIABLE AT X(1)= .00000

LEVEL 3 ***** U-VEL *****

IY	R	I7= THETA=	1 .0000	2 .1667+01	3 .3333+01	4 .5000+01	5 .6667+01	6 .8333+01	7 .1000+02	8 .1167+02	9 .1333+02
20	.93268+00	.12742+00	.20069+00	.20263+00	.20418+00	.20501+00	.20501+00	.20501+00	.20501+00	.20501+00	.20501+00
19	.90018+00	.12115+00	.22719+00	.22954+00	.23131+00	.23225+00	.23225+00	.23225+00	.23225+00	.23225+00	.23225+00
18	.86676+00	.11501+00	.23055+00	.23434+00	.24451+00	.26333+00	.29787+00	.30521+00	.30521+00	.30521+00	.30521+00
17	.83335+00	.10904+00	.57636+00	.64786+00	.61221+00	.26974+00	.33523+00	.37106+00	.37143+00	.37143+00	.37143+00
16	.80005+00	.10328+00	.93833+00	.90559+00	.75112+00	.47542+00	.32857+00	.38823+00	.40895+00	.40895+00	.40895+00
15	.76691+00	.97673-01	.96482+00	.95558+00	.84550+00	.67610+00	.49018+00	.36486+00	.41507+00	.42529+00	.42529+00
14	.73392+00	.92103-01	.97168+00	.97168+00	.92410+00	.78656+00	.58549+00	.32778+00	.39406+00	.43720+00	.44065+00
13	.70109+00	.86514-01	.97944+00	.97944+00	.95817+00	.85986+00	.69340+00	.30475+00	.38661+00	.44244+00	.45536+00
12	.66845+00	.80847-01	.98524+00	.98524+00	.97771+00	.88024+00	.72525+00	.28539+00	.38122+00	.44349+00	.46979+00
11	.63603+00	.75052-01	.99225+00	.99225+00	.98715+00	.90030+00	.75598+00	.41381+00	.37395+00	.44063+00	.48109+00
10	.60384+00	.69101-01	.99356+00	.99356+00	.99559+00	.92009+00	.78633+00	.59046+00	.36448+00	.43456+00	.48503+00
9	.57190+00	.62967-01	.10073+01	.10073+01	.10062+01	.93964+00	.81662+00	.66025+00	.35091+00	.42604+00	.48358+00
8	.54028+00	.56600-01	.10158+01	.10158+01	.10158+01	.95911+00	.84708+00	.70893+00	.32554+00	.41575+00	.47771+00
7	.50900+00	.49978-01	.10251+01	.10251+01	.10251+01	.97862+00	.87775+00	.75175+00	.32902+00	.40335+00	.46840+00
6	.47807+00	.43098-01	.10355+01	.10355+01	.10355+01	.99826+00	.90866+00	.79295+00	.63814+00	.38595+00	.45679+00
5	.44754+00	.35940-01	.10471+01	.10471+01	.10471+01	.10182+01	.93983+00	.83410+00	.71052+00	.34756+00	.39217+00
4	.41750+00	.28446-01	.10052+01	.10052+01	.10052+01	.99893+00	.95877+00	.90315+00	.85706+00	.82137+00	.78708+00
3	.38795+00	.20632-01	.90597+00	.90597+00	.90597+00	.90597+00	.90597+00	.90597+00	.90394+00	.89489+00	.88291+00
2	.35895+00	.12517-01	.78404+00	.78404+00	.78404+00	.78404+00	.78404+00	.78404+00	.78404+00	.78404+00	.78404+00
1	.33220+00	.00000	.70105+00	.70105+00	.70105+00	.70105+00	.70105+00	.70105+00	.70105+00	.70105+00	.70105+00

		I7= THETA=	10 .1500+02
20	.93268+00	.12742+00	.20501+00
19	.90018+00	.12115+00	.23225+00
18	.86676+00	.11501+00	.30521+00
17	.83335+00	.10904+00	.37143+00
16	.80005+00	.10328+00	.40895+00
15	.76691+00	.97673-01	.42529+00
14	.73392+00	.92103-01	.44065+00
13	.70109+00	.86514-01	.45536+00
12	.66845+00	.80847-01	.46979+00
11	.63603+00	.75052-01	.48630+00
10	.60384+00	.69101-01	.49912+00
9	.57190+00	.62967-01	.51420+00
8	.54028+00	.56600-01	.52050+00
7	.50900+00	.49978-01	.52007+00
6	.47807+00	.43098-01	.53085+00
5	.44754+00	.35940-01	.41857+00
4	.41750+00	.28446-01	.76141+00
3	.38795+00	.20632-01	.87710+00
2	.35895+00	.12517-01	.78404+00
1	.33220+00	.00000	.70105+00

Figure B13. - Sample printout of flow field variables.

1. Report No.	2. Government Accession No.	3. Recipient's Catalog No.
NASA CR-3494		

4. Title and Subtitle	5. Report Date
TURBOFAN FORCED MIXER-NOZZLE INTERNAL FLOWFIELD III - A COMPUTER CODE FOR 3-D MIXING IN AXISYMMETRIC NOZZLES	April 1982
	6. Performing Organization Code
7. Author(s)	8. Performing Organization Report No.
J. P. Kreskovsky, W. R. Briley, and H. McDonald	R81-912929
	10. Work Unit No.
9. Performing Organization Name and Address	
United Technologies Research Center East Hartford, CT 06108, and Scientific Research Associated, Inc. P.O. Box 498, Glastonbury, CT 06033	11. Contract or Grant No. NAS3-20951
	13. Type of Report and Period Covered
12. Sponsoring Agency Name and Address	Contractor Report
National Aeronautics and Space Administration Washington, D.C. 20546	14. Sponsoring Agency Code 505-32-12

15. Supplementary Notes

Final report. Project Manager, Louis A. Povinelli, Aerothermodynamics and Fuels Division, NASA Lewis Research Center, Cleveland, Ohio 44135.

16. Abstract

A finite-difference method is developed for making detailed predictions of three-dimensional subsonic turbulent flow in turbofan lobe mixers. The governing equations are solved by a forward-marching solution procedure which corrects an a priori inviscid potential flow solution for viscous and thermal effects, secondary flows, total pressure distortion and losses, internal flow blockage and pressure drop. Test calculations for a turbulent coaxial jet flow verify that the turbulence model performs satisfactorily for this relatively simple flow for which lobe mixer flows are presented for two geometries typical of current mixer design. These calculations included both hot and cold flow conditions, and both matched and mismatched Mach number and total pressure in the fan and turbine streams.

17. Key Words (Suggested by Author(s))	18. Distribution Statement
Three dimensional Turbulent Compressible Mixing	Unclassified - unlimited STAR Category 34

19. Security Classif. (of this report)	20. Security Classif. (of this page)	21. No. of Pages	22. Price*
Unclassified	Unclassified	128	A07

* For sale by the National Technical Information Service, Springfield, Virginia 22161

NASA-Langley, 1982